Netherlands Enterprise Agency

Site Studies Wind Farm Zone Borssele

Metocean study for the Borssele Wind Farm Zone Site I

>> *Sustainable. Agricultural. Innovative. International.*

Author   Deltares

Netherlands Enterprise Agency (RVO.nl)
Croeselaan 15 | 3521 BJ | Utrecht
P.O.Box 8242 | 3503 RE | Utrecht
Netherlands

Det Norske Veritas, Danmark A/S
DNV GL Energy
Technical
Tuborg Parkvej 8, 2nd Floor
DK2900 Hellerup
Denmark
Tel: +45 39 45 48 00
Fax: +45 39 45 48 01

Date:	**Our reference**:	**Your reference**:
2015-02-19	DNV Doc. No:1KI2TUA-3	[Your Ref]
	Sign:IPL	
	Corresp. No.:	

Zone Borssele Site Data

This Letter provides a status of DNV GL's review of the Deltares Report '*Metocean Study Borssele Wind Farm Zone, Site 1*' Final version 2 issued February 16 2015.

DNV GL finds that the metocean conditions presented in the report are appropriate to be applied as background for design for offshore wind turbines.

Upper bounds parameters (conservative parameters) can be applied directly for design without further justification.

Sincerely
for Det Norske Veritas, Danmark A/S

Erik Asp Hansen
Project Manager and Head of Project
Certification

Mobile: +45 20 27 38 71
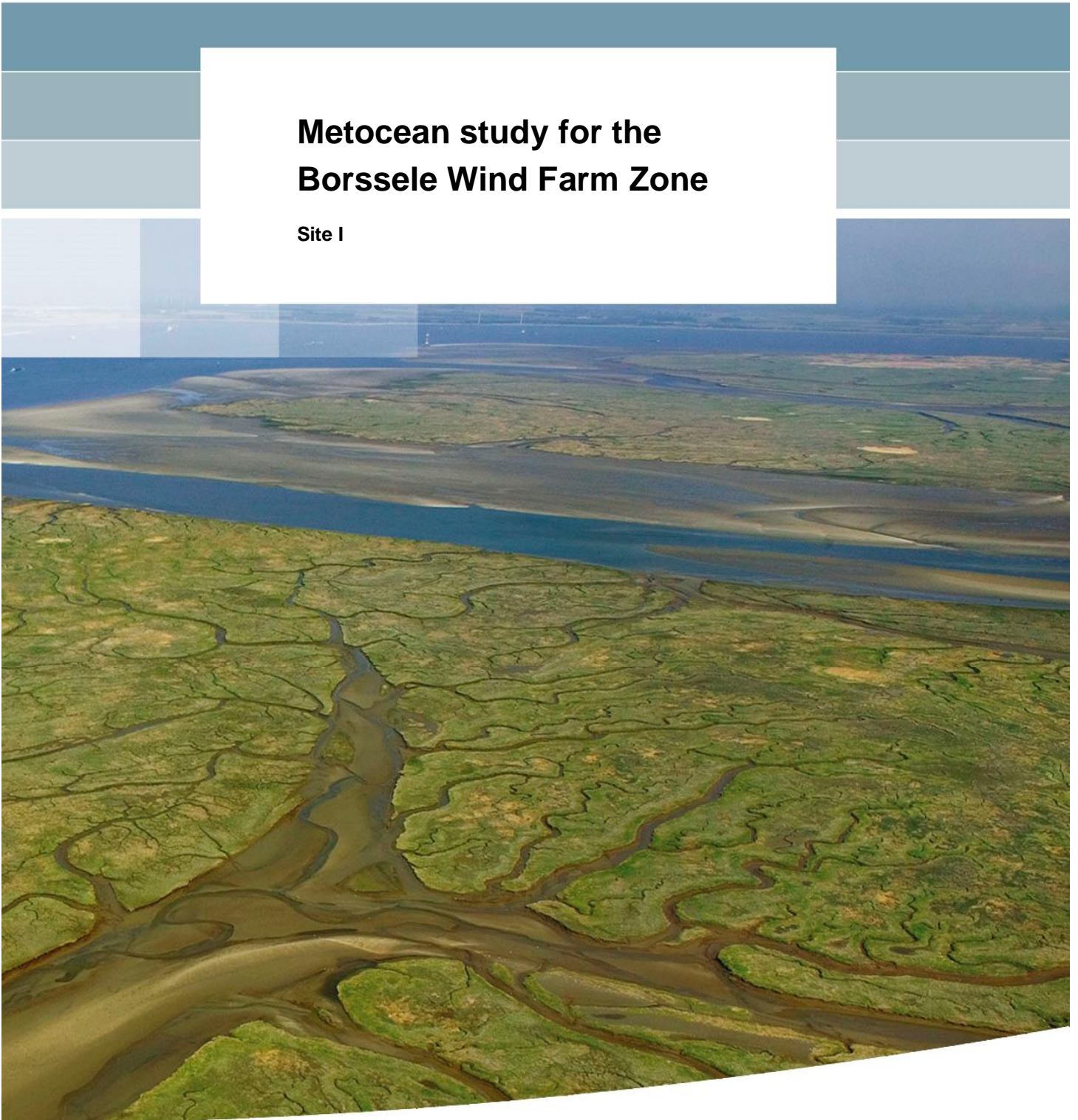Direct: +45 39 45 48 71
erik.asp.hansen@dnvgl.com

Iris Pernille Lohmann
Senior Engineer

Mobile: +45 60 35 15 56
Direct: +45 39 45 49 53
iris.lohmann@dnvgl.com

DNV GL Headquarters, Veritasveien 1, P.O.Box 300, 1322 Høvik, Norway. Tel: +47 67 57 99 00. www.dnvgl.com

1KI2TUA-3_1-N1KX59_CT.docx

Metocean study for the Borssele Wind Farm Zone

Site I

Deltares

Title
Metocean study for the Borssele Wind Farm Zone

Project	**Reference**	**Pages**
1210467-000	1210467-000-HYE-0010	109

Keywords
Offshore wind farm, metocean conditions, Borssele

Summary
In the Dutch Energy Agreement for Sustainable Growth the goal of having 4,450 MW of offshore wind power capacity operational before 2023 has been established. This means that in addition to the operational wind farms a total of 3,500 MW will be contracted by means of phased tender procedures. Several zones on the Dutch continental shelf are being identified for this development, of which the Borssele wind farm zone (BWFZ) is the first zone to be tendered. This zone is divided in four wind farm sites (in Dutch: *kavels*). In order to support the tendering phase RVO requested Deltares to setup a metocean study per wind farm site of the BWFZ. This report describes the metocean conditions that can be used as basis for design (where the appropriate interpretation of parameters and application of safety factors still need to be considered) for Site I. The requested parameters are determined for one location per site and cover wind, wave, water level and current conditions. Also, other types of metocean conditions are analysed, which are, amongst others, marine growth, air- and water temperature. The analyses comprised normal conditions and extreme conditions (several recurrence periods of 1, 2, 5, 10, 50 and 100 years, depending on the requirements following the DNV standard).

References
1210467-000-HYE-0002-o-Deltares proposal for determining metocean conditions for Borssele offshore wind farm zone CV Experts.pdf

Version	Date	Author	Initials	Review	Initials	Approval	Initials
	jan. 2015	H.J. Riezebos		S. Caires		W.M.K Tilmans	
		R. de Graaff		R. Boers(KNMI)			
		J. Schouten					

State
final

Contents

Managementsamenvatting

In het Nederlandse Energieakkoord voor Duurzame Groei is het doel vastgesteld om voor 2023 een vermogen van 4450 MW te hebben opgesteld aan windenergie op zee. Dit betekent dat 3500 MW aan de reeds operationele windparken dient te worden toegevoegd, hetgeen gedaan wordt door middel van gefaseerde aanbestedingsprocedures. Verscheidene zones in de Nederlandse Noordzee zijn hiervoor geïdentificeerd, waarvan het windgebied Borssele als eerste wordt ontwikkeld. Dit gebied is opgedeeld in vier kavels. Ter ondersteuning van de aanbestedingsprocedure heeft de Rijksdienst voor Ondernemend Nederland (RVO.nl) aan Deltares gevraagd om een metoceanstudie uit te voeren voor elk van de kavels van het windgebied Borssele. Dit rapport beschrijft de metoceancondities die –met de juiste interpretatie van de parameters en inachtneming van geschikte veiligheidsfactoren– kunnen worden gebruikt als ontwerpbasis voor kavel I van het windgebied Borssele.

Wind

De windcondities zijn gebaseerd op HARMONIE data van 1979 tot 2013. Een karakteristiek windprofiel voor extreme condities is op basis van deze hoge resolutie data bepaald. Er is geconcludeerd dat een logaritmisch windprofiel (met een Charnock-constante van 0.018) enkel geldig is gedurende gemiddelde omstandigheden. Vanaf windsnelheden boven de 5m/s fit een machtsfunctieprofiel de data over het algemeen beter. Daarom wordt aangeraden om voor dergelijke windsnelheden het machtsfunctieprofiel toe te passen, met een alpha-waarde van 0.08 en een onzekerheidsband van ±0.03. Het windklimaat in windgebied Borssele wordt als volgt gekarakteriseerd:
* De wind waait het meest frequent (en krachtigst) uit het zuidwesten.
* Gedurende het jaar varieert de heftigheid van de windcondities significant, waarbij de zomermaanden milder zijn.
* De heftigste windcondities in windgebied Borssele komen uit de zuidwestelijke en noordwestelijke sectoren; de minst heftige windcondities uit de oostelijke sectoren. De meest extreme windsnelheden worden gevonden in de zuidwestelijke sector (ZW, 225°N - 255°N), met een windsnelheid op 10m hoogte van 29.9m/s bij een overschrijdingskans van eens per 50 jaar.

Golven

De ruimtelijk variërende golfcondities in het windgebied Borssele zijn gemodelleerd met SWAN, een derde-generatie fase-middelend ondiep-water golfmodel. De operationele golfcondities zijn gebaseerd op een modellering van 20 jaar aan condities (tussen 1992 en 2011) met dit model. De extreme golfcondities zijn gebaseerd op de ERA-interim en HARMONIE datasets, welke beide 35 jaar omvatten, gecombineerd met SWAN modellering. Het golfklimaat in windgebied Borssele wordt als volgt gekarakteriseerd:
* De golven komen overwegend uit het zuidwesten en noordwesten. De meest extreme golven arriveren ook uit deze sectoren.
* Gedurende het jaar varieert de heftigheid van de golfcondities significant, waarbij de zomermaanden milder zijn.
* Lange golven naderen het gebied vanaf open zee, waar ook de hogere golven vandaan komen. Golven die arriveren vanaf de kust zijn doorgaans korter en lager.
* Er is een sterke correlatie tussen de windsnelheid en de golfcondities in het windgebied Borssele, waarbij hogere windsnelheden resulteren in heftigere golfcondities.
* De meest extreme golven naderen het windgebied Borssele vanuit de westelijke sectoren, de minder extreme golven arriveren vanuit de oostelijke sectoren. De omnidirectionele golfhoogte met een overschrijdingskans van eens per 50 jaar is 8.7m.

Waterstanden
De waterstanden en stroomsnelheden zijn gebaseerd op een voorspellingsperiode van 20 jaar, gegeneerd door middel van numerieke modellering. Hiervoor is gebruik gemaakt van Delft3D-FLOW, een numeriek model dat in staat is instabiele waterbewegingen en transport van opgelost materiaal te modelleren. Delft3D-FLOW lost de driedimensionale ondiep watervergelijkingen op voor een gegeven set randvoorwaarden. Op basis van de voorspelling is in kavel I van windgebied Borssele het hoogste astronomische getij geschat op 1.95m (ten opzichte van het middenstandsvlak) en het laagste astronomische getij op -1.45m (ten opzichte van het middenstandsvlak). De extreme hoogwaterstand met een overschrijdingskans van eens per 50 jaar is 3.00m boven middenstandsvlak en de extreme laagwaterstand met dezelfde overschrijdingskans is -2.10m. Verder wordt, op basis van beschikbare data aangaande wereldwijde en regionale zeespiegelstijging, aangeraden om rekening te houden met een zeespiegelstijging van 0.2m in de komende 25 jaar en 0.4m in de komende 50 jaar.

Stroming
De operationele en extreme stromingscondities in windgebied Borssele zijn ook gebaseerd op de gedetailleerde Delft3D-FLOW voorspelling van 20 jaar. Het stromingsklimaat in windgebied Borssele wordt als volgt gekarakteriseerd:
*   De twee aan het getij gerelateerde dominante stromingsrichtingen zijn noordnoordoost en zuidzuidwest (gedefinieerd als stromend naar die richting).
*   De dieptegemiddelde stroomsnelheden met een overschrijdingskans van eens per 50 jaar voor de sectoren noordnoordoost en zuidzuidwest zijn respectievelijk 1.2m/s en 1.0m/s.

Overige metoceancondities
*   Mariene ijsaanwas is voorspeld voor 0.27% van de levensduur, gemiddeld bijna een dag per jaar. Dit is gebaseerd op de som van de voorvallen waarbij de luchttemperatuur beneden -2°C is en de zeewatertemperatuur beneden 8°C is.
*   Atmosferische ijsaanwas is voorspeld voor 0.64% van de levensduur, gemiddeld bijna tweeëneenhalve dag per jaar. Dit is gebaseerd op de som van de voorvallen waarbij de luchttemperatuur beneden 0°C is.
*   Aangaande biologische aangroei wordt verwacht dat de biologische groeigemeenschappen in Windgebied Borssele zich zullen ontwikkelen volgens vergelijkbare patronen als waargenomen bij het windpark C-power en het Prinses Amaliawindpark. Bij het Prinses Amaliawindpark werd na een periode van drieënhalf jaar een hoge biodiversiteit waargenomen en werden tevens hoge dichtheden van de mossel M. edulis aangetroffen. Het wordt daarom geadviseerd om in windgebied Borssele rekening te houden met een biologische aangroei van 150mm voor de eerste 7m onder water en 50mm voor het overige deel van de waterkolom.

Executive Summary

In the Dutch Energy Agreement for Sustainable Growth the goal of having 4,450 MW of offshore wind power capacity operational before 2023 has been established. This means that in addition to the operational wind farms a total of 3,500 MW will be contracted by means of phased tender procedures. Several zones on the Dutch continental shelf are being identified for this development, of which the Borssele wind farm zone (BWFZ) is the first zone to be tendered. This zone is divided in four wind farm sites (in Dutch: *kavels*). In order to support the tendering phase RVO requested Deltares to setup a metocean study per wind farm site of the BWFZ. This report describes the metocean conditions that can be used as basis for design (where the appropriate interpretation of parameters and application of safety factors still need to be considered) for Site I.

Wind

The wind conditions are based on high resolution HARMONIE data from 1979 to 2013. Using these data, a characteristic extreme wind profile for the Borssele region has been determined. In conclusion it can be stated that a log profile, with a Charnock-constant of 0.018 is only valid on average. In general, and in particular for wind speeds above 5m/s, a power-law profile fits the data better. For such conditions we recommend that a power-law profile be used, with an alpha value of 0.08 and an uncertainty bandwidth of ±0.03. The main wind climate characteristics at the BWFZ are the following:

- The most frequent (and extreme) winds at BWFZ are blowing from the Southwest.
- The severity of the wind conditions vary significantly during the year, with the summer months being characterised by milder wind conditions.
- The most extreme winds at BWFZ come from the Southwest-Northwest sectors and the less extreme from the Northeast-Southeast sectors. The sector with the most extreme wind conditions is the Southwest sector (SW, 225°N: 255°N) for which the 50-yr return value of the wind speed at 10m height is 29.9m/s.

Wave

In order to model temporal and spatial variations of the wave conditions in the BWFZ a 3rd generation phase-averaging shallow-water wave model, SWAN, was set-up. The normal wave conditions are based on a 20-year hindcast period (1992 – 2011) generated by means of numerical modelling using SWAN. The extreme wave conditions are based on estimates from the 35-years long ERA-interim and HARMONIE dataset and SWAN modelling. The main wave climate characteristics at the BWFZ are the following:

- The most frequent (and extreme) waves reaching the BWFZ are from the Southwest and the Northwest.
- The severity of the wave conditions vary significantly during the year, with the summer months being characterised by milder wave conditions.
- Longer waves approach the site from offshore, the directions from where the most extreme waves also come from. The waves reaching the site from the coast are, as expected, shorter.
- There is high correlation between the wind speed and the wave conditions at the BWFZ, with higher values of wind speed being associated with more severe wave conditions.
- The most extreme waves reaching the BWFZ come from the Southwest-Northwest sectors. The less extreme waves reaching the BWFZ come from the Northeast-Southeast sectors. The omni-directional estimate of the 50-year return value of the significant wave height is of 8.7m.

Water levels
The water level and current conditions are based on a 20-year hindcast period, generated by means of numerical modelling. The modelling was based on the Delft3D-FLOW modelling program for the modelling of unsteady water flow and transport of dissolved matter. Delft3D-FLOW solves the three-dimensional shallow-water equations for given boundary conditions. This study estimates that at the BWFZ the highest astronomical tide (HAT) is of 1.95m (relative to MLS) and the lowest astronomical tide (LAT) is -1.45m (relative to MSL). The 50-year return value of the extreme high total water level is 3.00m and of the extreme low water level is -2.10m. Furthermore, based on the available data on global and regional mean sea level rise, we recommend accounting for a sea level rise of 0.2m in the coming 25 years and of 0.4m in the coming 50 years.

Currents
The operational and extreme current conditions at the BWFZ were also assessed by means of detailed analyses of the hindcast simulations with Delft3D-FLOW for the period 1992 – 2011 (20-year hindcast). The main current climate characteristics at the BWFZ are the following:
- The two dominant tide-related flow directions North-Northeast and South-Southwest (going to) can be clearly observed.
- The 50-year return value estimates of the depth-averaged current for the main directional sectors North-Northeast and South-Southwest at the BWFZ are 1.2(m/s) respectively 1.0(m/s).

Other metocean data
- Marine ice accretion is predicted to occur for 0.27 % of time (the sum of the occurrences with air temperature below -2°C and seawater temperature below 8°C), which is almost one day per year on average.
- Atmospheric icing is predicted to occur for 0.64 % of time (the sum of the occurrences with air temperature below 0°C), which is almost two and a half days per year on average.
- Marine growth: It is to be expected that the biofouling communities at the BWFZ will develop in similar ways to the observed communities at the C-Power and Princess Amalia wind farms. As the Princess Amalia wind farm showed a higher biodiversity and higher densities of mussel M. edulis after a longer period (3.5 years) of operation, it is advised to take into account a marine growth thickness of 150 mm for the top 7 m below water level of the BWFZ monopoles and 50 mm for the lower zone.

List of abbreviations

ADI	Implicit finite difference method (Delft3D-FLOW numerical scheme)
API	American Petroleum Institute
BSBT	Backward space, backward time (SWAN numerical scheme)
BWFZ	Borssele Wind Farm Zone
cdf	cumulative distribution function
CFSR	Climate Forecast System Reanalysis
CoastDat	Model based data bank for the North Sea
DCSM	Dutch Continental Shelf Model
DD	Domain Decomposition
Delft3D-FLOW	Software program to simulate non-steady flows in relatively shallow water
DNV	Det Norske Veritas
DONAR	Data Opslag NAtte Rijkswaterstaat (Dutch water database)
ECMWF	European Center for Medium-range Weather Forecasting
EMS	European Macroseismic Scale (seismicity)
ESS	Extreme Sea States
ERA-interim	Global atmospheric reanalysis from 1979, continuously updated in real time
ETRS89	European Terrestrial Reference System 1989
eva	Extreme value analysis
FINO[1]	Offshore measurement platform in the North Sea
GPD	Generalized Pareto Distribution
HARMONIE	Non-hydrostatic convection-permitting atmospheric model
HAT	Highest Astronomical Tide
HWL	High Water Level
IPCC	Intergovernmental Panel on Climate Change
ISO	International Organization for Standardization
JONSWAP	Joint North Sea Wave Project
KEMA	Keuring van Elektrotechnische Materialen te Arnhem (certification body)
KNMI	Royal Dutch Meteorological Institute (Koninklijk Nederlands Meteorologisch Instituut)
LAT	Lowest Astronomical Tide
LWL	Low Water Level
MHWN	Mean High Water Neap
MHWS	Mean High Water Spring
MLLWS	Mean Lowest Low Water Spring
MLWN	Mean Low Water Neap
MLWS	Mean Low Water Spring
MSL	Mean Sea Level
MW	Megawatt
MWD	Mean Wave Direction

Deltares

MWL	Mean Water Level
NCEP-CFSR	National Center for Environmental Prediction – Climate Forecast System Reanalysis
NOAA	National Oceanic and Atmospheric Administration
NSS	Normal Sea States
NWP	Numerical Weather Prediction
ORCA	metOcean data tRansformation, Classification and Analysis tool
OWEZ	Offshore Windpark Egmond aan Zee
OWP	Offshore Wind Park
PAWF	Prinses Amalia Wind Farm
PGA	Peak Ground Acceleration (seismicity)
POT	Peak over Threshold
PSU	Practical Salinity Init
PWM	Probability-Weighted Moments
RCP	IPCC emission scenario
RMSE	root-mean-square error
RP	Return Period
RVO	Netherlands Enterprise Agency (Rijksdienst voor Ondernemend Nederland)
SCW	Scheur West Wandelaar wave buoy
S&L	Second order upwind scheme with third order diffusion (SWAN numerical scheme)
SORDUP	Second-order upwind scheme with second order diffusion (SWAN numerical scheme)
SSS	Severe Sea States
SWAN	Simulating WAves Nearshore (numerical wave model)
SWB	Schouwenbank wave buoy
TNO	Dutch Organisation for Applied Scientific Research (Nederlandse Organisatie voor Toegepast Natuurwetenschappelijk Onderzoek)
WGS84	World Geodetic System 1984

Deltares

1 Introduction

1.1 Project background

In the Dutch Energy Agreement for Sustainable Growth the goal of having 4,450 MW of offshore wind power capacity operational before 2023 has been established. Currently two offshore wind farms are operational – Prinses Amalia Wind Park and Offshore Wind Farm Egmond aan Zee - and two wind farms are being set up – Luchterduinen and Gemini. In addition to these, a total of 3,500 MW will be contracted by means of phased tender procedures from 2015 onwards. Several zones on the Dutch continental shelf are being identified for this development. One of these zones is the Borssele wind farm zone (Hereafter: BWFZ). The BWFZ is the first zone to be tendered. It is located in the southern part of the Dutch North Sea, close to the Dutch-Belgian border. The area's location with respect to the coast can be visualised in Figure 1.1.
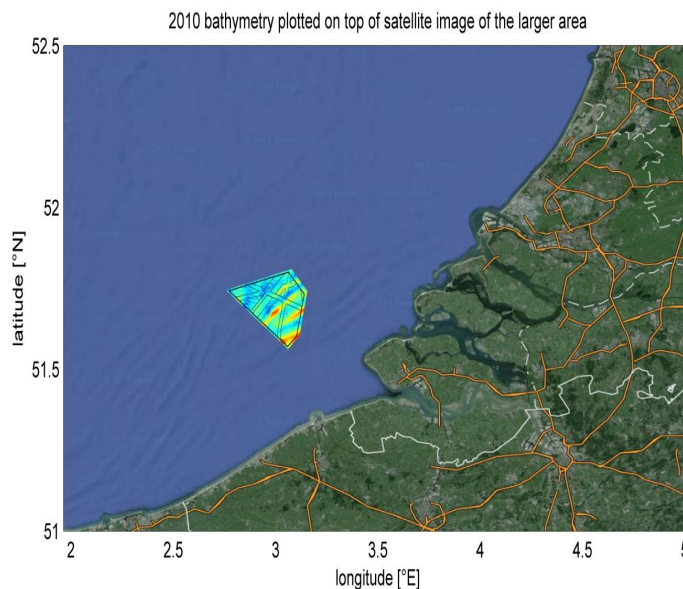
Figure 1.1 Location of the Borssele Wind Farm Zone in the southern part of the Dutch North Sea.

In order to support developers in competitive bids for the tenders for the further development of offshore wind farms, the Netherlands Enterprise Agency (RVO.nl) aims to make specific site data available. The area's meteorological and ocean conditions (commonly abbreviated into "metocean" conditions) are among the data to be provided.

RVO.nl requested Deltares to provide a proposal for a study into the metocean conditions that affect offshore operations in the BWFZ. The requested metocean data, which are to be determined in accordance with applicable norms and standards, including DNV-OS-J101 or equal, are required for supporting, amongst others, the wind resource assessment, the design of the offshore wind farm as well as the Environmental Impact Assessment. Deltares submitted this proposal on 25 September 2014.

The proposal was subsequently awarded by letter, dated 3 October 2014 and the contract was signed on 15 October 2014.

BWFZ is divided in four different sites, see Figure 1.2 below. The metocean parameters are determined for one location per site. Table 1.1 and Figure 1.2 present the locations and depths of the selected output locations.

Site:	Latitude	Longitude	Easting	Northing	Depth
Site I	3,038888°N	51,758979°E	502684m UTM31	5734232m UTM31	30.8m MSL
Site II	3,077777°N	51,668601°E	505379m UTM31	5724183m UTM31	25.4m MSL
Site III	2,961111°N	51,694424°E	497312m UTM31	5727053m UTM31	35.1m MSL
Site IV	2,863889°N	51,720246°E	490598m UTM31	5729933m UTM31	38.5m MSL

Table 1.1 Locations and depths of selected output locations for each site in the BWFZ, coordinate system: ETRS89 / UTM zone 31N.
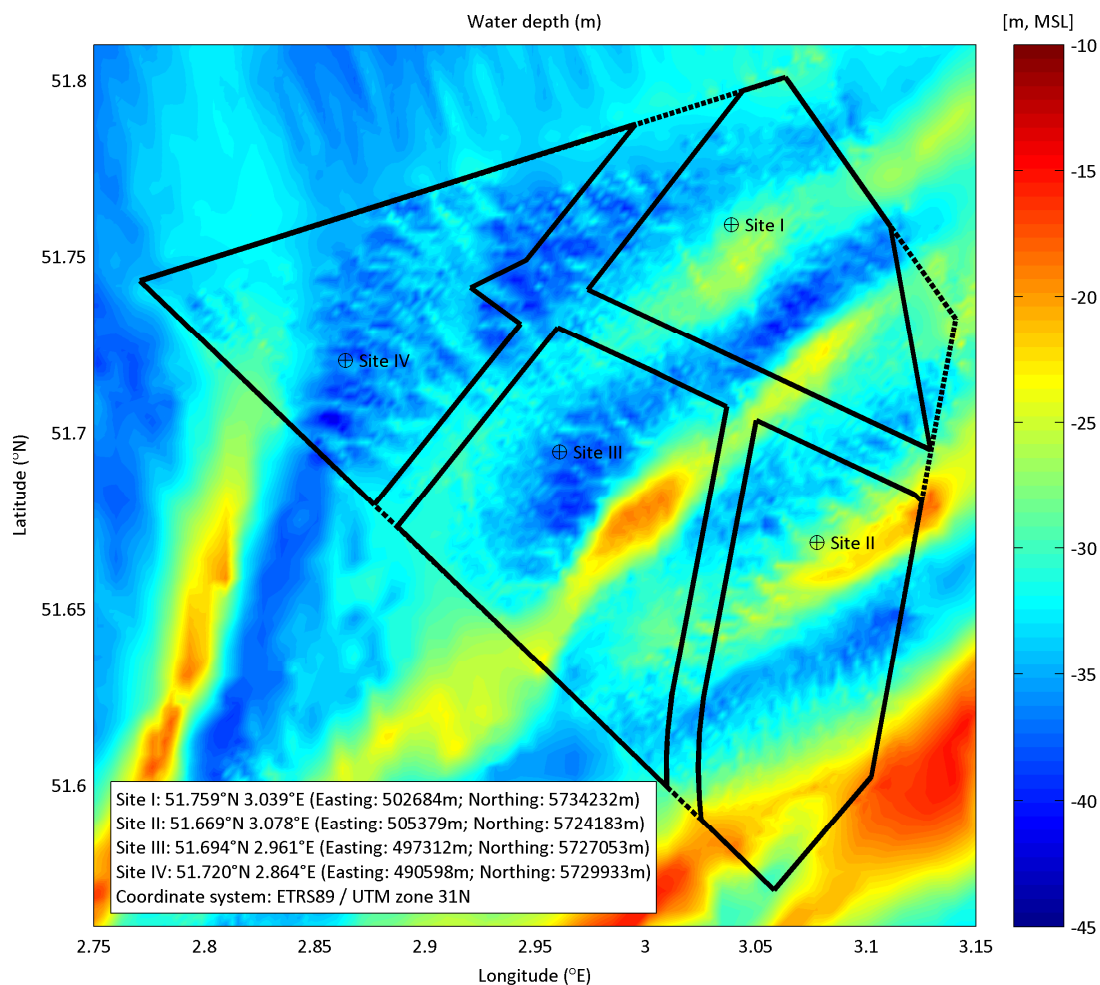
Figure 1.2   Output locations within the BWFZ.

This report presents the metocean conditions that can be used as basis for design (where the appropriate interpretation of parameters and application of safety factors still need to be considered) for Site I.

1.2 Objectives

The general objective of this study is to determine the metocean conditions that can be used as basis for design (where the appropriate interpretation of parameters and application of safety factors still need to be considered) (wind, wave, current and other meteorological parameters) present in Site I of the BWFZ. As specified in the scope description for this study:

1 Identify all meteorological and oceanographic parameters that can be used as basis when carrying out design calculations (where the appropriate interpretation of parameters and application of safety factors are taken into consideration) for offshore wind farm in the BWFZ.
2 Identify relevant meteorological and oceanographic parameters that are input for wave and wind persistence tables for the wind farms and offshore high voltage stations in the BWFZ.

This is done by means of a detailed analysis of the available data and numerical modelling of the area. For the analyses the in-house software package "ORCA" is used ("metOcean data tRansformation, Classification and Analysis tool", http://www.deltares.nl/nl/software/1023790/orca).

The methodology of each analysis will be presented and discussed. The resulting data is summed up next.

The analysis of the wind data will result in:
- Extreme wind speed profiles
- Extreme wind speeds
    o The directional dependent all year extreme wind speed:
        ▪ for return periods of 1, 2, 5, 10, 50 and 100 years;
        ▪ averaged over 1h, 10min, 1min and 3sec;
        ▪ at heights of 10m, 70m, 80m, 90m, 100m and 150m.
- Wind spectral density
    o Wind spectra at 10m, 70m, 80m, 90m, 100m and 150m.
- Wind operational criteria
    o Monthly and annual wind roses at heights of 10m, 70m, 80m, 90m, 100m and 150m;
    o Monthly and annual joint occurrence tables of wind speed vs. wind direction at heights of 10m, 70m, 80m, 90m, 100m and 150;
    o Directional dependent Weibull parameters for normal wind speed distribution;
    o Persistence of wind speed with the following parameters:
        ▪ Wind speed thresholds 2m/s, 4 m/s, 6 m/s, 8 m/s, 9 m/s, 10 m/s, 11 m/s, 12 m/s and 15m/s
        ▪ Time windows of 1h, 6h, 12h, 24h, 48h and 72h
        ▪ Probabilities of exceedance of 20%, 50% and 80%;
- Turbulence intensity.

The analysis of the wave conditions will result in:
- Operational wave criteria (joint probability wind/waves)

- o Omni-directional monthly and all-year scatter diagrams of H_s vs T_z
- o Directional all-year scatter diagrams of H_s vs T_z
- o Omni-directional monthly and all-year scatter diagrams of H_s vs T_p
- o Omni-directional monthly and all-year scatter diagrams of H_s vs MWD
- o H_s and T_p wave roses
- o H_s persistence tables (monthly, H_s>threshold & H_s<threshold)
  - ▪ Thresholds (0.25m, 0.5m, 0.75m, 1.0m, 1.25m, 1.5m, 1.75m, 2.0m, 2.25m, 2.75m, 3.0m)
  - ▪ Spells (1h, 6h, 12h, 24h, 48h, 72h)
  - ▪ Probability of exceedance 20% / 50% / 80%
- Wave height fatigue tables
  - o All-year individual wave height and MWD and individual wave height and wave period joint occurrences tables (H(m)/T(s) 0-12m ranges 0.5m vs. frequency vs. direction)
- Extreme values
  - o $H_s/T_z/T_p$, $H_{max}/T_{maxlower}/T_{maxupper}$, Crest - return periods 1, 2, 5, 10, 50, 100 years (12 directions & non directional)
  - o Extreme sea-state
  - o 50-year extreme wave parameters combined with 50-year minimum still water levels
  - o 100-year extreme wave parameters combined with 100-year minimum still water levels
  - o Extreme wave crest height
  - o Local variations
  - o H_{max} interpolated depth (considering the complete BWFZ)
  - o Wave parameters for 10,000-year sea state
- Secondary parameters
  - o Wave energy density spectrum
    - ▪ Wave input parameters for the 100 years condition for the most severe direction
  - o Maximum wave height
  - o Storm duration
- Shoaling and wave breaking
- Extreme sea states

The analysis of the water levels will result in:
- Astronomical tidal levels
  - o LAT, MLLWS, MLWS, MLWN, MHWN, MHWS, HAT
- Extreme water levels
  - o 1, 2, 5, 10, 50, 100-year (HWL/LWL)
  - o Wave crest height above MWL (10, 50-year return period)
  - o Total wave crest elevation (10, 50-years return period)
- Long term seasonal sea level change

The analysis of the currents will result in:
- Extreme current profiles with directional dependency (1yr, 10yr, 50yr, 100yr return period)
  - o Extreme total steady (tide plus surge) current profiles (from MWL to seabed) and direction
- Operational conditions
  - o Joint occurrence of depth-averaged current speed and direction

  o Current roses (speed and direction)
  o Current velocity profiles (from MWL to seabed)

Furthermore the joint-probability of various metocean parameters will be analysed. This will result in:
- Extremes
  - o Omni-directional wind speeds associated with the H_s extremes and wave height an wave period associated with the wind speed extremes (1, 2, 5, 10, 50, 100yr)
- Operational
  - o Wind & waves
    - Joint occurrence of wind direction at hub height (for wind speed from 0m/s to 100 m/s)
    - H_s distribution of wave-wind misalignment cases (for wind speed from 0m/s to 100 m/s)
    - H_s distribution for wave height (0-7m H_s) – wind direction misalignment cases – wind speed (0-100m/s)
    - Directional wind speed versus wave height for 10m height and hub height
    - Persistence tables (probability of exceedance 20% / 50% / 80%
  - o Current & waves
    - H_s versus still water level – total of tide and surge
    - H_s versus residual water level (surge height)
    - H_s versus depth averaged current speed – total of tide and surge
    - H_s versus depth averaged residual (surge) current speed
    - H_s distribution for misalignment cases
  - o Water levels & waves
    - Water level versus significant wave height
    - Residual water level versus significant wave height by direction
  - o Water levels & current directions
    - Joint occurrence of water level and current (residual) direction
    - Joint occurrence of water level and current (total of tide and surge) direction
    - Example of time series of water levels and current

Also other metocean conditions will be analysed. This will result in:
- Snow and ice accretion criteria
- Sea ice conditions
- Seismicity
- Air temperature and air density
- Seawater salinity and seawater density
- Marine growth

1.3 Methodology

As already written in Section 1.1, the requested metocean parameters are determined for one location per site. This location (coordinates given in Table 1.1 and indicated in Figure 1.2) is deemed representative for Site I and was chosen based on initial numerical modelling results combined with expert judgement (see also Section 4.2). We note that it should not be expected that the estimates obtained for this location are the severest (most conservative) of the site. The location with the most conservative estimates varies depending on the

considered parameter (and the specific design purpose for which that parameter is needed). By using a single location, direct and consistent coupling of different parameters is possible, and over-conservatism can be prevented. However, if required for design purposes, the spatial variation of the extreme wave conditions over the whole site can be found in the Appendix B.3 and B.4. When looking in detail at these plots slightly higher values can be found at other locations in the site.

In order to determine the local variation over each one of the four sites of the BWFZ, dedicated numerical modelling is required for wave, water level and current modelling, all based on spatially varying wind data. The local modelling simulations cover a relative long period (20 years), sufficient for deriving the requested metocean parameters.

The metocean conditions will be assessed by means of detailed analyses of available model (reanalysis) and measurement data. These data will be analysed statistically for each selected output location with our in-house software package "ORCA" ("metOcean data tRansformation, Classification and Analysis tool", http://www.deltares.nl/nl/software/1023790/orca).

The analyses comprised normal conditions and extreme conditions (several recurrence periods of 1, 2, 5, 10, 50 and 100 years, depending on the requirements following the DNV standard). The wind, wave and current normal conditions are computed empirically and given in terms of frequencies of joint occurrences and the extreme climate in terms of return values obtained by means of extreme value analyses.

The extreme value analysis approach used in this study is based on the Peaks-Over-Threshold (POT) method, e.g. (Coles, 2001). It consists of fitting the Generalized Pareto Distribution (GPD) to the peaks of clustered excesses over a threshold, the excesses being the observations in a cluster minus the threshold, and calculating return values by taking into account the rate of occurrence of clusters. Under very general conditions this procedure ensures that the data can have only three possible, albeit asymptotic, distributions (the three forms of the GPD) and, moreover, that observations belonging to different peak clusters are (approximately) independent. More precisely, the peaks of clustered excesses over a high threshold u are assumed to occur in time according to a Poisson process with rate λ_u and to be independently distributed with a GPD, whose distribution function is given by

$$
F_u(y) = \begin{cases} 1 - \left(1 + \xi \dfrac{y}{\sigma_u}\right)^{-1/\xi} & \text{, for } \xi \neq 0 \\[2em] 1 - \exp\left(-\dfrac{y}{\sigma_u}\right), & \text{for } \xi = 0, \end{cases}
\tag{1.1}
$$

where $0 < y < \infty$, $\sigma_u > 0$ and $-\infty < \xi < \infty$. The two parameters of the GPD are called scale (σ_u) and shape (ξ) parameters.

The choice of threshold represents a trade-off between bias and variance: choosing too low a threshold is likely to violate the asymptotic basis of the model, leading to bias; a threshold which is too high will generate fewer excesses with which to estimate the model, leading to high variance. An important property of the POT/GPD approach is the threshold stability

property: if a GPD is a reasonable model for excesses of a threshold u_0, then for a higher threshold u a GPD should also apply; the two GPD's have identical shape parameter and their scale parameters bear a simple relation. This property of the GPD was used to find the optimal threshold to fit a GPD model to the data.

The sample to be used in the POT method has to be extracted from the original time series in such a way that the data can be modelled as independent observations. This is done by a process of declustering in which only the peak (highest) observations in clusters of successive exceedances of a specified threshold are retained and, of these, only those which in some sense are sufficiently apart (so that they belong to more or less 'independent storms') are considered as belonging to the collection of POT points. Specifically, in the present application we have treated cluster maxima at a distance of less than 48 h apart as belonging to the same cluster (storm). This period of 48h corresponds to the maximal storm duration in the data.

There are several methods available for the estimation of the parameters of the GPD. For the type of data we are concerned with in this report the method of Probability-Weighted Moments (PWM) represents an adequate choice (for details, see Hosking and Wallis, 1987, and Hosking et al., 1985). In order to provide reliable asymmetric confidence bands, the method of PWM has been combined with adjusted bootstrap estimates (see Coles and Simiu, 2003 and Delft Hydraulics, 2007) for computing confidence intervals.

To recap, the extreme value analysis procedure applied here consist of the following steps:
- POT samples of storm maxima are collected from the original time series using different thresholds.
- For each POT sample the GPD parameters and their uncertainties are estimated.
- Based on the variation of the shape parameter estimates with the threshold, the optimal threshold is chosen.

Fixing this threshold, the definite return values estimates and uncertainty are defined.

1.4 Project team

This project was managed by Jan-Joost Schouten. The analysis and computations were carried out by Wilbert Verbruggen and Hendrik Jan Riezebos (wind and waves), Reimer de Graaff (water level, currents and ice), Ger de Lange (seismicity) and Helena Hulsman (marine growth). The HARMONIE data were pre-processed and sent to Deltares by Mark Savenije (KNMI) and Henk van den Brink (KNMI) helped with the interpretation of some results. The reporting was carried out by Jan-Joost Schouten with help from the rest of the team. The review was carried out by Reinout Boers (KNMI, wind analysis), Luca van Duren (marine growth) and Sofia Caires (analyses of all remaining parameters not mentioned above).

1.5 Outline of the report

In chapter 2 the available data sources, the applicability of each source and the validation of the data is discussed. Next the data as summed up in section 1.2 is provided: the wind data in chapter 3, the wave data in chapter 4, the water levels in chapter 5, the current data in chapter 6, the joint probability conditions in chapter 7 and the other metocean data in chapter 8.

This report is accompanied with two separate excel files containing data:
- *1210467-000-HYE-0010-v2-r-Metocean study for the Borssele Wind Farm Zone Tables Site I.xls*
- *1210467-000-HYE-0010-r-Metocean study for the Borssele Wind Farm Zone Persistence Tables Site I.xlsx*

2 Data

2.1 Introduction

Given the availability of long-term reanalysis, hindcast and measurement wind and wave data in the vicinity of the Borssele Wind Farm Zone, we start this study by defining the most suitable data to use in the determination of the wind and wave metocean conditions in the next chapters.
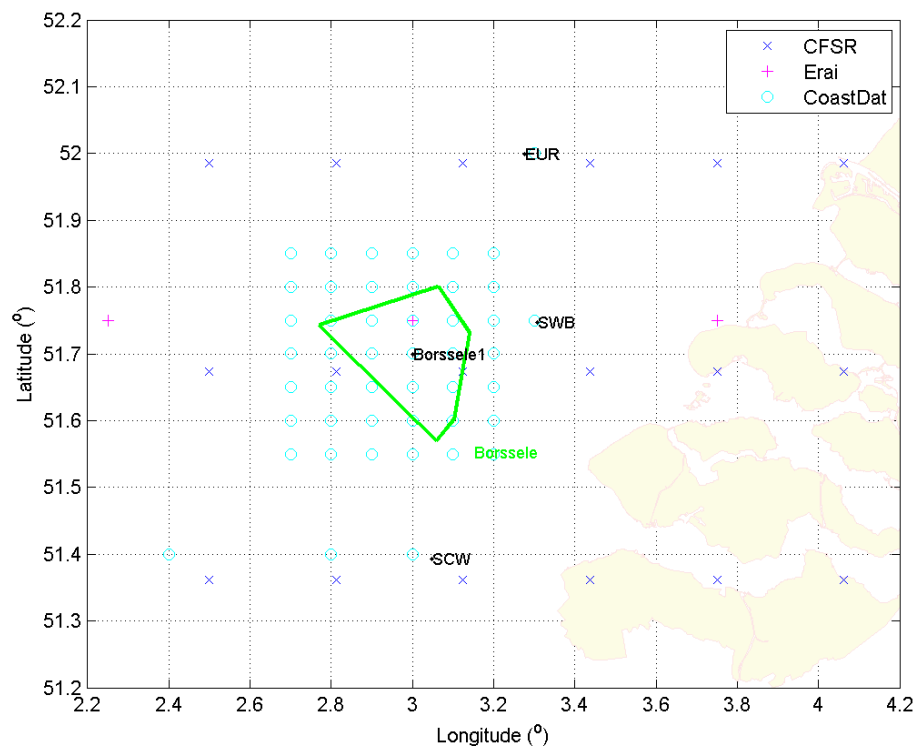
Figure 2.1 Aerial view of the region of interest with Dutch measurement stations marked with a black ●, CFSR grid points with a blue x, ERA-interim grid points with a magenta + and the coastDat grid points with a cyan o.

A number of datasets have been considered:
- Wave and wind measurements carried out by the Dutch Ministry of Public Works and Meteorological Institute. The wave data are 3-hourly from 1979 until 2008 and from the SCW, SWB and Euro platform measuring stations. The wind data are hourly and from 1983 to 2009 at the Euro platform.
- Meteorological data from HARMONIE. The high resolution atmospheric model HARMONIE has been chosen to model the winds and pressures leading to hydraulic loads in the Dutch primary water defences (Baas, 2014). HARMONIE is the operational Numerical Weather Prediction (NWP) model of KNMI. It is a limited-area model that has been developed in a consortium involving many European countries. Major differences between HARMONIE and its predecessors are that HARMONIE is intended to run on a very high resolution and that it is a so-called non-hydrostatic model. The latter means that instead of employing the hydrostatic approximation, which often breaks down in severe-weather events, that the vertical momentum equation is solved explicitly. The

model has been used to hindcast the relevant atmospheric variables in the period from 1979 until 2013 with a time resolution of 1 hour on a grid with a spacing of 2.5 km. The period from 1979 until 2013 was chosen because it is the period in which the ERA-interim data, needed to force the model at the boundaries and to provide initial conditions for the HARMONIE runs, are available. ERA-interim is the most reliable reanalysis dataset of the European Centre for Medium-Range Weather Forecasts (ECMWF). The strength of the ERA-Interim dataset is that it combines one of the leading numerical weather prediction models (the ECMWF model) with an advanced data assimilation system (Dee et al., 2011). The resulting data can be considered a best estimate of the state of the atmosphere, given the model information and the observations. A validation of the HARMONIE 10 m wind speeds and vertical wind profiles can be found in Baas (2014) and Bas et al. (2015). These publications show good comparisons between the HARMONIE wind velocities and measurements above water. Only two stations - the offshore Wind Farm Egmond aan Zee (OWEZ) tower and the FINO tower-with measurements of vertical wind profiles above water are considered in these studies, but a good comparison between the model results and the observations is found.

- Waves and winds from ERA-interim data. The data are 6 hourly, from 1979 until 2013 and on a global grid with a resolution of about 0.75° x 0.75°.
- Winds from the Climate Forecast system Reanalysis (CFSR, Saha et al., 2010) of the American National Oceanic and Atmospheric Administration (NOAA). The data are 6 hourly, from 1979 until 2012 and on a global grid with a resolution of about 0.31° x 0.31°. We were also intending to consider the CFSR waves (Chawla et al., 2012), but during the American government shutdown in October 2013, there was a hardware failure in the American NOAA server on which the processed wave data were stored. NOAA plans to reprocess the data, but it is still unclear when these data will become available.
- The German CoastDat reanalysis winds and waves (Weisse and Günther, 2007). The data are hourly from 1958 until 2003 and on a North Sea grid with a resolution of about 0.10° x 0.05°.

Figure 2.1 shows the locations and Table 2.1 provides an overview of the considered data.

Dataset	Location	Data type	Data availability	Variables	Source of data
SWB	3.3067°E 51.7467°N	measurements	Hourly (wind) and 3-hourly (waves), 1979 - 2008	Wind, Waves	Dutch Data-ICT-service
Euro Platform	3.2764°E 51.9986°N	measurements	Hourly (wind) and 3-hourly (waves), 1979 - 2008	Wind, Waves	Dutch Data-ICT-service
SCW	3.0481°E 51.3924°N	measurements	Hourly (wind) and 3-hourly (waves), 1979 - 2008	Wind, Waves	Dutch Data-ICT-service
HARMONIE	North Sea, on a 2.5x.25 km grid	dynamical downscalling	Hourly	Wind at several heights	KNMI
CFSR	Global, on a 0.31°x0.31° grid	reanalysis	6-hourly, 1979 - 2009	Wind	NOAA
ERA-interim	Global, on a 0.75°x0.75° grid	reanalysis	6-hourly, 1979 - 2013	Wind and waves	ECMWF
coastDat-1	North Sea, on a 0.10° x 0.05° grid	hindcast	hourly, 1958 - 2007	Waves	http://www.coastdat.de/

Table 2.1   Overview of the considered data.

In the next sections we validate the wave (Section 2.2), wind data (Section 2.3).

We note that the wind and wave directions are given using the nautical (or meteorological) convention: the coming from direction, clockwise from the North (coming from North=0°N, East=90°N, South=180°N, West=270°N).

2.2   Waves

The comparisons between the measured data and ERA-Interim and CoastDat data are quantified by means of error statistics such as the bias, root-mean-square error (RMSE), correlation and slope. Table 2.2 presents estimated performance classification for the error statistics used in this report (correlation and slope) to quantify the comparison between two datasets. Note, however, that the classifications are based on general experience with these types of data, since no standard classification of wind and wave data error statistics exist.

Error statistics	Performance		
	Moderate/poor	**Good**	**Excellent**
Correlation (ρ)	< 0.8	0.8 – 0.9	0.9 – 1.0
Slope	<0.8 or >1.2	0.8–0.9 or 1.1–1.2	0.9 – 1.1

Table 2.2   Performance classification of correlation and slope.

2.2.1   Comparison of ERA-Interim to measurements

Figure 2.2 and Figure 2.3 presents a comparison of the ERA-interim wave data at location 3°E and 51.75°N (the ERA-interim location closest to Borssele and the measurement locations, cf. Figure 2.1) with the SWB, Euro Platform and SCW measurements. We note that at SCW no wave direction measurements are available and that at SWB the wave direction measurements have only been carried out from November 2005. Furthermore, the wave

period variable used in these comparisons is $T_{m-1,0}$ [1] because this is the wave period parameter freely available from the ERA-interim dataset.

At both SWB and Euro Platform, an excellent comparison between the measured and ERA-interim significant wave height can be observed (correlation of 0.931 and 0.954). The comparison of the wave period shows a good agreement between the measurements and the ERA-interim data (correlation of 0.804 and 0.833). As expected given its relative locations and depths, the ERA-interim data slightly overestimates the significant wave height at SWB (+6%), and underestimates the wave height at Euro Platform (-7%).

At SCW, the ERA-Interim data shows a lower correlation for both the significant wave height (0.872) and the wave period (0.694), see Figure 2.4. This can be explained by the fact that SCW is located at significantly shallower water.

2.2.2 Comparison of CoastDat data to measurements

Figure 2.5 shows a comparison of the CoastDat wave data to wave measurements at SWB and Euro Platform. Although the considered CoastDat data are at the grid locations closer to the respective measurements locations and these are nearer the measuring locations than the considered ERA-interim location (cf. Figure 2.1), the correlations between the CoastDat and the measurements are lower than those between the ERA-interim data and the measurements. We, therefore, consider that the ERA-interim data are more suitable to form the basis of this study than the CoastDat data. Still, we acknowledge that the expected spatial variations in the wave conditions in the considered region are well described in the CoastDat data. To illustrate this Figure 2.6 shows the comparisons between the measured significant wave height at Euro Platform and SWB and the comparisons between the CoastDat significant wave height data at the Euro Platform and SWB locations. The CoastDat data shows that the significant wave height at the Euro Platform location is on average 16% larger than that at SWB (Figure 2.6, right panel). This is close to what the measurements show: the significant wave height at the Euro Platform location is on average 14% larger than that at SWB (Figure 2.6, left panel).

The CoastDat data have therefore been used to check whether the obtained differences between the ERA-interim data and the SWB measurements can be explained by the spatial variability of the significant wave height. Figure 2.7 shows that the significant wave height in the CoastDat data at 3°E and 51.7°N, which is very close to the ERA-Interim location and within the Borssele Wind Farm Zone, and SWB is 1.070 which is close to the 1.057 ratio between the ERA-interim and the SWB significant wave height data (see Figure 2.2). We, therefore, conclude that the ERA-interim wave data provide a good basis for the determination of the wave conditions at the Borssele Wind Farm Zone.

---

[1] *There are several parameters for describing the sea state period. One of these is $T_{m-1,0} = (m_1 / m_0)^{-1}$ where m_n, the n order spectral moment, is , $m_n = \int_0^\infty f^n S(f) df$, f is the frequency and $S(f)$ the spectral wave energy. Using different moments other period parameters can be defined. Such as $T_{m0,1} = m_0 / m_1$ and $T_{m0,2} = \sqrt{m_0 / m_2}$. Another commonly used wave period is the peak wave period, T_p , the period corresponding to the spectral maximum.*

2.2.3 Calibration

Based on the present wave comparisons, the ERA-interim data at location 3°E and 51.75°N are considered further to generate boundary conditions for the wave modelling. The wave comparisons indicate that the ERA-interim gives an accurate prediction of the wave parameters in this area. The ERA-interim output location however is not representative for the whole Borssele Wind Farm Zone, see Figure 2.8. The figure shows spatial gradients based on the CoastDat data, indicating that the significant wave height in the south-eastern corner of the project site is on average about 15% lower than at the ERA-interim output location, whereas in the north-western part, the significant wave height is about 2% higher than at the ERA-interim output location. This variability in significant wave height has been taken into account for the generation of boundary conditions for the wave model, see Section 4.1.

The only wave period parameter available in the considered ERA-interim dataset is $T_{m-1,0}$. In order to convert $T_{m-1,0}$ to $T_{m0,1}$ or T_p we propose that the relation between these parameters in the SWB measurements be used. These, as shown in Figure 2.9, are:

$$T_{m0.1} = 0.899 T_{m-1,0},$$

$$(2.1)$$

and

$$T_p = 1.134 T_{m-1,0}.$$

$$(2.2)$$
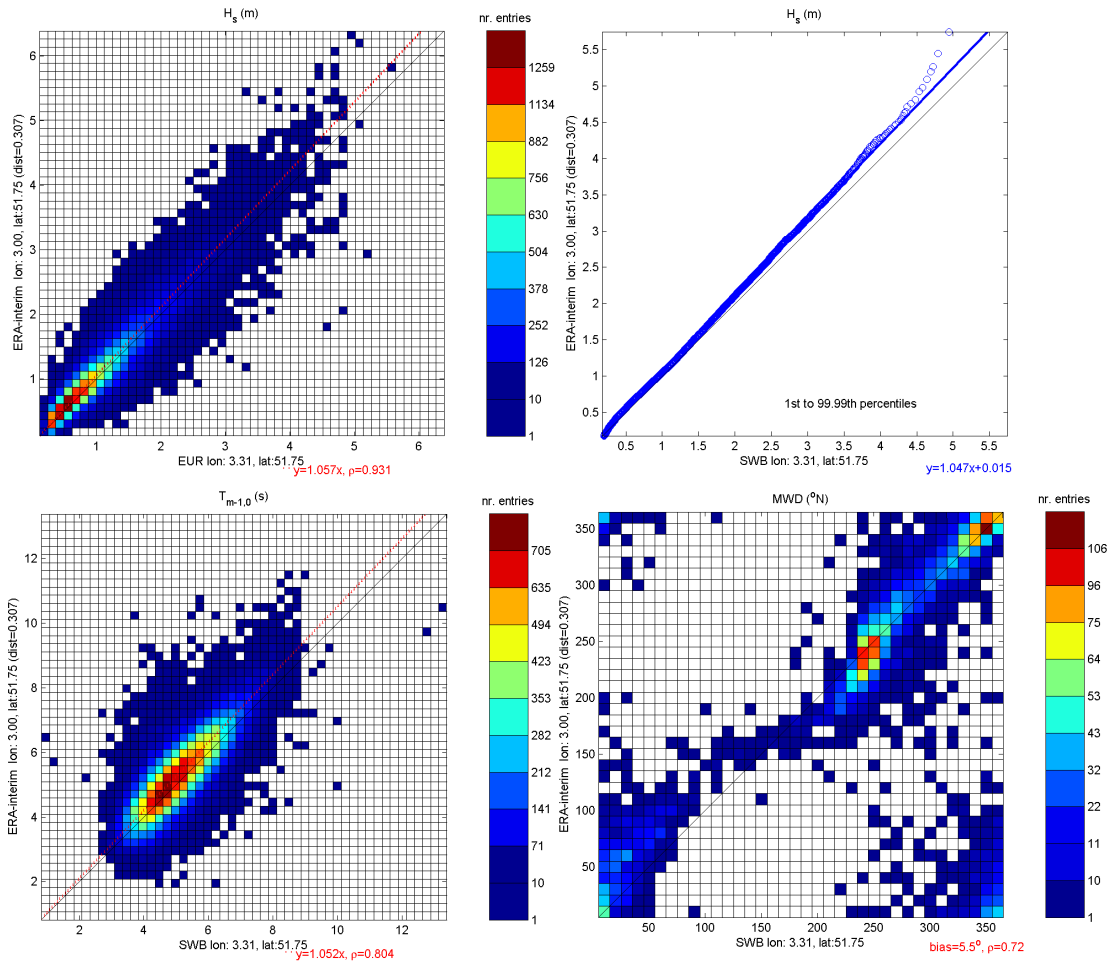
Figure 2.2   Comparison between ERA-interim and SWB wave measurements.
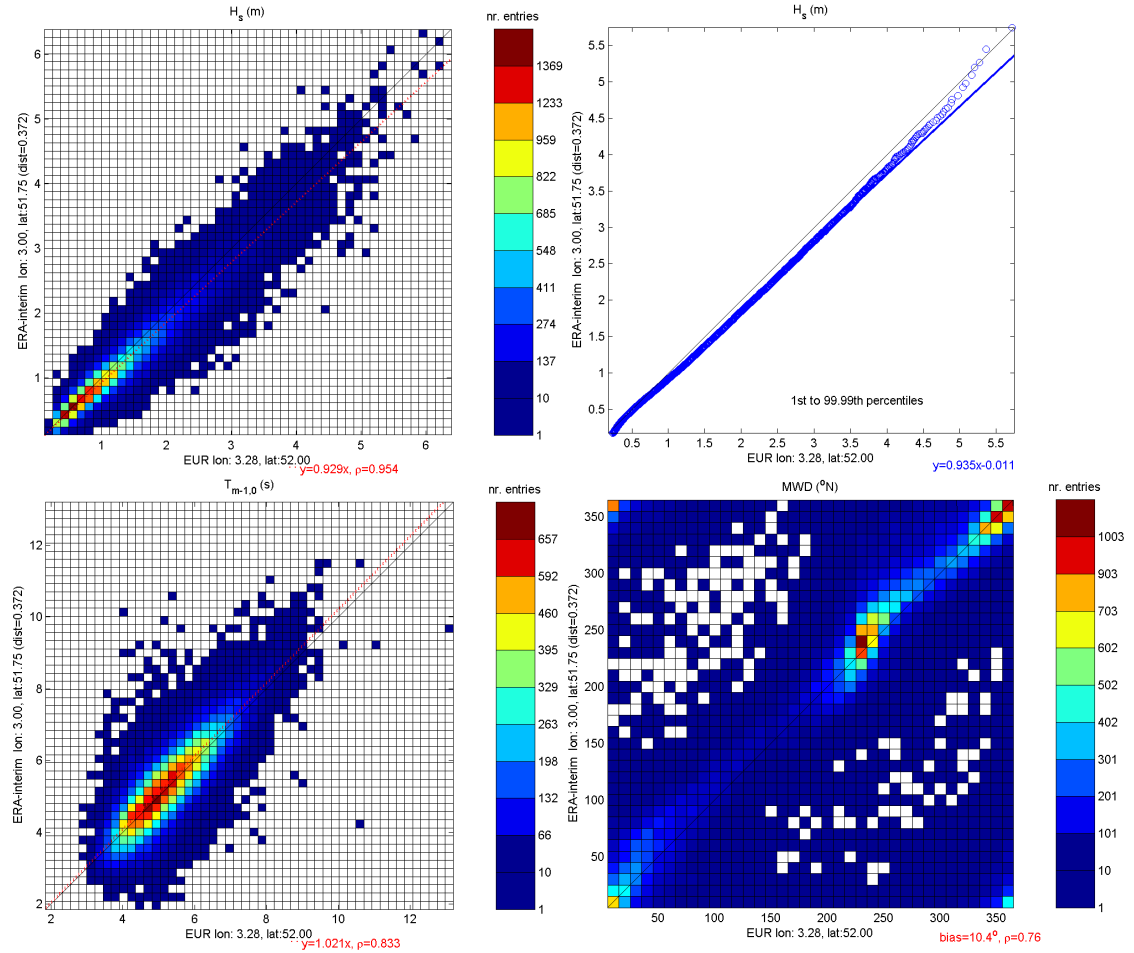
Figure 2.3   Comparison between ERA-interim and Euro Platform wave measurements.
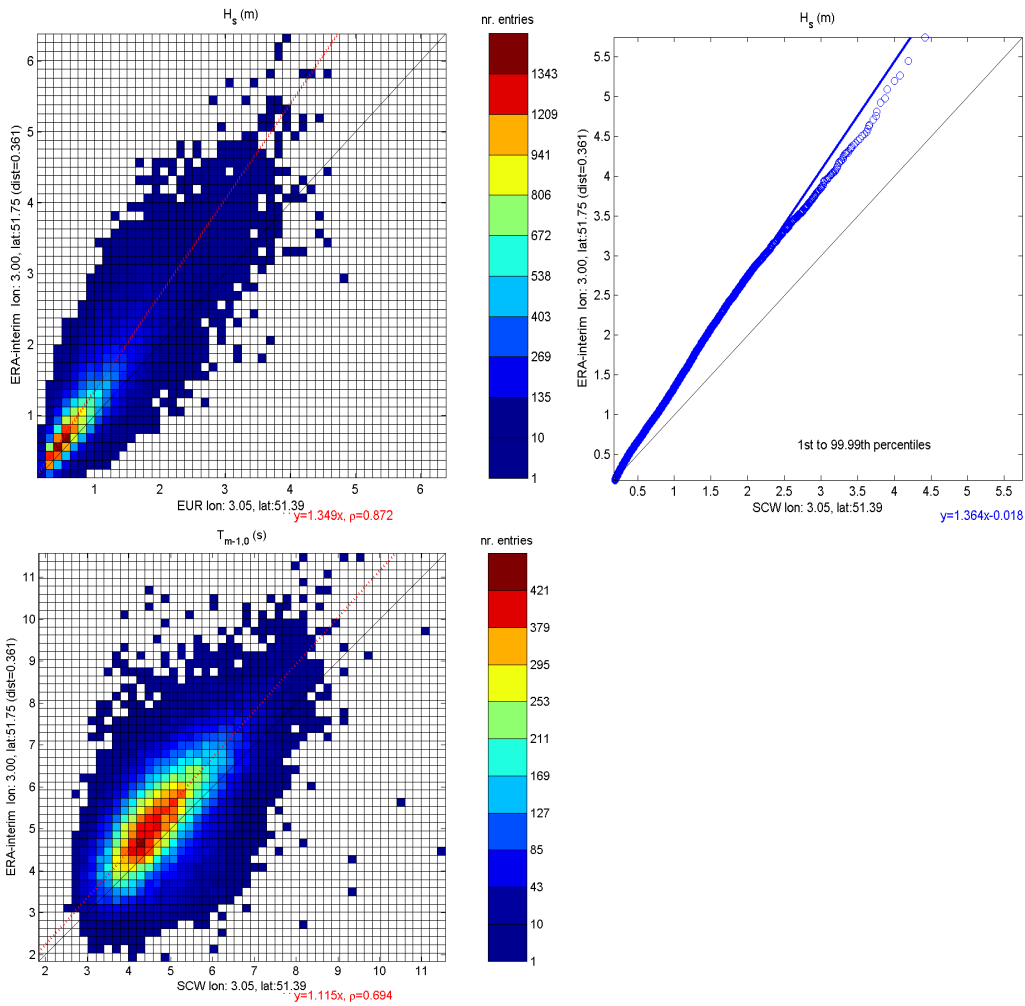
Figure 2.4   Comparison between ERA-interim and SCW wave measurements.

Deltares
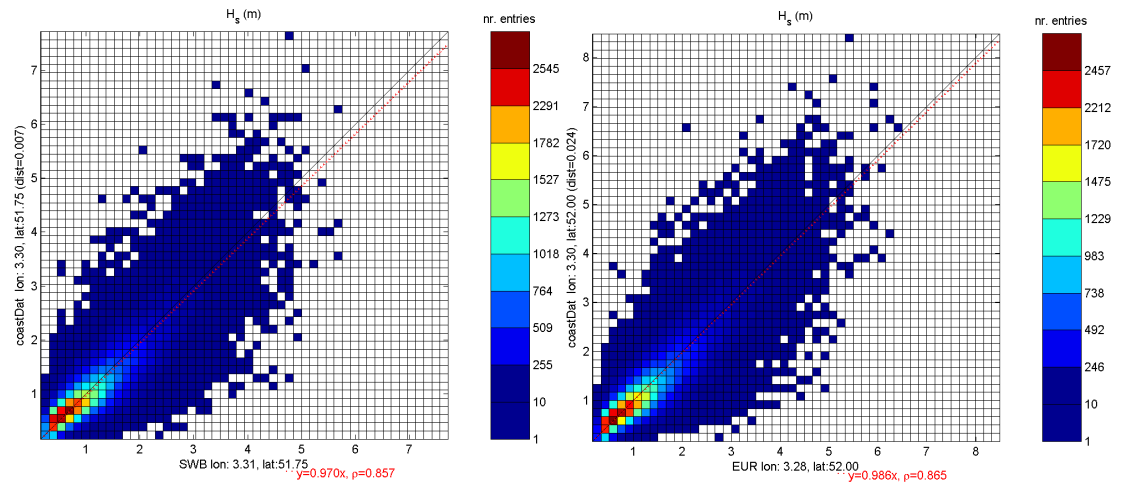
Figure 2.5   Comparison between CoastDat and SWB (left) and Euro Platform (right) wave measurements.
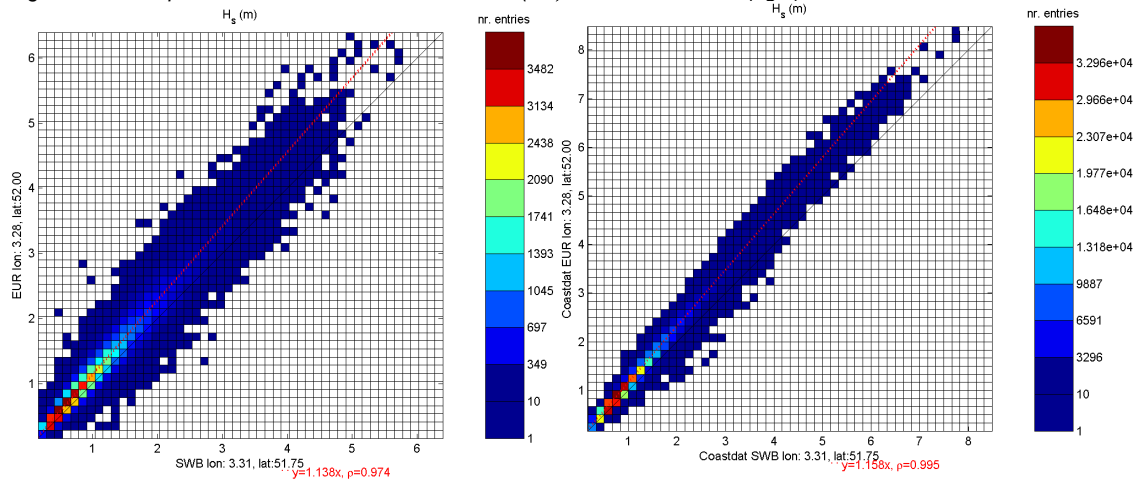
Figure 2.6   Comparison between measured wave heights at SWB and Euro Platform (left) and between CoastDat data at SWB and at Euro Platform (right).
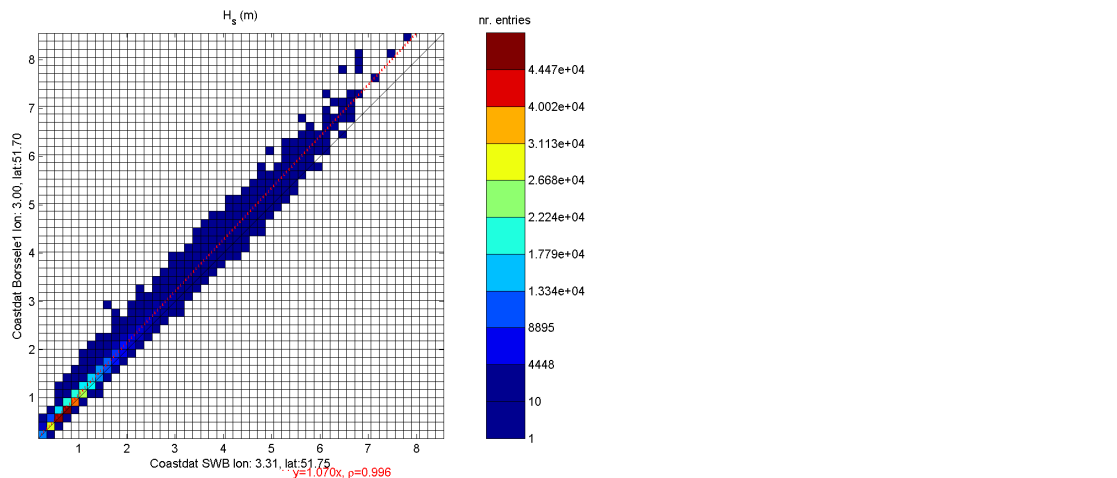
Figure 2.7   Comparison between CoastDat data at SWB and the ERA-interim location within the Borssele Wind Farm Zone.
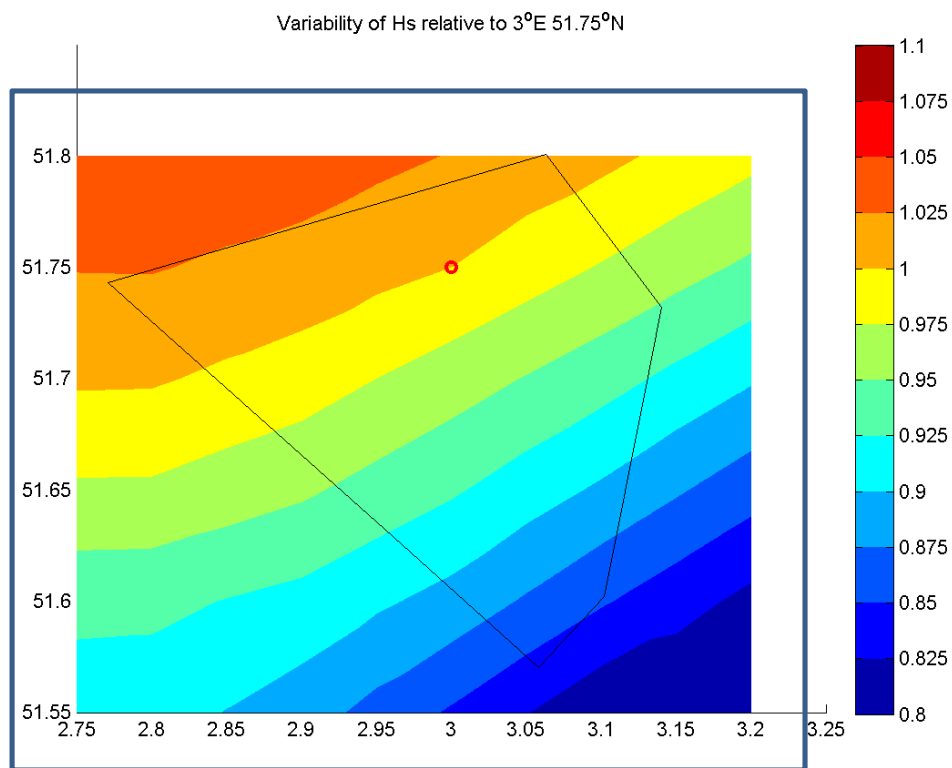
Figure 2.8   Spatial significant wave height gradients according to CoastDat data. Gradients are given relatively to location 3°E 51.75°N.
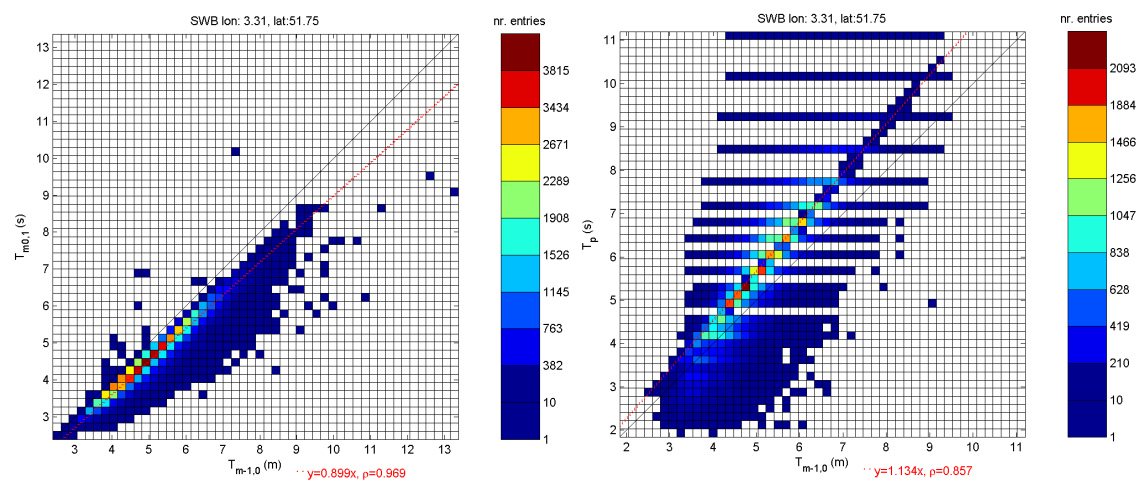
Figure 2.9   Relation between $T_{m-1,0}$ and $T_{m0,1}$ (left) and T_p (right) measurements at SWB.

2.3 Wind

The different wind model datasets are validated against wind measurements at Euro Platform, see Figure 2.10 to Figure 2.14. The results of the comparisons are summarised in Table 2.3. The CoastDat data shows the lowest correlation for both the wind speed and direction and will not be considered further. The HARMONIE, ERA-Interim and CFSR datasets have a similar correlation for the wind speed and direction. Compared to the other datasets, the HARMONIE data has an optimal regression coefficient for the wind speed (1.000) and has the lowest bias in wind direction (+26.3°). In addition, the HARMONIE data has the highest resolution and will therefore be considered further in this study without further calibration.

Figure 2.14 shows a comparison of the HARMONIE data at Euro Platform to HARMONIE data at Borssele (3.02°E 51.70°N). As expected, the wind speed and direction is very similar for both locations.

Dataset	Wind speed		Wind direction	
	$U_{10,dataset}$ / $U_{10,measured}$ [-]	Correlation [-]	Bias [°]	Correlation [-]
HARMONIE	1.000	0.923	+26.3	0.70
ERA-Interim	0.880	0.923	+37.0	0.68
CFSR	1.046	0.938	+29.2	0.70
CoastDat	0.963	0.814	+38.3	0.53

Table 2.3   Summary of wind data comparisons.
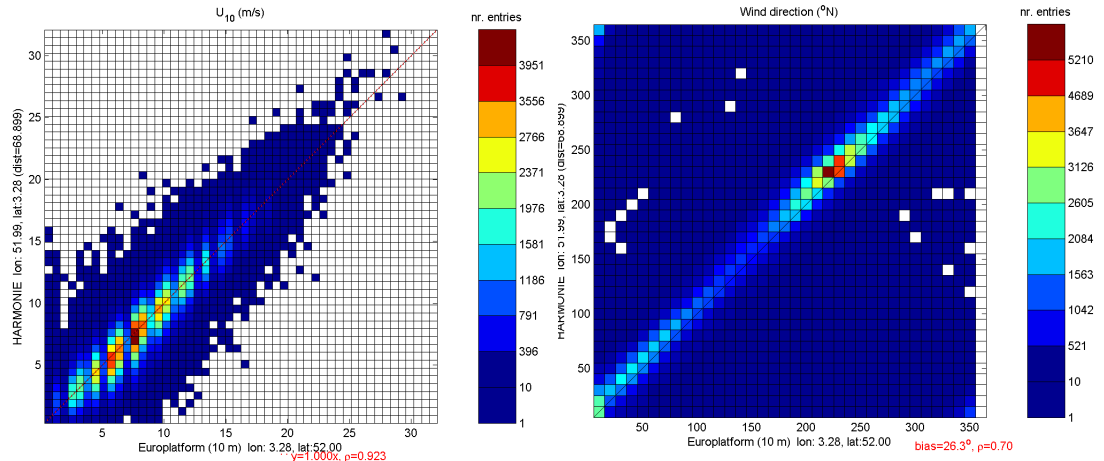
Figure 2.10 Comparison between HARMONIE and Euro Platform wind measurements.
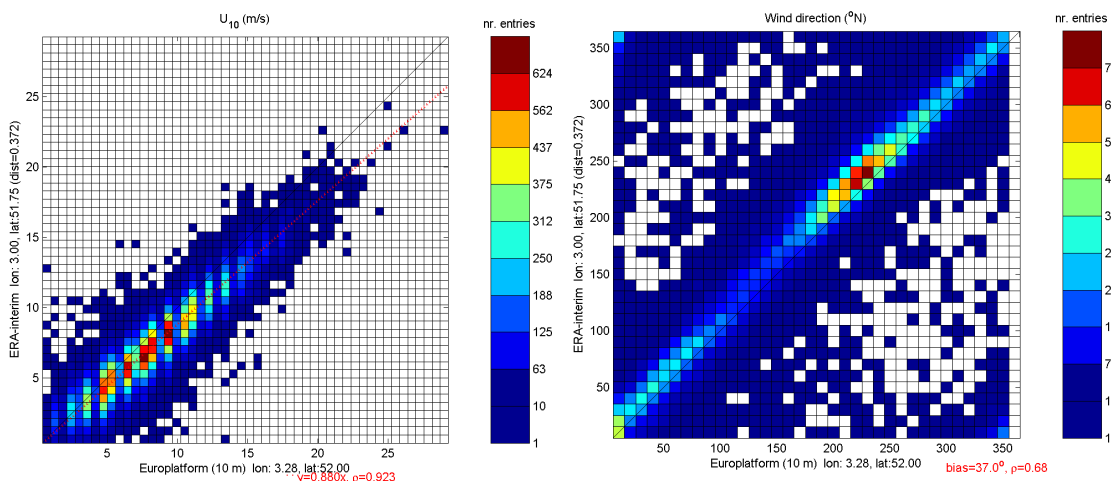
Figure 2.11 Comparison between ERA-Interim and Euro Platform wind measurements.
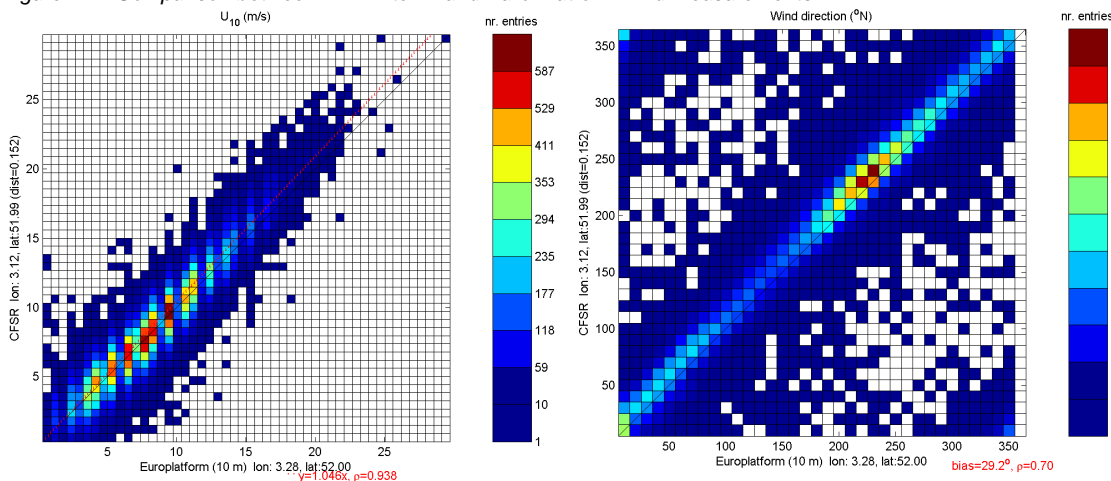
Figure 2.12 Comparison between CFSR and Euro Platform wind measurements.
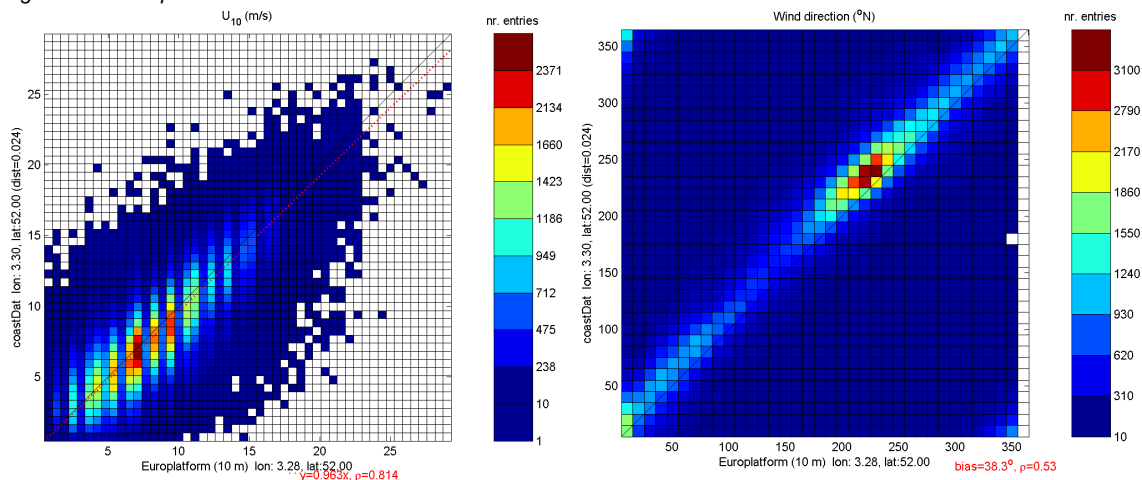
Figure 2.13 Comparison between CoastDat at Euro Platform and 3°E 51.75°N (within the Borssele Wind Farm Zone).
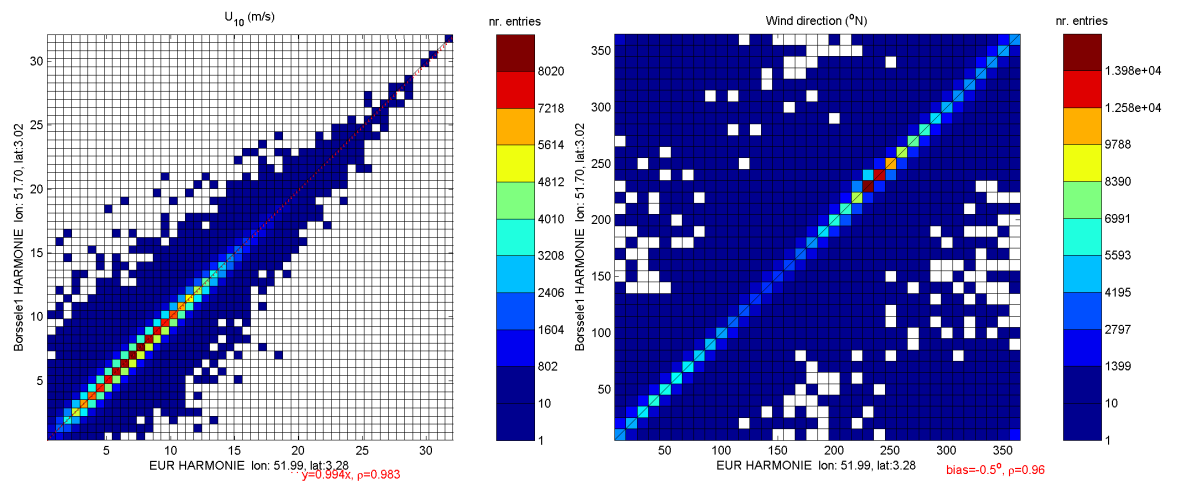
Figure 2.14 Comparison between HARMONIE data at Euro Platform and Borssele (3.02°E 51.70°N).

3 Wind Conditions

3.1 Introduction

This chapter presents the wind conditions in the BWFZ. These conditions are based on the HARMONIE data at 3.02°E 51.70°N (see also section 2.3). The considered data are 1-hour average hourly 10-metre height wind velocities ($U_{10,1h}$)[2] from 1979 until 2013 and 1-hour average hourly 70-, 80-, 90-, 100- and 150-metre height wind velocities from 1989 until 2013.

The determined wind conditions include:
a. Extreme wind speed profile
b. Extreme wind speeds:
- The directional dependent all year extreme wind speed:
  – for return periods of 1, 2, 5, 10, 50 and 100 years;
  – averaged over 1h, 10min, 1min and 3sec;
  – at heights of 10m, 70m, 80m, 90m, 100m and 150m
c. Wind spectral density:
- Wind spectra at 10m, 70m, 80m, 90m, 100m and 150m.
d. Wind operational criteria:
- Monthly and annual wind roses at heights of 10m, 70m, 80m, 90m, 100m and 150m
- Monthly and annual joint occurrence tables of wind speed vs. wind direction at heights of 10m, 70m, 80m, 90m, 100m and 150m
- Directional dependent Weibull parameters for normal wind speed distribution
- Persistence of wind speed with the following parameters:
  – Wind speed thresholds 2m/s, 4 m/s, 6 m/s, 8 m/s, 9 m/s, 10 m/s, 11 m/s, 12 m/s and 15m/s
  – Time windows of 1h, 6h, 12h, 24h, 48h and 72h
  – Probabilities of exceedance of 20%, 50% and 80%
e. Turbulence intensity

In Section 3.2 the determination of the vertical wind profile using the HARMONIE data is described. The extreme winds conditions are presented in Section 3.3. The wind spectral density is discussed in Section 3.4. Wind operational criteria are given in Section 3.5. Finally, the turbulence intensity is discussed in Section 3.6.

In order to minimize the effects of the statistical uncertainty as much as possible, the analysis of extreme conditions will be applied solely to the HARMONIE data at 10 metres height (U_{10}). The values obtained for this height are subsequently translated to the other required heights (70m, 80m, 90m, 100m and 150m) by means of determined extreme wind speed vertical profile. Given that the length of the available time series at heights other than 10 metres (25 years) is shorter than the length of the time series at 10m (35 years) this approach leads to more reliable estimates and given that a fixed profile is used to translate the 10m results to other heights there is consistency between the estimates at different levels.

---

[2] *We use $U_{10,1h}$ or U_{10} to represent the 1-hour average 10-metre height wind speed. In general U_h represents the 1-hour average wind speed at height h and $U_{h,t}$ represents the wind speed at height h for an averaging time of t.*

3.2 Wind profile

A characteristic wind profile for the BWFZ has been determined based on HARMONIE data (see also section 2.3). The data used to determine the wind profile is a continuous hourly time series from 01-01-1987 till 31-12-2013, with data at heights of 10m, 70m, 80m, 90m, 100m and 150m. For this analysis we consider three generally accepted wind profile formulas: the log-profile, the power law profile and the profile advised in the API guideline (API, 2000) and DNV (2014), referred to as the DNV profile.

The log-profile is described by:

$$U(z) = \frac{u_*}{\kappa} \ln\left(\frac{z}{z_0}\right), \text{ with } z_0 = Ch\frac{u_*^2}{g} \tag{3.1}$$

where z is the height, U(z) is the wind speed at height z, u_* is the friction velocity, z_0 is the surface roughness, $Ch = 0.018$ is the Charnock constant, $\kappa = 0.4$ the von Karman constant and $g = 9.81$ m/s^2 the acceleration of gravity.

The power law profile is described by:

$$U(z) = U_{10}\left(\frac{z}{10}\right)^{\alpha} \tag{3.2}$$

where U_{10} is the wind speed at 10m above the surface and α is the power-law constant.

The DNV profile is described by:

$$U(z) = U_{10}\left[1 + C\ln\left(\frac{z}{10}\right)\right], \text{ with } C = 5.73\cdot 10^{-2}\sqrt{1 + 0.15U_{10}}. \tag{3.3}$$

In our analysis we have for each hour at which the HARMONIE data were available at 10m, 70m, 80m, 90m, 100m and 150m computed the corresponding log-profile, power law and DNV profiles. In the case of the log and DNV profiles this was done by using the HARMONIE U_{10} to compute u_* and z_0 the wind velocity at 70m, 80m, 90m, 100m and 150m, In the case of the power law profile α was estimated by fitting, using least square to the HARMONIE data.

The resulting hourly profile estimates and original data were normalized using the hourly HARMONIE U_{10}. The data were further analysed considering a few U_{10} thresholds. We start with presenting our results for a threshold of 10m/s. The omnidirectional, normalised wind speed profiles for which $U_{10} > 10$ m/s are plotted in Figure 3.1; the figure shows
- in grey the HARMONIE hourly profiles, with their mean, 5th and 95th percentiles being given in black;
- in red the mean, 5th and 95th percentiles of the fitted power law profiles, the α values corresponding to these lines being given in the caption; and
- in green the mean, 5th and 95th percentiles of the computed log-profiles with the z_0 values corresponding to these lines being given in the caption and
- in blue the mean, 5th and 95th percentiles of the computed DNV profiles.

Deltares

Figure 3.1 clearly shows that the power-law profile fits best with the profiles observed in the data; both for the mean profile as for the 95%-profiles. The same plots for thresholds of 0m/s, 5m/s, 15m/s, 20m/s and 25m/s can be seen in Figure 3.2, Figure 3.3, Figure 3.4, Figure 3.5 and Figure 3.6, respectively.

The figures show that in all cases power-law profile fits best with the profiles observed in the data. Furthermore, a higher threshold results in less data and smaller band widths (less spreading) of the obtained profiles. Please also note the small mismatch between the 95th percentile lines of the HARMONIE data and of power law profile fits. For higher thresholds the mean alpha-value of the power profile fits increases, while the alpha-values of the 5th and 95th percentiles draw closer to the mean and the 95th percentile power law profile fits then the data better. The figures also show a clear offset between log-profiles and the data, except for when no threshold is applied, see Figure 3.2. The DNV profiles are close to the log-profiles with Ch=0.018. From this analysis we conclude that only when considering all the data do the log and DNV profiles seem adequate. In all other situations, and especially for extremer conditions, power law profile fits the data means and percentiles better.
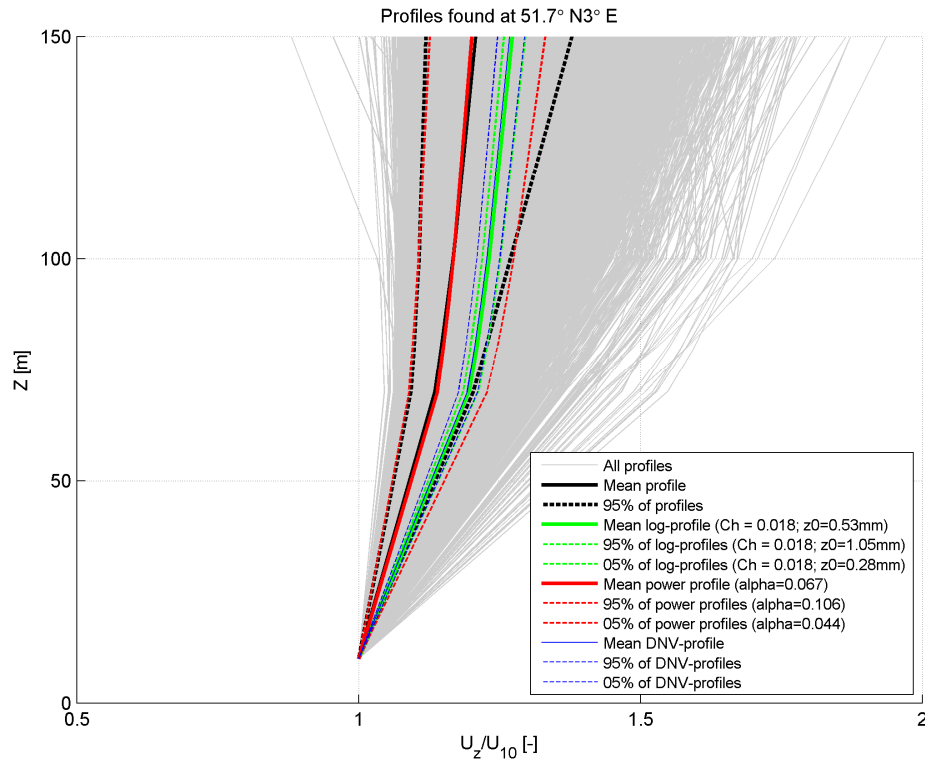
Figure 3.1   Normalised wind profiles obtained in the HARMONIE dataset, for a threshold value of U_{10} = 10m/s.
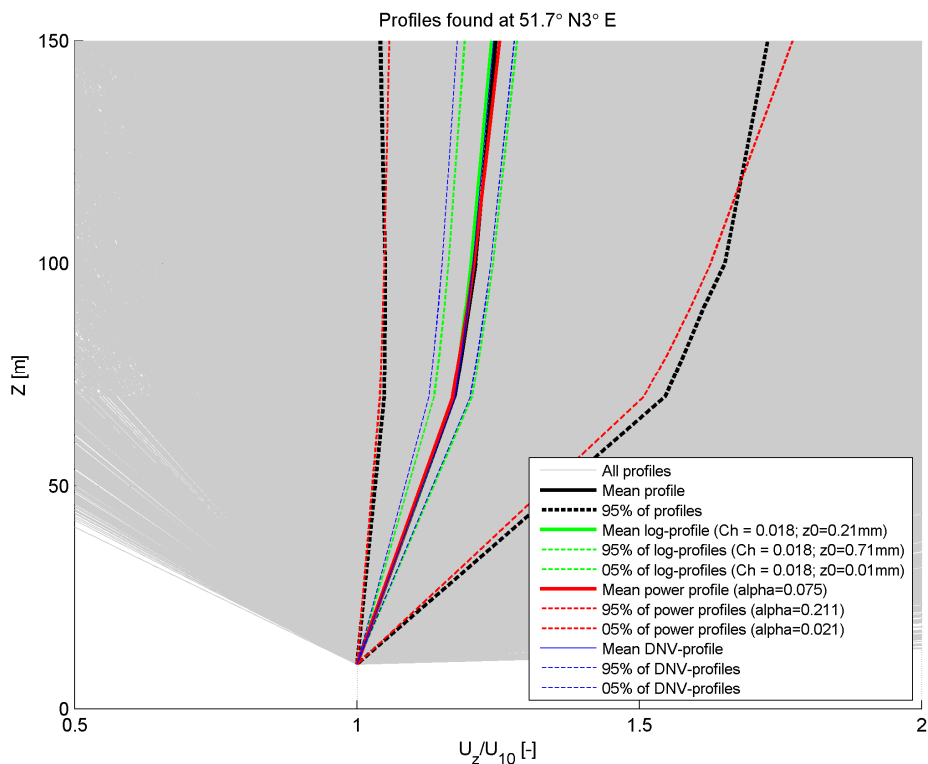
Figure 3.2   *Normalised wind profiles obtained in the HARMONIE dataset, for a threshold value of $U_{10} = 0m/s$.*
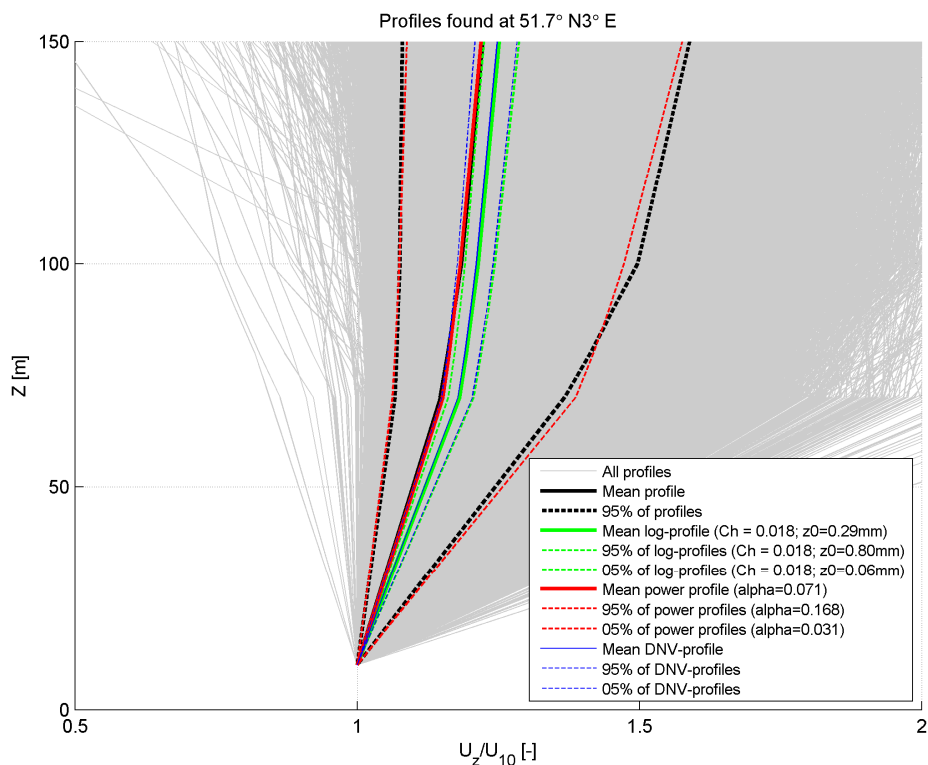
Figure 3.3   *Normalised wind profiles obtained in the HARMONIE dataset, for a threshold value of $U_{10} = 5m/s$.*
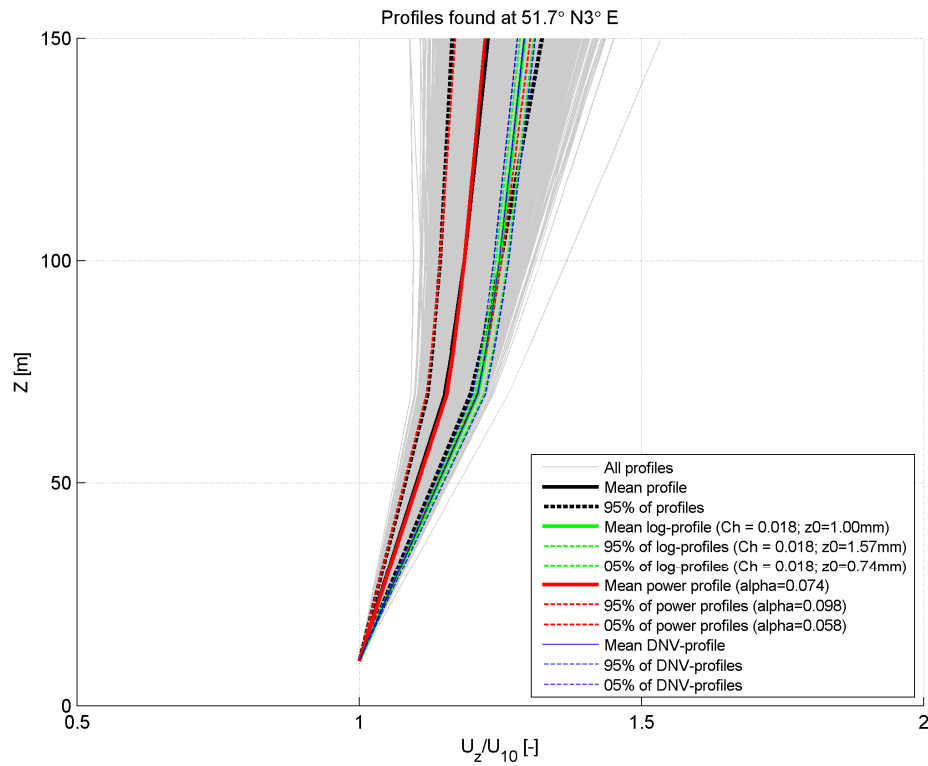
Figure 3.4 Normalised wind profiles obtained in the HARMONIE dataset, for a threshold value of $U_{10} = 15m/s$.
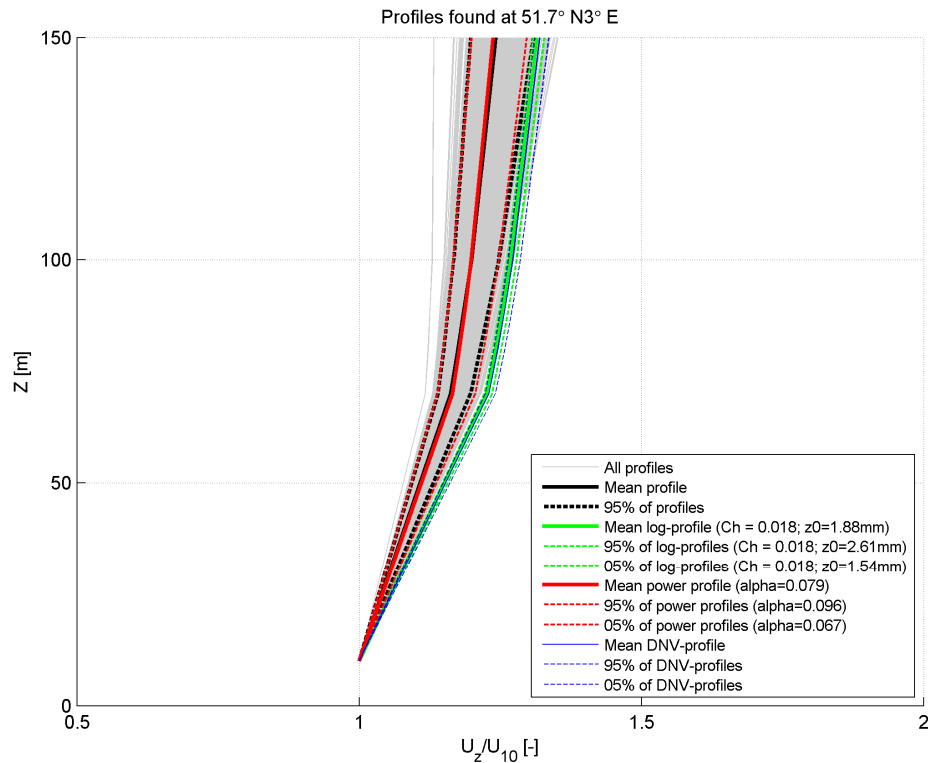
Figure 3.5 Normalised wind profiles obtained in the HARMONIE dataset, for a threshold value of $U_{10} = 20m/s$.
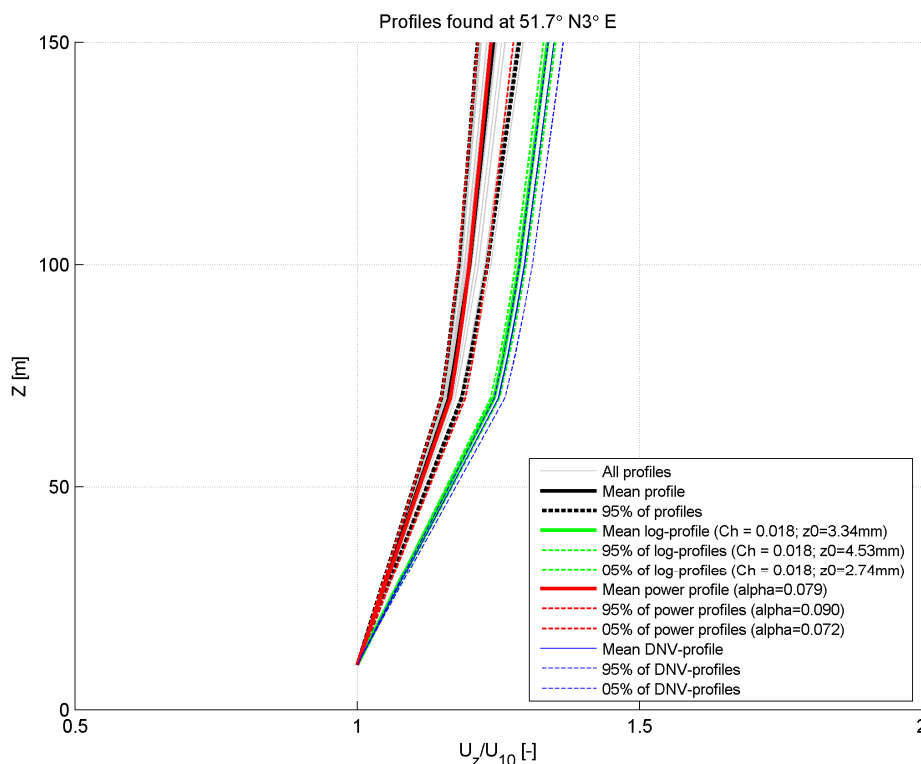
Figure 3.6 Normalised wind profiles obtained in the HARMONIE dataset, for a threshold value of $U_{10} = 25m/s$.

The mean, 5th and 95th percentiles of the estimated α values considering different thresholds are given in Table 3.1.

Threshold	$\alpha_{5\%}$	α_{mean}	$\alpha_{95\%}$
0 m/s	0.021	0.075	0.211
5 m/s	0.031	0.071	0.168
10 m/s	0.044	0.067	0.106
15 m/s	0.058	0.074	0.098
20 m/s	0.067	0.079	0.096
25 m/s	0.072	0.079	0.090

Table 3.1   alpha-values obtained for different wind speed thresholds.

As the table shows, for the higher thresholds a mean alpha value of approximately 0.8 is found. In Figure 4.7 this profile is plotted along log profiles considering different Charnock-constants and to a power law profile with an α value of 0.11. A power-law constant of 0.11 is used by Dong Energy for the Irish Sea (see Graaff et al., 2011).

From the comparison it becomes clear that a Charnock-constant (Ch) of 0.0003 is needed to fit a log-profile fit to the power-law 0.07 profile (which correlated well to the observed mean profile in the HARMONIE data at the BWFZ). Such a low Charnock constant corresponds to virtually no surface roughness, which is unrealistic. Therefore the log-profile is not considered a realistic description of the extreme wind speed profile observed in the data and will not be considered for the description of the extreme profile.
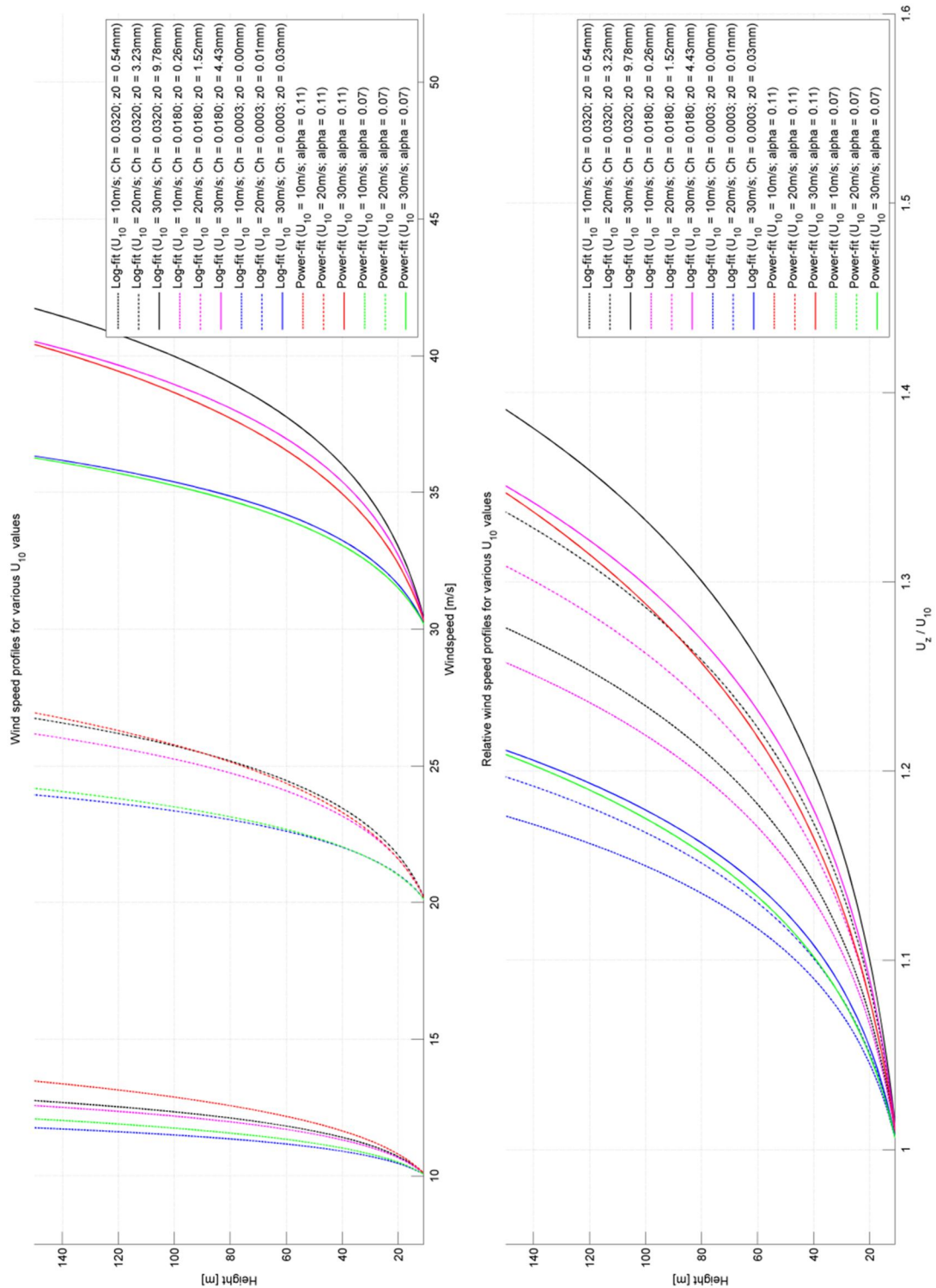
Figure 3.7   Comparison between various profile fit-functions, and different fitting constants.

We note that alpha values observed in this analysis are in correspondence with the alpha values estimated elsewhere in the North Sea. Figure 3.8 shows the alpha values based on the HARMONIE data for 1990. Similar alpha values are found in the ERA-interim data, see Figure 3.9. The fact that the observed alpha values are relatively low is due to the fact that the wind profiles above the North Sea often deviate from a neutral wind profile.
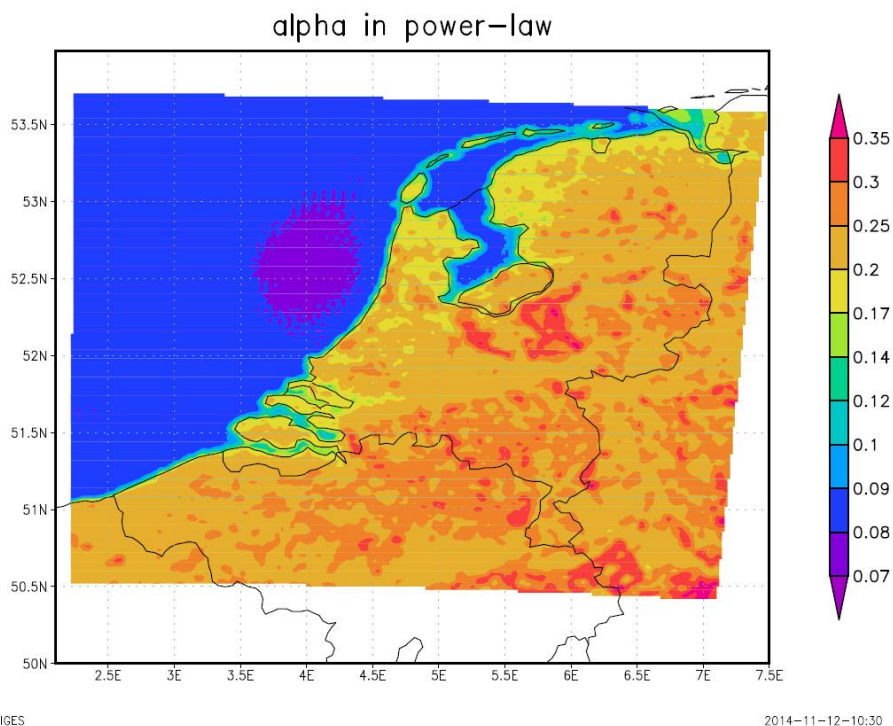
*Figure 3.8   Spatial variation in alpha-values near the Dutch coast, based on the HARMONIE-data from 1990
(source: Dr. Henk van den Brink, KNMI).*
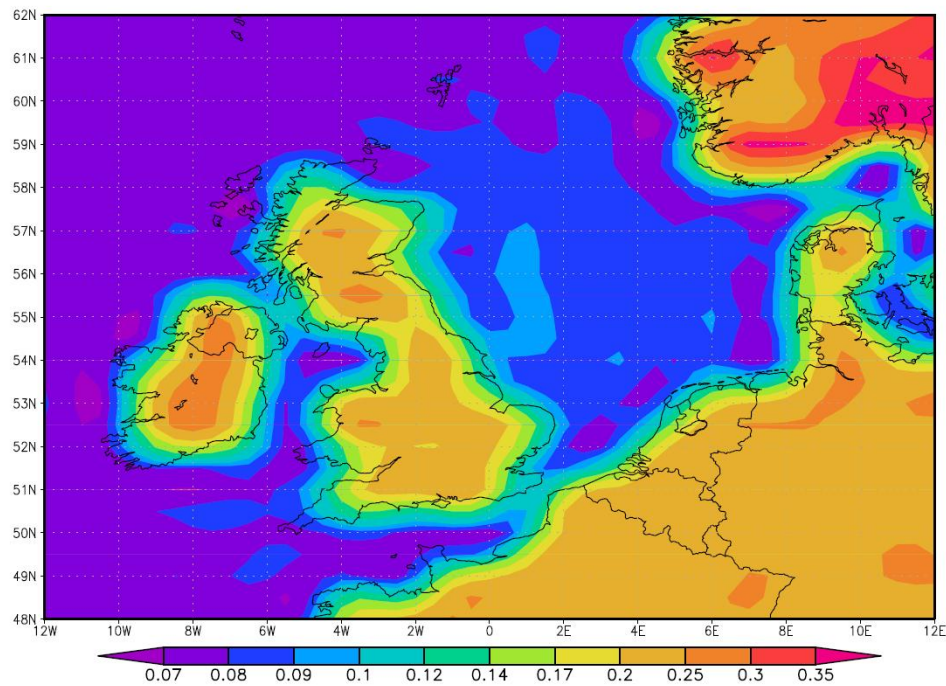
Figure 3.9   Spatial variation in alpha-values over the North Sea; based on the EAR-I data from 1990 (source: Dr. Henk van den Brink, KNMI).

In conclusion it can be stated that, as observed in the HARMONIE data, a log profile, with a Charnock-constant of 0.018 and the DNV profile, are only valid on average. In general, and in particular for wind speeds above 10 m/s, a power-law profile fits the data better. For extreme conditions we recommend that a power-law profile be used, with an alpha value of 0.08 and an uncertainty bandwidth of α±0.03. The recommended (normalised) extreme wind speed profiles are given in Figure 3.10. Note that the profile of the upper bandwidth (α-0.11) is close to the DNV profile and used therefore as upper band.
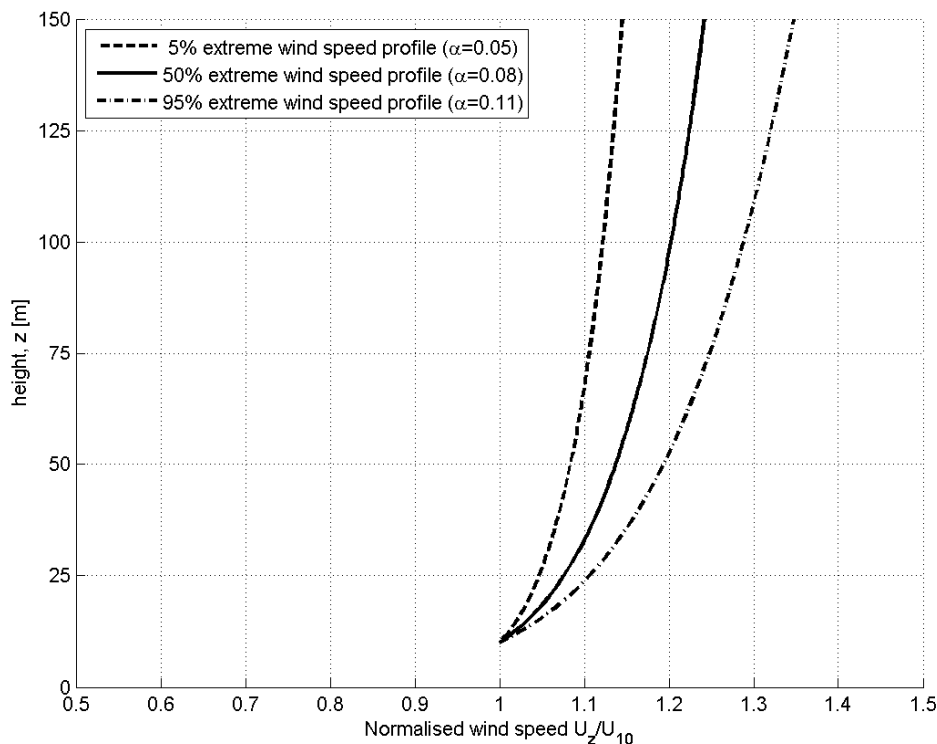
Figure 3.10   Proposed normal and extreme wind speed profiles, based on the wind speed profiles observed in the HARMONIE-database at location 51.7°N, 3.02°E.

We note further that the recommended values for alpha are also applicable to a relation in the form

$$U(z) = U_{100} \left(\frac{z}{100} \right)^{\alpha}.$$

(3.4)

Furthermore, that the given uncertainty bands for alpha should be taken into account when considering the mean and extreme wind speed estimates given in this report.

3.3   Extreme wind speeds

An extreme value analysis (EVA) of the 35-year long time series of the 10-m wind speed was carried out using the POT method. The EVA of the data included omni-directional analyses and directional analyses over 30° sectors. The sectors considered are: 345ºN-15ºN, 15ºN-45ºN, ..., 285ºN-315ºN and 315ºN-345ºN. In the omni-directional analysis all data are considered. In the directional analysis only the data falling in the sector of interest are taken into account. The data are stratified into sectors before the EVA is carried out, meaning that a given storm may be considered in more than one sector. The stratification into sectors before the analysis is necessary because we are interested in the return value for the above enumerated fixed sectors. If only storm peaks were to be stratified, the return values obtained for a given sector could have been underestimates.

The output of the EVA include 1, 2, 5, 10, 50 and 100 years return values of hourly averaged 10-m wind speed. These have been translated to other mean wind speed durations (10 minutes, 1 minute and 3 seconds) using the API guideline (API, 2000) and DNV (2014),:

$$U(t) = U_{10,1h} \cdot \left[1 - 0.41 \cdot I_u \cdot \ln\left(\frac{t}{t_{1h}}\right) \right]; \tag{3.5}$$

$$I_u = 0.06 \cdot (1 + 0.043 \cdot U_{10,1h}), \tag{3.6}$$

where U(t) is the wind speed for a certain duration, t (in seconds), $U_{10,1h}$ is the input 1-hour averaged wind speed at a height of 10-m; the value of t_{1h} is fixed at 3600s.

Furthermore, these data have been translated to heights of 10m, 70m, 80m, 90m, 100m and 150m using the extreme wind profile determined in the previous section. The U10 wind speeds are translated to other heights by means of a power-law fit profile (equation 3.2), with α=0.08 for the mean wind speed and α=0.05 and α=0.11 respectively for the 95%-confidence interval (as explained in Section 3.2).

The hourly extreme wind speeds for the BWFZ at heights 10m, 70m and 80m are given in Table 3.2 to Table 3.3. The hourly extreme wind speeds at heights 90m, 100m and 150m can be found in Table 3.4 to Table 3.5. The tables for these heights and other durations can be found in the excel-file provided with this report (see Section 1.5). The tables show that the most extreme winds at BWFZ come from the Southwest-Northwest sectors and the less extreme from the Northeast-Southeast sectors. The sector with the most extreme wind conditions is the Southwest sector (SW, 225°N - 255°N) for which the 50-yr return value of the hourly averaged wind speed at 10m height is 29.9m/s.

Sector	Return period	Dir. (°N)	U10 (m/s)	U70 (m/s)	U80 (m/s)
N (345°N -15°N)	1-yrs	356.20	16.33 (15.98 - 16.72)	19.08 (17.61 - 20.71)	19.29 (17.73 - 21.02)
	2-yrs	356.20	17.35 (16.85 - 17.84)	20.27 (18.57 - 22.10)	20.49 (18.70 - 22.43)
	5-yrs	356.20	18.53 (17.90 - 19.11)	21.65 (19.73 - 23.67)	21.88 (19.86 - 24.02)
	10-yrs	356.20	19.30 (18.46 - 20.06)	22.55 (20.35 - 24.85)	22.79 (20.48 - 25.22)
	50-yrs	356.20	20.77 (19.27 - 22.71)	24.27 (21.24 - 28.13)	24.53 (21.38 - 28.55)
	100-yrs	356.20	21.29 (19.47 - 23.94)	24.88 (21.46 - 29.65)	25.14 (21.60 - 30.09)
NE (15°N - 45°N)	1-yrs	29.70	15.11 (14.72 - 15.50)	17.66 (16.22 - 19.20)	17.84 (16.33 - 19.48)
	2-yrs	29.70	16.18 (15.64 - 16.72)	18.91 (17.24 - 20.71)	19.11 (17.35 - 21.02)
	5-yrs	29.70	17.55 (16.77 - 18.37)	20.51 (18.48 - 22.75)	20.73 (18.61 - 23.09)
	10-yrs	29.70	18.54 (17.45 - 19.78)	21.66 (19.23 - 24.50)	21.90 (19.36 - 24.86)
	50-yrs	29.70	20.76 (18.57 - 23.81)	24.26 (20.47 - 29.49)	24.52 (20.60 - 29.93)
	100-yrs	29.70	21.66 (18.92 - 25.89)	25.31 (20.85 - 32.07)	25.58 (20.99 - 32.54)
ENE (45°N - 75°N)	1-yrs	57.30	14.42 (14.25 - 14.65)	16.85 (15.71 - 18.15)	17.03 (15.81 - 18.42)
	2-yrs	57.30	15.24 (14.87 - 15.66)	17.81 (16.39 - 19.40)	18.00 (16.50 - 19.68)
	5-yrs	57.30	16.29 (15.70 - 16.84)	19.03 (17.30 - 20.86)	19.24 (17.42 - 21.17)
	10-yrs	57.30	17.06 (16.28 - 17.70)	19.93 (17.94 - 21.92)	20.15 (18.06 - 22.25)
	50-yrs	57.30	18.78 (17.23 - 20.41)	21.94 (18.99 - 25.28)	22.18 (19.12 - 25.66)
	100-yrs	57.30	19.49 (17.50 - 22.04)	22.77 (19.29 - 27.30)	23.02 (19.42 - 27.70)
E (75°N - 105°N)	1-yrs	87.60	13.92 (13.92 - 13.93)	16.26 (15.34 - 17.25)	16.44 (15.45 - 17.51)
	2-yrs	87.60	14.61 (14.32 - 14.93)	17.07 (15.78 - 18.49)	17.25 (15.89 - 18.77)
	5-yrs	87.60	15.50 (14.94 - 16.07)	18.11 (16.47 - 19.91)	18.31 (16.58 - 20.20)
	10-yrs	87.60	16.16 (15.42 - 16.86)	18.88 (17.00 - 20.88)	19.08 (17.11 - 21.19)
	50-yrs	87.60	17.63 (15.98 - 19.32)	20.60 (17.61 - 23.93)	20.82 (17.73 - 24.29)
	100-yrs	87.60	18.24 (16.09 - 20.78)	21.31 (17.73 - 25.74)	21.54 (17.85 - 26.12)
ESE (105°N - 135°N)	1-yrs	119.10	13.38 (13.00 - 13.78)	15.63 (14.33 - 17.07)	15.80 (14.42 - 17.32)
	2-yrs	119.10	14.41 (13.89 - 14.92)	16.84 (15.31 - 18.48)	17.02 (15.41 - 18.75)
	5-yrs	119.10	15.65 (14.97 - 16.28)	18.29 (16.50 - 20.17)	18.48 (16.61 - 20.46)
	10-yrs	119.10	16.49 (15.63 - 17.43)	19.27 (17.23 - 21.59)	19.47 (17.34 - 21.91)
	50-yrs	119.10	18.19 (16.63 - 20.49)	21.25 (18.33 - 25.38)	21.48 (18.45 - 25.76)
	100-yrs	119.10	18.83 (16.90 - 22.09)	22.00 (18.63 - 27.36)	22.24 (18.75 - 27.77)
SE (135°N - 165°N)	1-yrs	155.40	15.17 (15.00 - 15.38)	17.73 (16.53 - 19.05)	17.92 (16.64 - 19.33)
	2-yrs	155.40	16.10 (15.69 - 16.59)	18.81 (17.29 - 20.55)	19.01 (17.41 - 20.85)
	5-yrs	155.40	17.32 (16.65 - 18.09)	20.24 (18.35 - 22.41)	20.45 (18.47 - 22.74)
	10-yrs	155.40	18.23 (17.32 - 19.29)	21.30 (19.09 - 23.89)	21.53 (19.22 - 24.25)
	50-yrs	155.40	20.28 (18.19 - 22.57)	23.70 (20.05 - 27.96)	23.95 (20.18 - 28.37)
	100-yrs	155.40	21.15 (18.56 - 24.55)	24.71 (20.46 - 30.41)	24.98 (20.59 - 30.86)
S (165°N - 195°N)	1-yrs	188.00	19.52 (19.13 - 19.91)	22.81 (21.08 - 24.66)	23.05 (21.23 - 25.03)
	2-yrs	188.00	20.60 (20.00 - 21.13)	24.07 (22.04 - 26.17)	24.33 (22.19 - 26.56)
	5-yrs	188.00	22.01 (21.23 - 22.69)	25.72 (23.40 - 28.11)	25.99 (23.56 - 28.52)
	10-yrs	188.00	23.06 (22.05 - 24.02)	26.94 (24.30 - 29.75)	27.23 (24.47 - 30.19)
	50-yrs	188.00	25.45 (23.42 - 28.30)	29.74 (25.81 - 35.05)	30.06 (25.99 - 35.57)
	100-yrs	188.00	26.46 (23.86 - 30.80)	30.92 (26.30 - 38.15)	31.25 (26.47 - 38.72)

Table 3.2   Directional return values of hourly-averaged wind speed at different heights for the BWFZ. The return value point estimates are given in front of the 95% confidence intervals given between parentheses. The associated wind directions given in the second column have been computed from the $U_{10,1h}$ POT data. (Continues in Table 3.3.)

Deltares

Sector	Return period	Dir. (°N)	U10 (m/s)	U70 (m/s)	U80 (m/s)
SSW (195°N - 225°N)	1-yrs	215.80	21.61 (21.14 - 22.07)	25.25 (23.30 - 27.34)	25.52 (23.46 - 27.74)
	2-yrs	215.80	22.93 (22.32 - 23.54)	26.79 (24.60 - 29.16)	27.08 (24.77 - 29.59)
	5-yrs	215.80	24.65 (23.65 - 25.70)	28.80 (26.07 - 31.83)	29.11 (26.24 - 32.31)
	10-yrs	215.80	25.93 (24.44 - 27.59)	30.30 (26.94 - 34.18)	30.62 (27.12 - 34.68)
	50-yrs	215.80	28.81 (25.86 - 32.76)	33.66 (28.50 - 40.58)	34.02 (28.69 - 41.18)
	100-yrs	215.80	30.03 (26.35 - 35.39)	35.09 (29.04 - 43.84)	35.47 (29.24 - 44.49)
SW (225°N - 255°N)	1-yrs	233.30	21.83 (21.33 - 22.36)	25.51 (23.51 - 27.70)	25.78 (23.67 - 28.11)
	2-yrs	233.30	23.25 (22.55 - 23.97)	27.17 (24.85 - 29.69)	27.46 (25.02 - 30.13)
	5-yrs	233.30	25.13 (24.00 - 26.32)	29.36 (26.45 - 32.60)	29.68 (26.63 - 33.08)
	10-yrs	233.30	26.55 (24.96 - 28.43)	31.02 (27.51 - 35.22)	31.36 (27.69 - 35.74)
	50-yrs	233.30	29.87 (26.55 - 34.40)	34.90 (29.26 - 42.61)	35.28 (29.46 - 43.24)
	100-yrs	233.30	31.30 (27.16 - 37.79)	36.57 (29.94 - 46.81)	36.97 (30.14 - 47.50)
W (255°N - 285°N)	1-yrs	266.80	20.13 (19.54 - 20.67)	23.52 (21.54 - 25.60)	23.77 (21.68 - 25.98)
	2-yrs	266.80	21.56 (20.88 - 22.22)	25.19 (23.01 - 27.52)	25.46 (23.17 - 27.93)
	5-yrs	266.80	23.30 (22.38 - 24.28)	27.22 (24.67 - 30.08)	27.52 (24.83 - 30.52)
	10-yrs	266.80	24.53 (23.26 - 25.97)	28.66 (25.64 - 32.17)	28.97 (25.81 - 32.64)
	50-yrs	266.80	27.09 (24.66 - 30.50)	31.65 (27.18 - 37.78)	31.99 (27.36 - 38.34)
	100-yrs	266.80	28.09 (25.04 - 32.66)	32.82 (27.60 - 40.46)	33.17 (27.78 - 41.05)
NNW (285°N - 315°N)	1-yrs	296.30	19.15 (19.05 - 19.28)	22.38 (21.00 - 23.88)	22.62 (21.14 - 24.24)
	2-yrs	296.30	20.05 (19.63 - 20.52)	23.43 (21.64 - 25.42)	23.68 (21.78 - 25.79)
	5-yrs	296.30	21.30 (20.51 - 22.18)	24.89 (22.61 - 27.47)	25.16 (22.76 - 27.88)
	10-yrs	296.30	22.27 (21.15 - 23.64)	26.02 (23.31 - 29.28)	26.30 (23.47 - 29.72)
	50-yrs	296.30	24.68 (21.99 - 28.64)	28.84 (24.24 - 35.48)	29.15 (24.40 - 36.00)
	100-yrs	296.30	25.78 (22.22 - 32.05)	30.12 (24.49 - 39.70)	30.45 (24.65 - 40.29)
NW (315°N - 345°N)	1-yrs	327.80	17.56 (17.11 - 18.01)	20.52 (18.86 - 22.31)	20.74 (18.98 - 22.64)
	2-yrs	327.80	18.71 (18.08 - 19.31)	21.86 (19.93 - 23.92)	22.10 (20.06 - 24.27)
	5-yrs	327.80	20.18 (19.34 - 21.01)	23.58 (21.32 - 26.02)	23.83 (21.46 - 26.41)
	10-yrs	327.80	21.24 (20.08 - 22.55)	24.82 (22.13 - 27.93)	25.08 (22.28 - 28.35)
	50-yrs	327.80	23.57 (21.05 - 27.21)	27.54 (23.20 - 33.70)	27.84 (23.36 - 34.20)
	100-yrs	327.80	24.51 (21.25 - 29.65)	28.64 (23.42 - 36.73)	28.95 (23.58 - 37.27)
OMNI	1-yrs	232.00	22.83 (22.57 - 23.12)	26.68 (24.88 - 28.64)	26.96 (25.04 - 29.06)
	2-yrs	232.00	24.10 (23.48 - 24.74)	28.16 (25.88 - 30.65)	28.46 (26.05 - 31.10)
	5-yrs	232.00	25.78 (24.77 - 26.86)	30.12 (27.30 - 33.27)	30.45 (27.48 - 33.76)
	10-yrs	232.00	27.05 (25.59 - 28.72)	31.61 (28.20 - 35.58)	31.95 (28.39 - 36.10)
	50-yrs	232.00	30.02 (26.60 - 34.71)	35.08 (29.32 - 42.99)	35.45 (29.51 - 43.63)
	100-yrs	232.00	31.30 (26.82 - 38.38)	36.57 (29.56 - 47.54)	36.97 (29.76 - 48.24)

Table 3.3   Directional return values of hourly-averaged wind speed at different heights for the BWFZ. The return value point estimates are given in front of the 95% confidence intervals given between parentheses. The associated wind directions given in the second column have been computed from the $U_{10,1h}$ POT data. (Continuation of Table 3.2 and continues in Table 3.4.)

Sector	Return period	Dir. (°N)	U90 (m/s)	U100 (m/s)	U150 (m/s)
N (345°N -15°N)	1-yrs	356.20	19.47 (17.84 - 21.29)	19.63 (17.93 - 21.54)	20.28 (18.30 - 22.52)
	2-yrs	356.20	20.68 (18.81 - 22.72)	20.86 (18.91 - 22.98)	21.55 (19.29 - 24.03)
	5-yrs	356.20	22.09 (19.98 - 24.33)	22.28 (20.08 - 24.62)	23.01 (20.50 - 25.74)
	10-yrs	356.20	23.01 (20.60 - 25.54)	23.20 (20.71 - 25.84)	23.97 (21.14 - 27.02)
	50-yrs	356.20	24.76 (21.51 - 28.92)	24.97 (21.62 - 29.26)	25.79 (22.06 - 30.59)
	100-yrs	356.20	25.38 (21.73 - 30.49)	25.60 (21.85 - 30.84)	26.44 (22.29 - 32.25)
NE (15°N - 45°N)	1-yrs	29.70	18.01 (16.43 - 19.74)	18.17 (16.52 - 19.97)	18.77 (16.85 - 20.88)
	2-yrs	29.70	19.29 (17.46 - 21.29)	19.45 (17.55 - 21.54)	20.09 (17.91 - 22.52)
	5-yrs	29.70	20.92 (18.72 - 23.39)	21.10 (18.82 - 23.67)	21.80 (19.20 - 24.74)
	10-yrs	29.70	22.10 (19.48 - 25.19)	22.29 (19.58 - 25.48)	23.02 (19.98 - 26.64)
	50-yrs	29.70	24.75 (20.73 - 30.32)	24.96 (20.84 - 30.67)	25.78 (21.26 - 32.07)
	100-yrs	29.70	25.82 (21.12 - 32.97)	26.04 (21.23 - 33.35)	26.90 (21.66 - 34.87)
ENE (45°N - 75°N)	1-yrs	57.30	17.19 (15.90 - 18.66)	17.34 (15.99 - 18.87)	17.91 (16.32 - 19.73)
	2-yrs	57.30	18.17 (16.60 - 19.94)	18.32 (16.68 - 20.17)	18.93 (17.03 - 21.09)
	5-yrs	57.30	19.42 (17.52 - 21.44)	19.58 (17.62 - 21.69)	20.23 (17.98 - 22.68)
	10-yrs	57.30	20.34 (18.17 - 22.54)	20.51 (18.27 - 22.80)	21.19 (18.64 - 23.84)
	50-yrs	57.30	22.39 (19.23 - 25.99)	22.58 (19.33 - 26.29)	23.32 (19.73 - 27.49)
	100-yrs	57.30	23.24 (19.53 - 28.07)	23.43 (19.64 - 28.39)	24.20 (20.04 - 29.69)
E (75°N - 105°N)	1-yrs	87.60	16.60 (15.54 - 17.74)	16.74 (15.62 - 17.95)	17.29 (15.94 - 18.76)
	2-yrs	87.60	17.42 (15.98 - 19.01)	17.57 (16.07 - 19.23)	18.14 (16.40 - 20.11)
	5-yrs	87.60	18.48 (16.67 - 20.46)	18.64 (16.76 - 20.70)	19.25 (17.11 - 21.65)
	10-yrs	87.60	19.27 (17.21 - 21.47)	19.43 (17.30 - 21.72)	20.07 (17.66 - 22.71)
	50-yrs	87.60	21.02 (17.84 - 24.60)	21.20 (17.93 - 24.89)	21.89 (18.30 - 26.02)
	100-yrs	87.60	21.75 (17.96 - 26.46)	21.93 (18.05 - 26.77)	22.65 (18.42 - 27.99)
ESE (105°N - 135°N)	1-yrs	119.10	15.95 (14.51 - 17.55)	16.09 (14.59 - 17.75)	16.62 (14.88 - 18.56)
	2-yrs	119.10	17.18 (15.50 - 19.00)	17.32 (15.58 - 19.22)	17.90 (15.90 - 20.10)
	5-yrs	119.10	18.66 (16.71 - 20.73)	18.82 (16.80 - 20.97)	19.44 (17.14 - 21.93)
	10-yrs	119.10	19.66 (17.45 - 22.20)	19.83 (17.54 - 22.45)	20.48 (17.90 - 23.48)
	50-yrs	119.10	21.69 (18.56 - 26.09)	21.87 (18.66 - 26.40)	22.59 (19.04 - 27.60)
	100-yrs	119.10	22.45 (18.86 - 28.13)	22.64 (18.96 - 28.46)	23.39 (19.35 - 29.76)
SE (135°N - 165°N)	1-yrs	155.40	18.09 (16.74 - 19.58)	18.24 (16.83 - 19.81)	18.84 (17.17 - 20.72)
	2-yrs	155.40	19.19 (17.51 - 21.13)	19.36 (17.60 - 21.37)	19.99 (17.97 - 22.35)
	5-yrs	155.40	20.65 (18.58 - 23.04)	20.82 (18.68 - 23.30)	21.51 (19.06 - 24.37)
	10-yrs	155.40	21.73 (19.33 - 24.56)	21.92 (19.43 - 24.85)	22.64 (19.83 - 25.98)
	50-yrs	155.40	24.18 (20.30 - 28.74)	24.38 (20.41 - 29.08)	25.19 (20.83 - 30.40)
	100-yrs	155.40	25.21 (20.72 - 31.26)	25.43 (20.82 - 31.63)	26.27 (21.25 - 33.07)
S (165°N - 195°N)	1-yrs	188.00	23.27 (21.35 - 25.35)	23.47 (21.46 - 25.65)	24.24 (21.90 - 26.82)
	2-yrs	188.00	24.56 (22.32 - 26.91)	24.77 (22.44 - 27.22)	25.58 (22.90 - 28.46)
	5-yrs	188.00	26.24 (23.70 - 28.89)	26.46 (23.82 - 29.23)	27.33 (24.31 - 30.56)
	10-yrs	188.00	27.49 (24.61 - 30.59)	27.72 (24.74 - 30.94)	28.64 (25.25 - 32.36)
	50-yrs	188.00	30.34 (26.14 - 36.04)	30.60 (26.28 - 36.46)	31.61 (26.82 - 38.12)
	100-yrs	188.00	31.54 (26.63 - 39.22)	31.81 (26.77 - 39.68)	32.86 (27.32 - 41.49)

Table 3.4   Directional return values of hourly-averaged wind speed at different heights for the BWFZ. The return value point estimates are given in front of the 95% confidence intervals given between parentheses. The associated wind directions given in the second column have been computed from the $U_{10,1h}$ POT data. (Continuation of Table 3.3 and continues in Table 3.5.)

Sector	Return period	Dir. (°N)	U90 (m/s)	U100 (m/s)	U150 (m/s)
SSW (195°N - 225°N)	1-yrs	215.80	25.76 (23.59 - 28.10)	25.98 (23.72 - 28.43)	26.84 (24.21 - 29.73)
	2-yrs	215.80	27.34 (24.91 - 29.98)	27.57 (25.04 - 30.33)	28.48 (25.56 - 31.71)
	5-yrs	215.80	29.39 (26.40 - 32.73)	29.64 (26.54 - 33.11)	30.61 (27.08 - 34.62)
	10-yrs	215.80	30.91 (27.28 - 35.13)	31.17 (27.42 - 35.54)	32.20 (27.98 - 37.16)
	50-yrs	215.80	34.35 (28.86 - 41.72)	34.64 (29.02 - 42.20)	35.78 (29.61 - 44.13)
	100-yrs	215.80	35.80 (29.41 - 45.07)	36.10 (29.57 - 45.59)	37.29 (30.17 - 47.67)
SW (225°N - 255°N)	1-yrs	233.30	26.03 (23.81 - 28.47)	26.25 (23.93 - 28.81)	27.11 (24.42 - 30.12)
	2-yrs	233.30	27.72 (25.17 - 30.52)	27.95 (25.30 - 30.88)	28.87 (25.82 - 32.29)
	5-yrs	233.30	29.96 (26.79 - 33.52)	30.21 (26.93 - 33.91)	31.21 (27.48 - 35.45)
	10-yrs	233.30	31.65 (27.86 - 36.20)	31.92 (28.01 - 36.62)	32.97 (28.58 - 38.30)
	50-yrs	233.30	35.61 (29.63 - 43.81)	35.91 (29.79 - 44.32)	37.10 (30.40 - 46.34)
	100-yrs	233.30	37.32 (30.31 - 48.12)	37.63 (30.47 - 48.68)	38.87 (31.10 - 50.90)
W (255°N - 285°N)	1-yrs	266.80	24.00 (21.81 - 26.32)	24.20 (21.92 - 26.63)	25.00 (22.37 - 27.84)
	2-yrs	266.80	25.70 (23.30 - 28.30)	25.92 (23.43 - 28.62)	26.78 (23.91 - 29.93)
	5-yrs	266.80	27.78 (24.98 - 30.92)	28.01 (25.11 - 31.28)	28.94 (25.63 - 32.71)
	10-yrs	266.80	29.24 (25.96 - 33.07)	29.49 (26.10 - 33.46)	30.46 (26.63 - 34.98)
	50-yrs	266.80	32.30 (27.52 - 38.84)	32.57 (27.67 - 39.29)	33.64 (28.24 - 41.08)
	100-yrs	266.80	33.49 (27.95 - 41.59)	33.77 (28.10 - 42.07)	34.89 (28.67 - 43.99)
NNW (285°N - 315°N)	1-yrs	296.30	22.83 (21.26 - 24.55)	23.02 (21.37 - 24.84)	23.78 (21.81 - 25.97)
	2-yrs	296.30	23.90 (21.91 - 26.13)	24.11 (22.03 - 26.43)	24.90 (22.48 - 27.64)
	5-yrs	296.30	25.39 (22.89 - 28.24)	25.61 (23.01 - 28.57)	26.45 (23.48 - 29.88)
	10-yrs	296.30	26.55 (23.61 - 30.10)	26.77 (23.73 - 30.45)	27.66 (24.22 - 31.84)
	50-yrs	296.30	29.42 (24.54 - 36.47)	29.67 (24.67 - 36.90)	30.65 (25.18 - 38.58)
	100-yrs	296.30	30.73 (24.80 - 40.81)	30.99 (24.93 - 41.29)	32.02 (25.44 - 43.17)
NW (315°N - 345°N)	1-yrs	327.80	20.93 (19.10 - 22.93)	21.11 (19.20 - 23.20)	21.81 (19.59 - 24.26)
	2-yrs	327.80	22.31 (20.18 - 24.59)	22.49 (20.29 - 24.88)	23.24 (20.70 - 26.01)
	5-yrs	327.80	24.06 (21.59 - 26.75)	24.26 (21.70 - 27.07)	25.06 (22.14 - 28.30)
	10-yrs	327.80	25.32 (22.41 - 28.72)	25.54 (22.53 - 29.05)	26.38 (22.99 - 30.38)
	50-yrs	327.80	28.10 (23.49 - 34.65)	28.34 (23.62 - 35.05)	29.27 (24.10 - 36.65)
	100-yrs	327.80	29.22 (23.72 - 37.76)	29.47 (23.84 - 38.20)	30.44 (24.33 - 39.94)
OMNI	1-yrs	232.00	27.22 (25.19 - 29.44)	27.45 (25.32 - 29.78)	28.35 (25.84 - 31.14)
	2-yrs	232.00	28.73 (26.21 - 31.50)	28.97 (26.34 - 31.87)	29.93 (26.88 - 33.32)
	5-yrs	232.00	30.73 (27.65 - 34.20)	30.99 (27.79 - 34.60)	32.02 (28.36 - 36.18)
	10-yrs	232.00	32.25 (28.56 - 36.57)	32.52 (28.71 - 37.00)	33.59 (29.30 - 38.69)
	50-yrs	232.00	35.79 (29.69 - 44.20)	36.09 (29.85 - 44.72)	37.28 (30.46 - 46.75)
	100-yrs	232.00	37.32 (29.93 - 48.87)	37.63 (30.09 - 49.44)	38.87 (30.71 - 51.70)

Table 3.5   Directional return values of hourly-averaged wind speed at different heights for the BWFZ. The return value point estimates are given in front of the 95% confidence intervals given between parentheses. The associated wind directions given in the second column have been computed from the $U_{10,1h}$ POT data. (Continuation of Table 3.4.)

3.4 Wind spectra

The hourly-averaged HARMONIE wind speed data from 1989 to 2013 at all available heights were used to determine the wind speed spectra. The spectra were computed by means of a fast Fourier analysis. The computed wind spectra are presented in Figure 3.11, Figure 3.12, Figure 3.13, Figure 3.14, Figure 3.15 and Figure 3.16, for respectively 10m, 70m, 80m, 90m, 100m and 150m height. The figures show the energy density of the y-axis and the frequency along the x-axis. These spectra show, as expected, a high peak at a frequency of 1 year. This peak is associated with the seasonal variation. The energy at frequencies below 10^{-4} hours^{-1} indicates multi-annual and decadal variations in the dataset. The bulk of the energy is located

between 10^{-2} and 10^{-3} hours^{-1} (100 to 1000 hours). This energy is typically associated with the passage of large scale structures (e.g. storm depressions). In the tail of the spectrum some spikes are visible; these are higher harmonics: an artefact of the Fourier analysis.

In order to illustrate the effect of the uncertainties in the vertical wind profile in the spectra at levels other than 10 m, in Figure 3.12, Figure 3.13, Figure 3.14, Figure 3.15 and Figure 3.16 the spectra of the wind speeds obtained from the HARMONIE 10m wind using the DNV profile (cf. Eq. (3.3)) have been added. These spectral energies are, as expected, higher than those of the HARMONIE data.
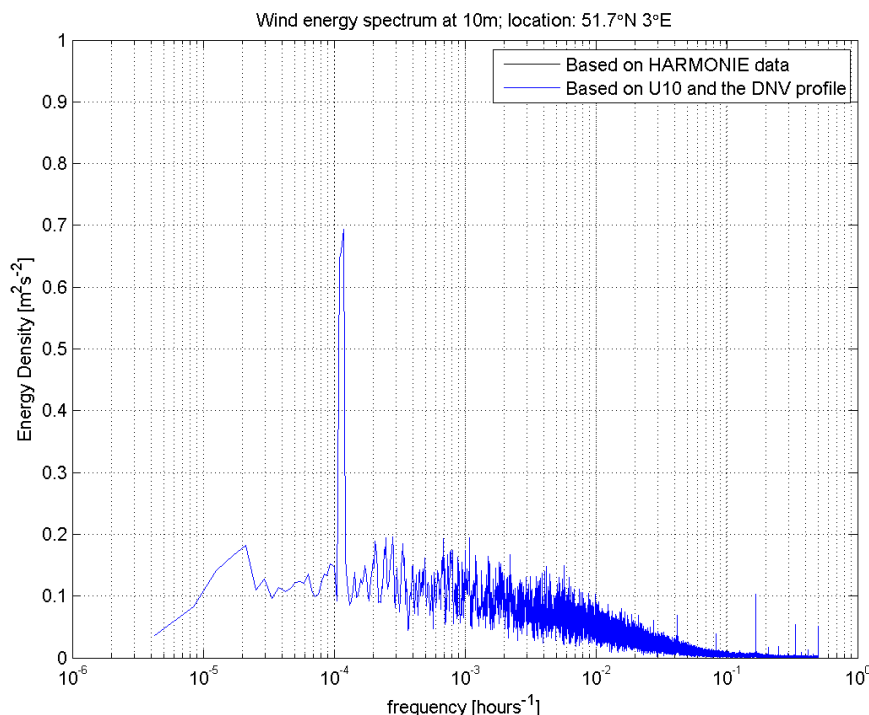
Figure 3.11 Wind energy spectrum at a height of 10m.
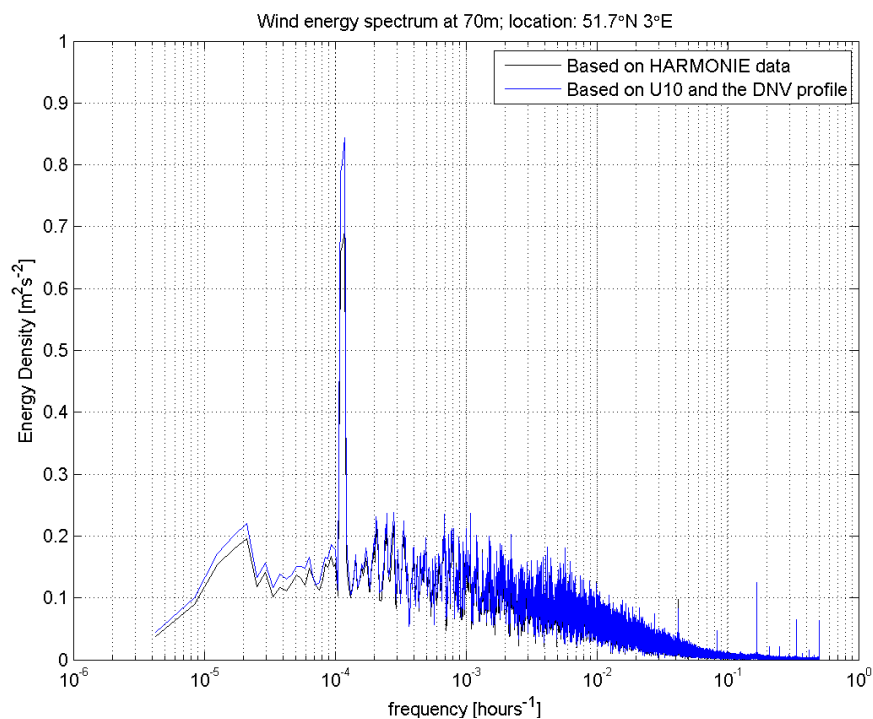
Figure 3.12 Wind energy spectrum at a height of 70m.
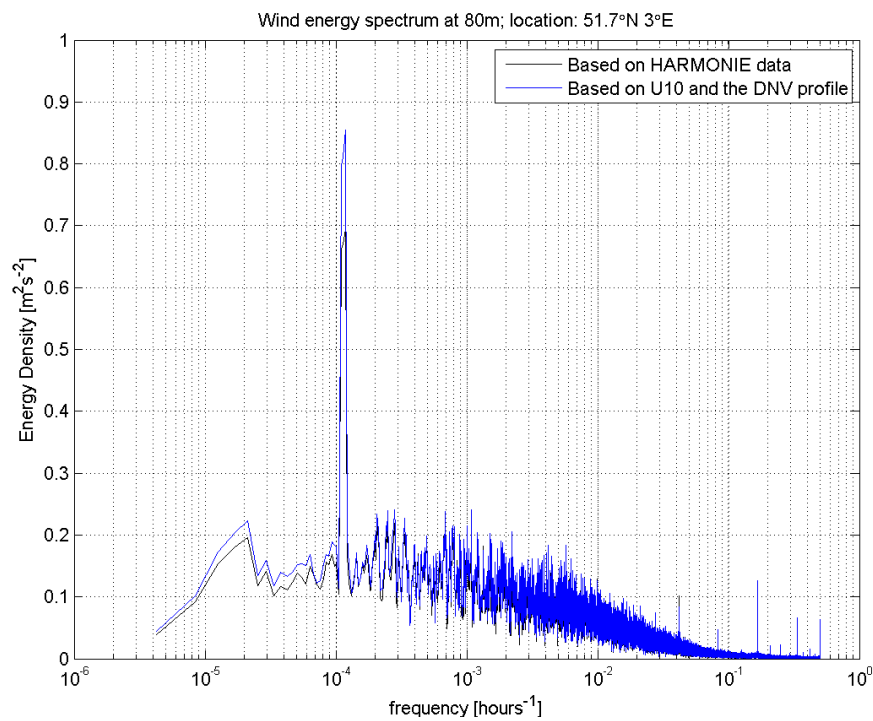
Figure 3.13 Wind energy spectrum at a height of 80m.
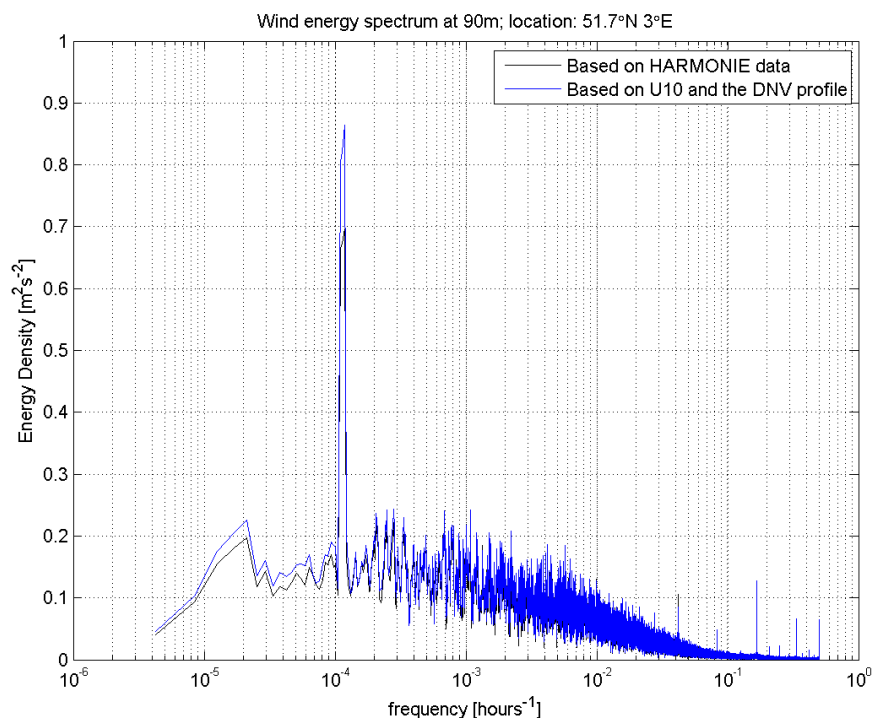
Figure 3.14 Wind energy spectrum at a height of 90m.
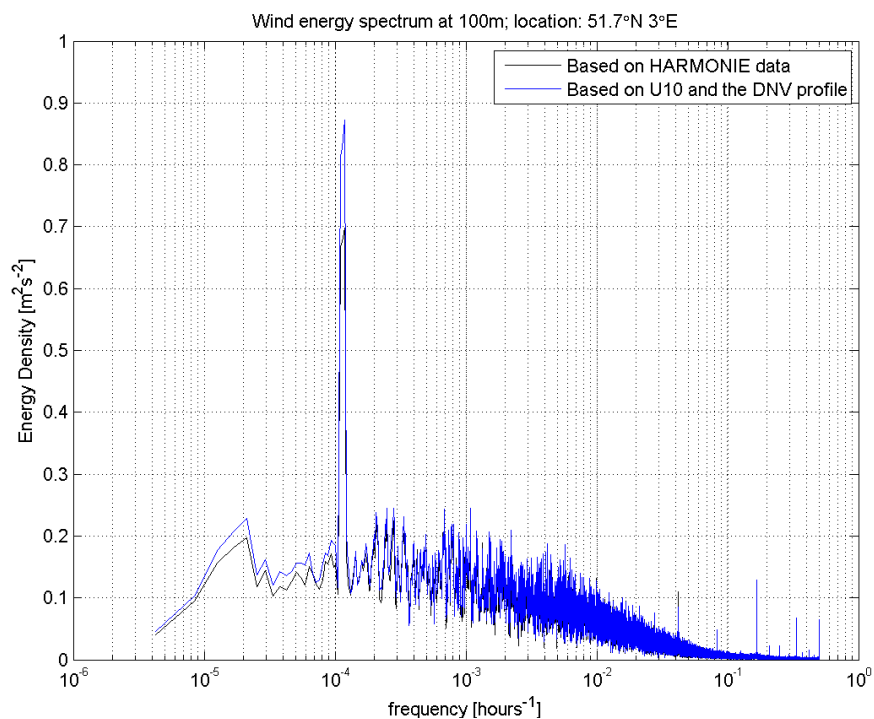
Figure 3.15 Wind energy spectrum at a height of 100m.

Wind energy spectrum at 150m; location: 51.7°N 3°E
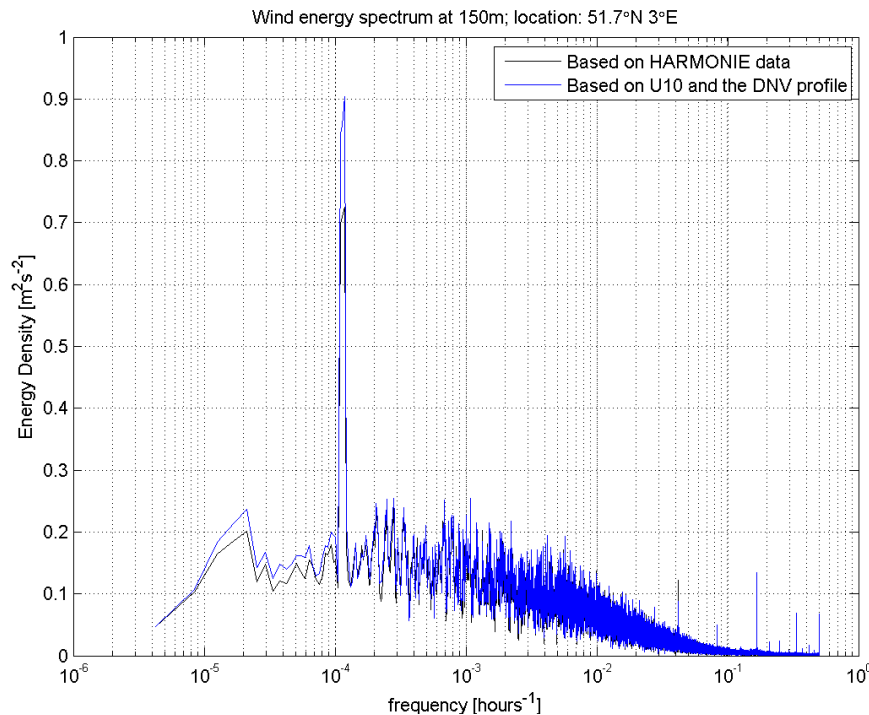
Figure 3.16 Wind energy spectrum at a height of 150m.

3.5 Wind operational criteria

The following wind operational criteria have been determined:
- Monthly and annual wind roses at heights of 10m, 70m, 80m, 90m, 100m and 150m;
- Monthly and annual joint occurrence tables of wind speed vs. wind direction at heights of 10m, 70m, 80m, 90m, 100m and 150m;
- Directional dependent Weibull parameters for normal wind speed distribution;
- Persistence of wind speed with the following parameters:
  - Wind speed thresholds 2m/s, 4 m/s, 6 m/s, 8 m/s, 9 m/s, 10 m/s, 11 m/s, 12 m/s and 15m/s
  - Time windows of 1h, 6h, 12h, 24h, 48h and 72h
  - Probabilities of exceedance of 20%, 50% and 80%
  - At heights of 10m, 70m, 80m, 90m, 100m and 150m.

The annual wind rose of $U_{10,1hour}$ is presented in Figure 3.17; the monthly roses are shown in Figure 3.18. The annual and monthly wind roses at the other heights are given in Appendix A.1. The yearly joint occurrence table of wind speed and direction at 10m height is given in Figure 3.19. The monthly joint occurrence tables at a height of 10m and all other joint occurrence tables for different heights are given in Appendix A.2. The directional dependent Weibull parameters are presented in Section 3.5.1. Both the joint occurrence tables and the Weibull parameters are also available in the excel-file provided with this report.

The persistence tables, which are based on the HARMONIE data, are provided in a separate excel-file, for all given criteria.

Data from 01-Jan-1987 01:00:00 until 01-Jan-2014 (mean=7.8 m/s, max=31.7m/s)
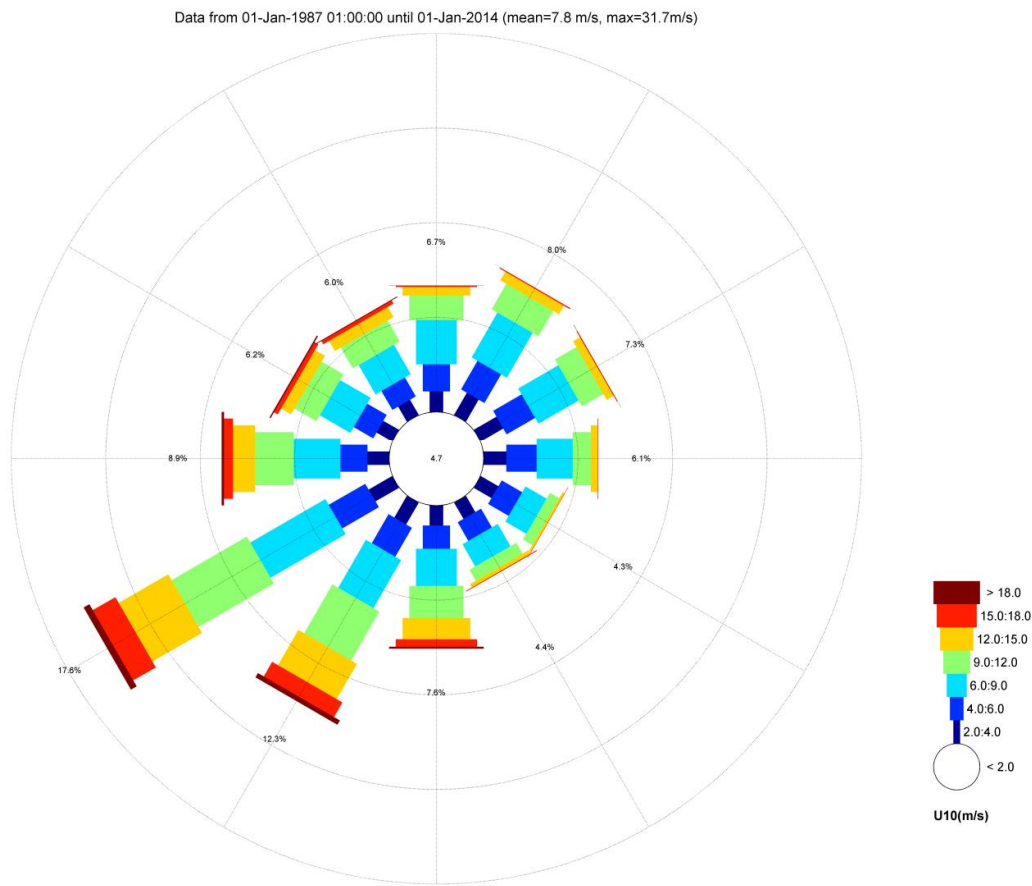
Figure 3.17 Annual wind rose of $U_{10,1h}$.
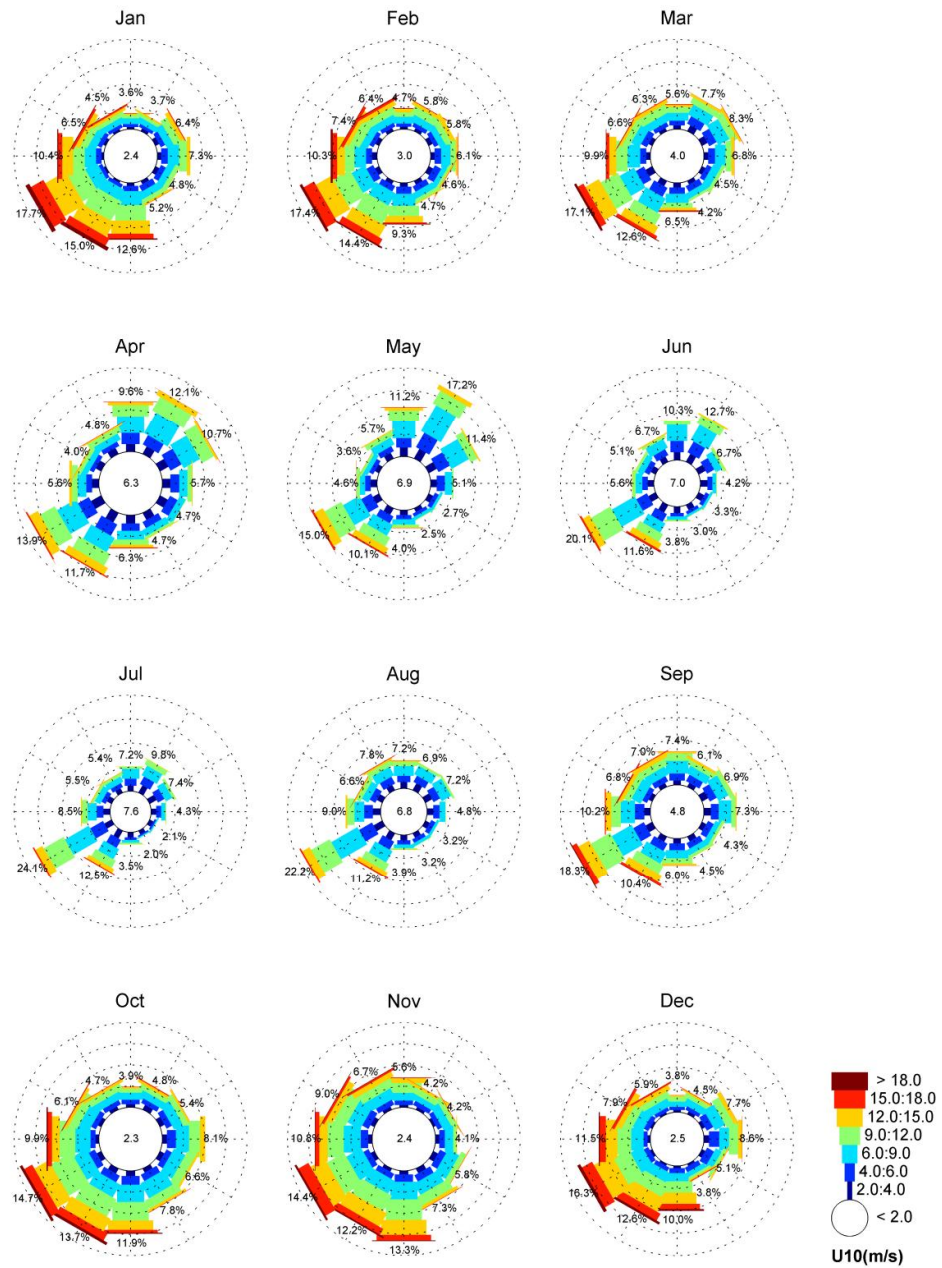
Figure 3.18 Monthly wind roses of $U_{10,1h}$.

Dir10 (° N)

U10 (m/s)	345-15	15-45	45-75	75-105	105-135	135-165	165-195	195-225	225-255	255-285	285-315	315-345	Total
>18.0	0.01	0.00	0.00			0.00	0.11	0.26	0.34	0.12	0.06	0.04	0.94
15.0-18.0	0.08	0.05	0.04	0.02	0.01	0.04	0.40	0.89	1.37	0.47	0.23	0.19	3.80
12.0-15.0	0.44	0.53	0.41	0.36	0.11	0.21	1.12	2.15	3.03	1.17	0.61	0.62	10.75
9.0-12.0	1.30	1.55	1.31	0.96	0.57	0.67	1.70	2.99	4.60	2.05	1.34	1.27	20.29
6.0-9.0	2.34	2.74	2.46	1.92	1.29	1.35	1.96	2.93	4.59	2.47	1.87	1.79	27.72
4.0-6.0	1.43	1.75	1.74	1.60	1.25	1.14	1.23	1.77	2.24	1.43	1.19	1.15	17.91
2.0-4.0	1.07	1.35	1.38	1.21	1.08	0.99	1.05	1.33	1.44	1.15	0.95	0.92	13.92
0.0-2.0	0.37	0.39	0.40	0.42	0.39	0.36	0.40	0.43	0.44	0.39	0.34	0.34	4.67
	7.05	8.30	7.74	6.47	4.71	4.76	7.90	12.74	18.05	9.25	6.59	6.32	100.00

All year   Total

Figure 3.19 Yearly joint frequency table of wind speed and direction at 10m height.

To summarise the normal wind climate at the BWFZ:
• The most frequent winds at BWFZ are from the Southwest.
• The severity of the wind conditions vary significantly during the year, with the summer months being characterised by milder wind conditions.
• The most severe winds at BWFZ come from the Southwest-Northwest sectors and the less severe winds from the Northeast-Southeast sectors.

3.5.1 Weibull parameters

The Weibull parameters for the omnidirectional wind speed and per directional section are determined based on the HARMONIE data at heights of 10m, 70m, 80m, 90m, 100m and 150m. The Weibull probability density function for wind speed U is given by:

$$p(U) = \left(\frac{k}{c}\right)\left(\frac{U}{c}\right)^{k-1} \exp\left[-\left(\frac{U}{c}\right)^{k}\right],$$ (3.7)

where k is the shape parameter and c is a scale parameter. The Weibull distribution function is given by:

$$F(U) = 1 - \exp\left[-\left(\frac{U}{c} \right)^k \right]. \tag{3.8}$$

An example of the cumulative distribution function (cdf) of the omnidirectional wind speed at 10m height is given in Figure 3.20. The parameters for all heights and directional sectors are given in Table 3.6. The mean wind speed, calculated from the estimated omni-directional Weibull parameters is given in the last row of the table.

Figure 3.20 Weibull fit of HARMONIE data at a height of 10m.

Heights	10m		70m		80m		90m		100m		150m	
Sector	c	k	c	k	c	k	c	k	c	k	c	k
N (345°N: 15°N)	7.84	2.22	9.90	2.64	8.85	2.23	8.90	2.22	8.96	2.22	9.12	2.18
NE (15°N: 45°N)	7.80	2.28	9.17	2.49	9.02	2.28	9.09	2.27	9.17	2.26	9.32	2.19
ENE (45°N: 75°N)	7.49	2.23	8.64	2.32	8.90	2.32	8.98	2.30	9.05	2.28	9.25	2.21
E (75°N: 105°N)	7.19	2.13	8.39	2.24	8.59	2.28	8.68	2.28	8.77	2.28	8.98	2.23
ESE (105°N: 135°N)	6.48	2.06	7.76	2.18	7.85	2.18	7.94	2.17	8.02	2.15	8.31	2.10
SE (135°N: 165°N)	6.98	2.02	8.06	2.01	8.44	2.12	8.53	2.12	8.64	2.11	8.84	2.05
S (165°N: 195°N)	9.30	2.04	9.59	1.97	10.99	2.13	11.10	2.13	11.22	2.13	11.55	2.07
SSW (195°N: 225°N)	10.20	2.21	11.56	2.17	12.10	2.29	12.26	2.29	12.41	2.29	12.88	2.25
SW (225°N: 255°N)	10.53	2.40	11.96	2.34	12.29	2.43	12.43	2.43	12.57	2.43	13.14	2.40
W (255°N: 285°N)	9.34	2.11	10.56	2.07	10.50	2.10	10.58	2.09	10.65	2.09	10.92	2.08
NNW (285°N: 315°N)	8.60	2.05	9.78	2.14	9.51	2.01	9.57	2.01	9.63	2.01	9.77	1.98
NW (315°N: 345°N)	8.49	2.06	10.02	2.25	9.43	2.04	9.47	2.03	9.50	2.01	9.62	1.99
OMNI	8.80	2.07	10.15	2.11	10.26	2.10	10.35	2.10	10.46	2.09	10.77	2.05
Omni Mean (m/s)	7.80		8.99		9.08		9.17		9.26		9.54	

Table 3.6   Weibull parameters for wind speed at different heights in the BWFZ based on HARMONIE data.

In order to account for the uncertainty in the vertical wind profile, the Weibull parameter were also computed from the HARMONIE 10m wind speed data and considering power law profile with an α value of 0.11 (the upper band given in Figure 3.10). In these fits the Weibull shape parameter estimates from the HARMONIE data have been kept unchanged. The computed parameters for all heights and directional sectors are given in Table 3.7. The given scale parameter values can be seen as the 95% upper bounds of the Weibull scale parameter estimates given in Table 3.6. Again, the mean wind speed, calculated from the estimated omni-directional Weibull parameters is given in the last row of the table.
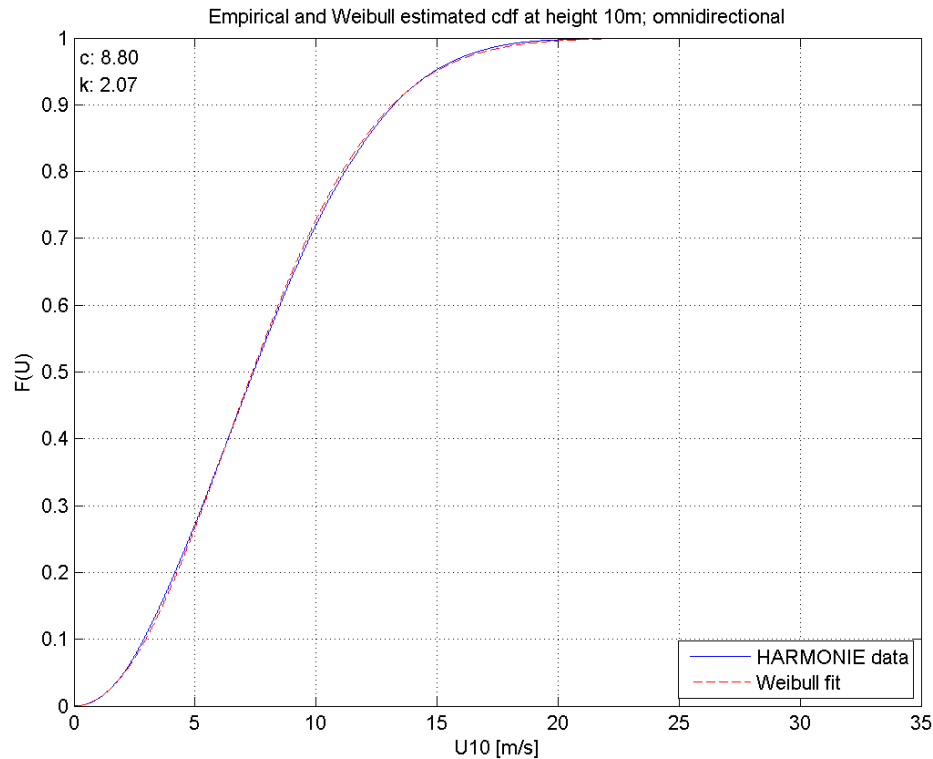
Heights	70m		80m		90m		100m		150m	
Sector	c	k	c	k	c	k	c	k	c	k
N (345°N: 15°N)	9.68	2.64	9.86	2.23	9.98	2.22	10.10	2.22	10.56	2.18
NE (15°N: 45°N)	9.64	2.49	9.80	2.28	9.93	2.27	10.04	2.26	10.50	2.19
ENE (45°N: 75°N)	9.28	2.32	9.41	2.32	9.54	2.30	9.65	2.28	10.09	2.21
E (75°N: 105°N)	8.90	2.24	9.03	2.28	9.15	2.28	9.25	2.28	9.68	2.23
ESE (105°N: 135°N)	8.03	2.18	8.15	2.18	8.26	2.17	8.35	2.15	8.73	2.10
SE (135°N: 165°N)	8.64	2.01	8.78	2.12	8.89	2.12	8.99	2.11	9.40	2.05
S (165°N: 195°N)	11.51	1.97	11.69	2.13	11.85	2.13	11.99	2.13	12.53	2.07
SSW (195°N: 225°N)	12.63	2.17	12.82	2.29	12.98	2.29	13.14	2.29	13.74	2.25
SW (225°N: 255°N)	13.05	2.34	13.24	2.43	13.41	2.43	13.57	2.43	14.19	2.40
W (255°N: 285°N)	11.57	2.07	11.74	2.10	11.89	2.09	12.03	2.09	12.58	2.08
NNW (285°N: 315°N)	10.65	2.14	10.80	2.01	10.94	2.01	11.07	2.01	11.57	1.98
NW (315°N: 345°N)	10.51	2.25	10.67	2.04	10.80	2.03	10.93	2.01	11.43	1.99
OMNI	10.90	2.11	11.06	2.10	11.21	2.10	11.34	2.09	11.85	2.05
Omni Mean (m/s)	9.66		9.80		9.93		10.04		10.50	

Table 3.7   Upper bounds of the Weibull parameters for wind speed at high heights in the BWFZ based on HARMONIE data.

3.6   Turbulence intensity

The most basic measure of turbulence is the turbulence intensity. It is defined by the ratio of the standard deviation of the wind speed to the 10-minute mean wind speed. Given that we had no turbulence data available we have carried out a literature review. Mol (2009) made use of the FINO measurements, which also include the variance of the wind speed for each 10-minute average value to assess the turbulence.

The standard deviation σ_{U_h} which is the square root of the variance is assumed to be a suitable parameter for expressing the amount of turbulence. Based on the analysis of the FINO data in Mol (2009) the following relation between the 10-min wind speed at a height higher than 70m and the turbulence is recommended.

$$\sigma_{U_h} = 0.03 U_h + 0.455. \tag{3.9}$$

We note, however, that this expression should be considered with care, given that we have no local turbulence data to verify whether the turbulence data at the FINO platform is applicable to the Borssele Wind Farm Zone.

4 Wave Conditions

4.1 Introduction

This chapter presents the wave conditions in the BWFZ. In order to model temporal and spatial variations of the wave conditions in the BWFZ a 3rd generation phase-averaging shallow-water wave model, SWAN (Booij et al., 1999), was set-up. The SWAN model was run in non-stationary mode to simulate the waves in the period 1992 – 2011 (20 years) and in stationary mode to simulate waves for a number of extreme events with return periods of 1, 2, 5, 10, 50 and 100 years. The wave model is described in the next section. The results of the SWAN non-stationary (hindcast) computations were used in the determination of the normal wave conditions presented in Section 4.3. The results of the SWAN stationary computations were used in the determination of the extreme wave conditions presented in Section 4.4. Sections 4.5, 4.6 and 4.7 discuss shoaling and wave breaking, the wave spectral form and the impact of currents and water levels on waves, respectively.

We note that next to the SWAN model, also a Delft3D-FLOW model was setup for simulating water levels and currents in the BWFZ, this is further explained in the next Chapter. For this project, SWAN has been run offline considering from the Delft3D-FLOW computations solely the water levels.

4.2 Wave modelling

4.2.1 Introduction

The next paragraph shortly explains the technical background of SWAN. Sections 4.2.3 to 4.2.6 describe the model setup for this study. In section 4.2.7 the qualitative validation of the model results that was carried out is described.

4.2.2 Description of SWAN

SWAN is the state-of-the-art third generation shallow water phase-averaging wave model. It can account for:

- Wave propagation in time and space, shoaling, refraction due to current and depth, frequency shifting due to currents and non-stationary depth.
- Wave generation by wind.
- Three- and four-wave interactions.
- Whitecapping, bottom friction and depth-induced breaking.
- Dissipation due to vegetation.
- Wave-induced set-up.
- Propagation from laboratory up to global scales.
- Transmission through and reflection (specular and diffuse) against obstacles.
- Diffraction.

Furthermore, SWAN computations can be made on a regular, a curvi-linear grid and a triangular mesh in a Cartesian or spherical co-ordinate system. Nested runs, using input, namely two-dimensional wave spectra, from other (larger scale) models can be made with SWAN.

The SWAN model has been validated and verified successfully under a variety of field cases and is continually undergoing further development. It sets today's standard for nearshore wave modelling.

For more information on SWAN, reference is made to http://swanmodel.sourceforge.net/online_doc/online_doc.htm from where the SWAN scientifical/technical documentation and used manual can be downloaded.

In short, the model solves the action balance equation, in Cartesian or spherical coordinates, without any ad hoc assumption on the shape of the wave spectrum. In Cartesian coordinates the equation is

$$\frac{\partial N}{\partial t} + \frac{\partial}{\partial x}(c_x N) + \frac{\partial}{\partial y}(c_y N) + \frac{\partial}{\partial \sigma}(c_\sigma N) + \frac{\partial}{\partial \theta}(c_\theta N) = \frac{S_{tot}}{\sigma}, \tag{3.10}$$

where N is the action density, t is the time, σ is the relative angular frequency, and θ the wave direction. The first term on the left-hand side of Eq. 4.1 represents the local rate of change of action density in time. The second and third terms represent propagation of action in geographical space. The fourth term represents shifting of the relative frequency due to variation in depth and currents. The fifth term represents depth-induced and current-induced refractions. The quantities c_x, c_y, c_θ and c_σ are the propagation speeds in the geographical x- and y-space, and in the θ- and the σ-space, respectively. The expressions of these propagation speeds are taken from linear wave theory. In Eq. 4.1 S_{tot} is the energy source term. This source term is the sum of separate source terms representing different types of processes: wave energy growth by wind input, wave energy transfer due to non-linear wave-wave interactions (both quadruplets and triads), and the decay of wave energy due to whitecapping, bottom friction, and depth induced wave breaking. For some source terms more than one formulation is implemented in SWAN, see http://swanmodel.sourceforge.net/online_doc/online_doc.htm

As to SWAN's numerical approach, the integration of the propagation and of the source terms of Eq. 4.1 has been implemented with finite difference schemes in all four dimensions (geographical space and spectral space). A constant time increment is used for the time integration. The model propagates the wave action density of all components of the spectrum across the computational area using implicit schemes in geographical and spectral space, supplemented with a central approximation in spectral space. In geographical space the scheme is upwind and applied to each of the four directional quadrants of wave propagation in sequence. Three of such schemes are available in SWAN: a first-order backward space, backward time (BSBT) scheme, a second-order upwind scheme with second order diffusion (the SORDUP scheme) and a second order upwind scheme with third order diffusion (the S&L scheme). The numerical schemes used for the source term integration are essentially implicit. In order to match physical scales at relatively high frequencies and to ensure numerical stability at relatively large time steps, a limiter controlling the maximum total change of action density per iteration at each discrete wave component is imposed.

4.2.3 Computational grid and bathymetry

The spatial grid and bathymetry on the SWAN model set up for this study is based on the detailed available bathymetry data of the BWFZ. The computational grid is defined in spherical coordinates (longitude, latitude), and the geodetic datum is WGS84. The grid

resolution is ~200x~200m and the extent approximately 45 x 45km. For directional space, the full circle is considered, divided in 36 sectors of 10° each. The frequency domain is from 0.03 to 2.5 Hz (0.4 – 33 s), with the frequencies logarithmically divided by SWAN in 46 bins. The model's domain and grid are shown in Figure 4.1 and the model's bathymetry in Figure 4.2.

The vertical reference level is Mean Sea Level (MSL). Reference is made to the Hydrodynamic Study (Deltares, 2014, Chapter 4) for the relation between MSL and other tidal levels.
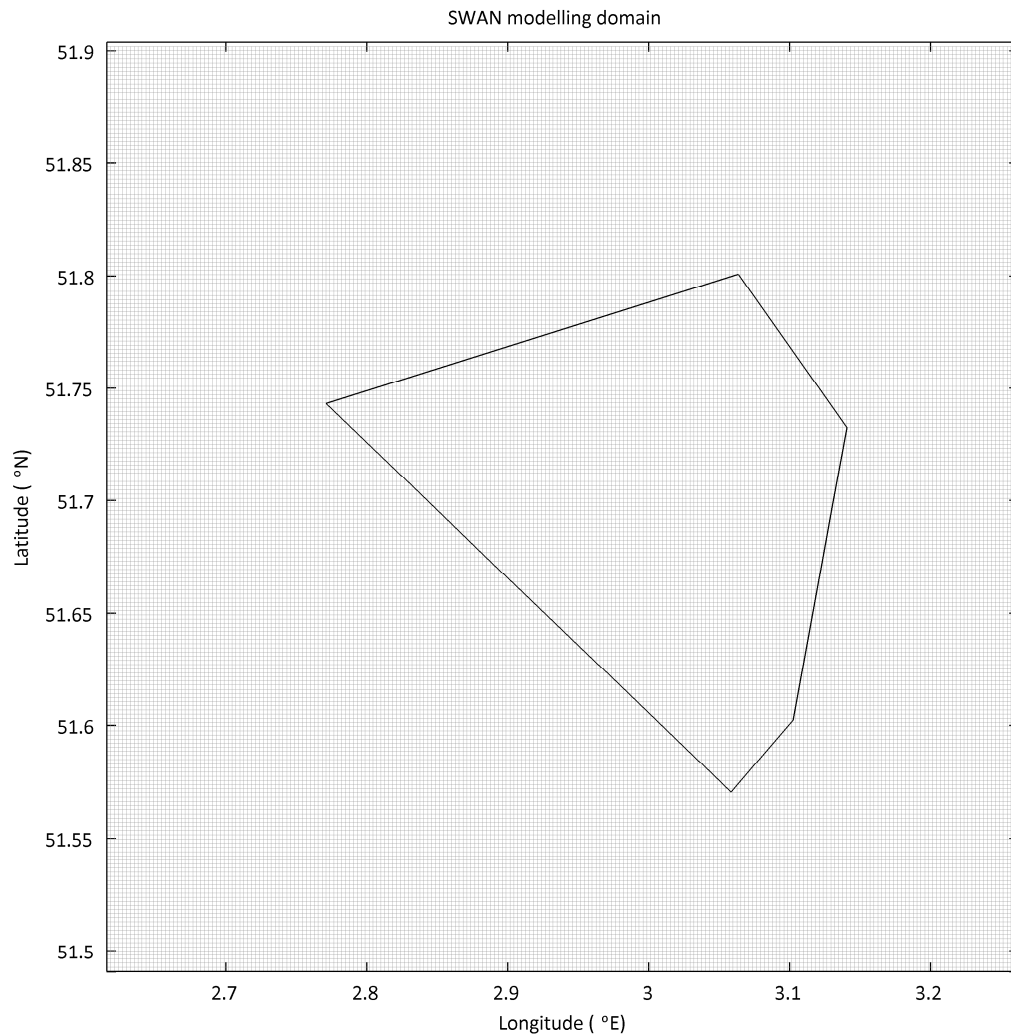
Figure 4.1   SWAN model computational grid.
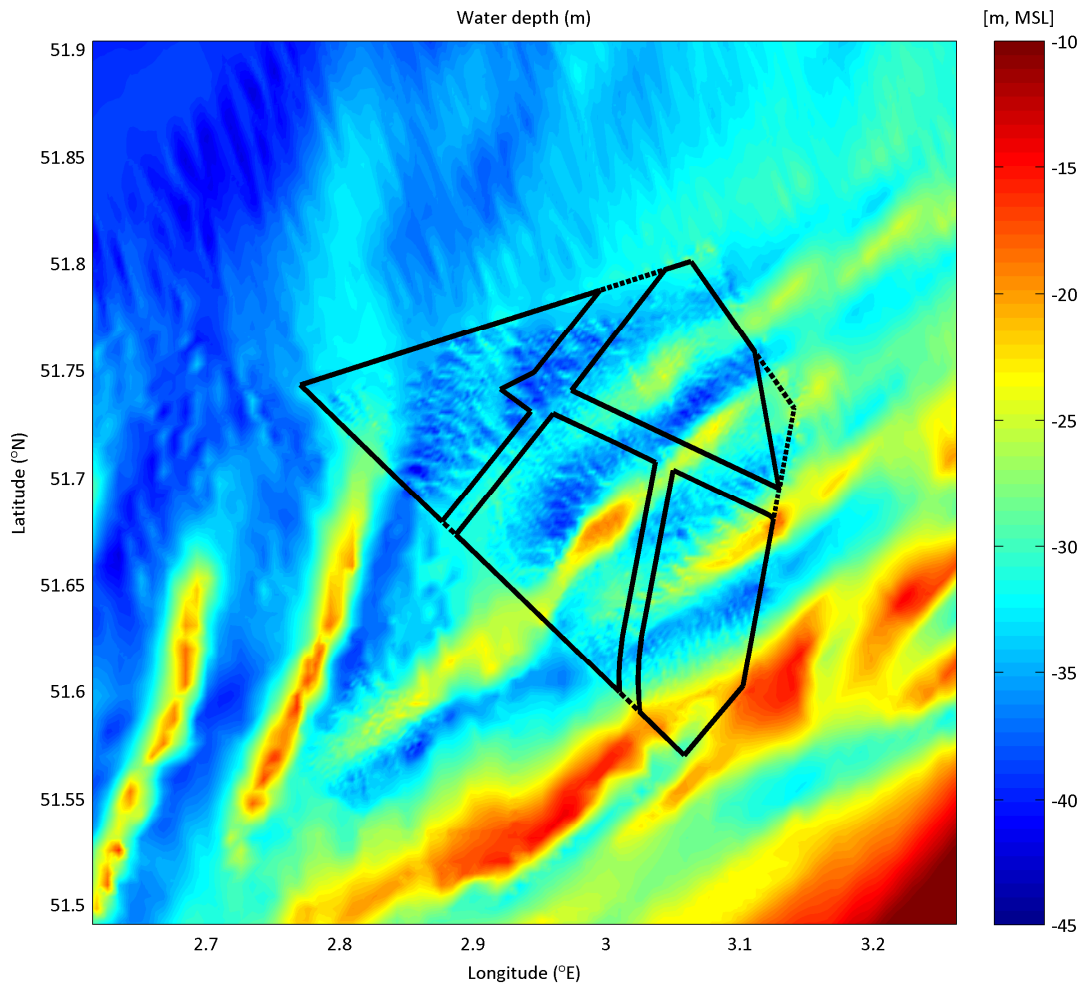
Figure 4.2   SWAN model bathymetry, coordinate system: ETRS89 / UTM zone 31N.

4.2.4   Forcing

The forcing applied in SWAN consisted of boundary waves, 10m wind velocities and water levels.

Boundary waves
For the hindcast time series of ERA-interim significant wave height (H_s), peak wave period (T_p, which has been computed from $T_{m-1,0}$ using Eq. (2.2)) and mean wave direction (MWD) at location 3°E and 51.75°N and from January 1992 until December 2011 (20 years) were used as boundary conditions for the SWAN computations.

For the extreme conditions, ERA-interim based return value estimates of H_s and associated T_p and MWD at location 3°E and 51.75°N were used as boundary conditions for the SWAN computations.

In both cases the spatial variation of the significant wave height (as found in the CoastDat database, see Figure 2.8) is taken into account by applying a correction on the ERA-interim H_s and T_p. An overview of the applied multiplication factors can be found in Table 4.1. The T_p

is adjusted such that the steepness of the waves remains unaltered, to prevent unrealistic breaking of waves.

Directional Bin	H_s factor
0°N - 60°N	1.02
60°N - 210°N	0.9
210°N - 290°N	1.05
290°N - 360°N	1.07

Table 4.1   Applied multiplication factor for H_s and T_p in the wave modelling.

Wind forcing
For the hindcast the hourly 10 m wind velocities from HARMONIE at the BWFZ (3.02°E 51.70°N) are imposed uniformly in the model domain.

For the extreme conditions, 100% correlation with the waves is assumed and the return value estimates of the 10 m wind velocities and their associated direction as given in the 2nd and 3rd columns of Table 3.2 are imposed uniformly in the model domain.

Water levels
Water levels from the hydrodynamic simulation (Chapter 5) and water level return value estimates are imposed also uniformly in the model domain in the hindcast and extreme conditions runs, respectively.

We note that, the boundaries of the computational spatial grid considered are all open (water), meaning that only the incoming wave energy is propagated into the model and can leave the area freely. The outgoing energy will be wave energy that propagated into the model plus all effects of the physical processes relevant in the considered model (such as refraction and wind forcing in the model domain). On the other hand, because the boundaries are open, these boundaries must be chosen sufficiently far away from the area where reliable computations are needed, so that they do not affect the computational results there. The computational grid shown in Figure 4.1 fulfils this requirement.

4.2.5   Model settings

The SWAN wave modelling was carried out in 3rd-generation mode for wind input, quadruplet interactions and white-capping (wave steepness induced wave breaking). The settings of other physical and numerical parameters in SWAN are listed in Table 4.2.

Model parameter	Settings
Mode	Non-stationary (normal conditions)
	Stationary (extreme conditions)
Generation	3rd generation including quadruplets
White-capping and wind input	Non-linear saturation-based whitecapping combined with wind input of Yan (1987)
Bottom friction	JONSWAP formulation ($c_{JON} = 0.038 m^2 s^{-3}$)
Integration time step	1 hour
Wind forcing	Time-varying and spatially uniform
Wave boundary input	JONSWAP spectra with a peakness parameter of 3.3, a directional spreading of about 25° and time-varying H_s and $T_{m0,1}$ and MWD
Triads	Off
Accuracy	Changes of less than 1% in H_s and $T_{m0,1}$ at 99% of the grid points relatively to the previous iterations, with a maximum of 100 iterations
Water levels	Time-varying and spatially uniform from off-line coupling with the Delft3D Flow model (Deltares, 2014)
Currents	None

Table 4.2   Various settings applied in the SWAN model.

The following comments apply to the parameters given in Table 4.2:
- Simulation mode: The model simulations for the determination of the normal conditions have been carried out in non-stationary mode. For the non-stationary simulations the Backward Space Backward Time (*BSBT)* numerical scheme was used. The time step was set to 60 minutes. When the time resolution of the input is coarser than the integration time step, SWAN interpolates the given input conditions linearly in time.
- Wind input and whitecapping: the SWAN default settings for wind growth and whitecapping are according to the formulation most recently implemented in SWAN; the formulation of Van der Westhuysen et al. (2007).
- Bottom friction: the SWAN default semi-empirical expression derived from the JONSWAP results for bottom friction dissipation (Hasselmann et al., 1973) is applied in this study. Due to the mixed sea and swell situation, the coefficient of 0.038 is considered to account for the effect of swell on bottom friction.
- Current: no currents were applied in the SWAN model since sensitivity runs (including currents) of previous studies indicated that this would not result in improved modeling results.

4.2.6   Model output

Table 4.3 and Figure 4.3 present the locations and depths of the selected model output locations.

The output of the hindcast consists of hourly time series of spectral wave parameters for the period 1 January 1992 till 31 December 2011 at the four output locations. For each stationary simulation (extreme conditions) a set of spectral wave parameters is output 11 at the four output locations

Site:	Latitude	Longitude	Easting	Northing	Depth
Site I	3,038888°N	51,758979°E	502684m UTM31	5734232m UTM31	30.8m MSL
Site II	3,077777°N	51,668601°E	505379m UTM31	5724183m UTM31	25.4m MSL
Site III	2,961111°N	51,694424°E	497312m UTM31	5727053m UTM31	35.1m MSL
Site IV	2,863889°N	51,720246°E	490598m UTM31	5729933m UTM31	38.5m MSL

Table 4.3   Locations and depths of selected output locations for each site in the BWFZ, coordinate system: ETRS89 / UTM zone 31N.
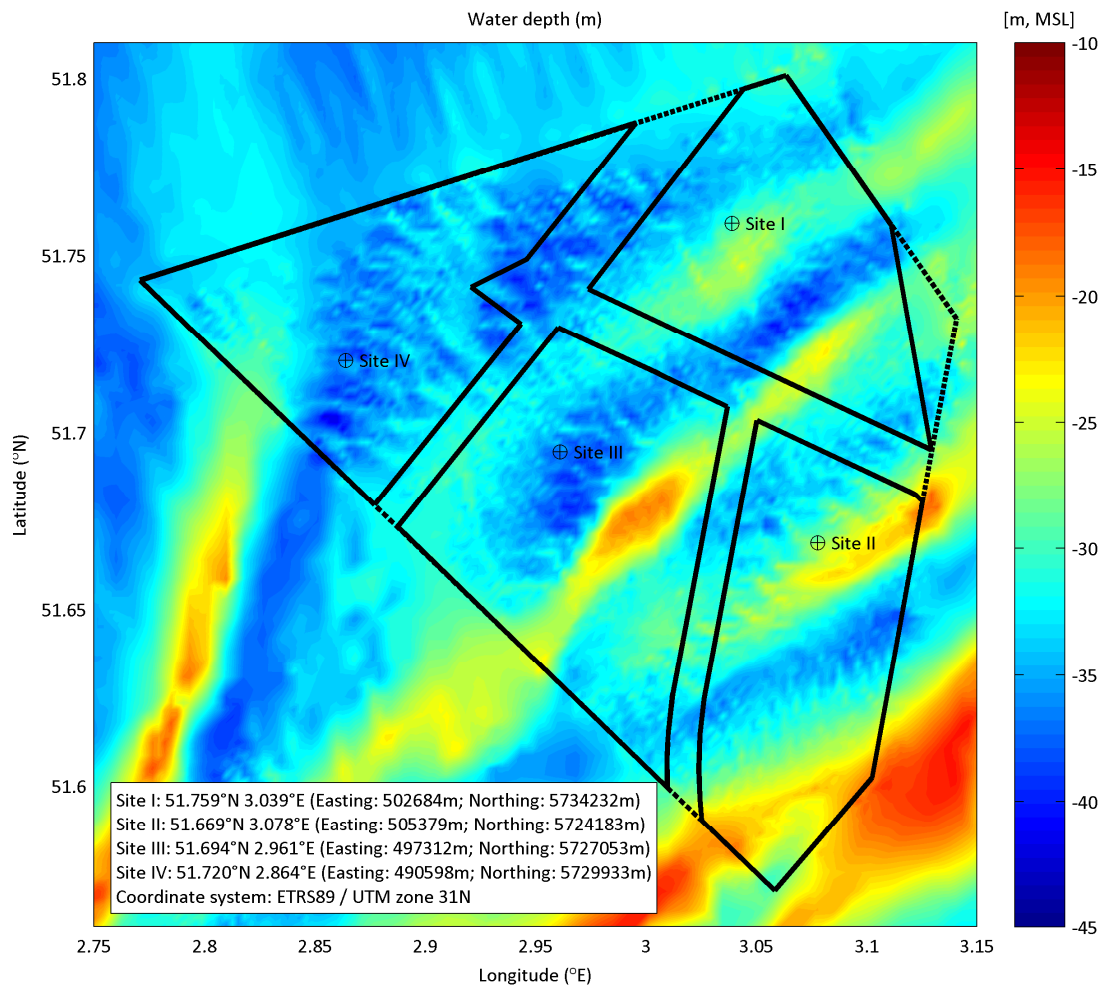
Figure 4.3   Output locations within the BWFZ.

4.2.7   Validation of the results

Given that there are no observations yet available, we have validated the model results by means of a number of checks on the convergence of the model results, boundary effects, and the sensitivity of the results to different model settings (not shown). The settings applied lead, according to our investigations, to a proper modelling of the wave conditions in the model domain. For illustration, Figure 4.4 shows surface plots of significant wave height for two instants of the hindcast. The influence of the sand banks on the wave propagation - the shoaling and de-shoaling of the waves - can be seen in the figure.
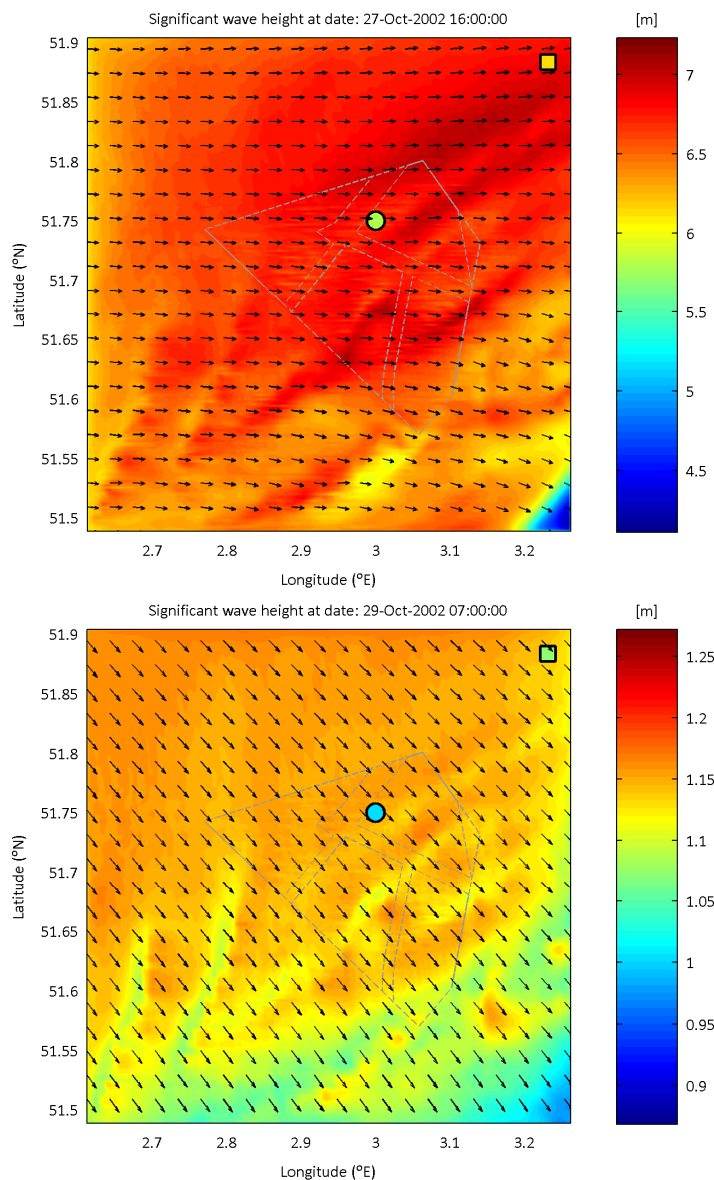
Figure 4.4 Significant wave heights observed in the computational domain of the SWAN model, at two timestamps during the hindcast.

4.3 Normal wave conditions

As said above, for the determination of the normal wave conditions non-stationary wave computations were carried out for a 20-year hindcast period, a period considered long enough for the determination of operational conditions. The associated HARMONIE hourly wind data was used in the joint analyses. The presented normal wave conditions consist of wave roses, joint occurrences tables and *Normal Sea States* (DNV-OS-J101, C402).

The annual wave rose of H_s is presented in Figure 3.17; the monthly roses are shown in Figure 3.18. The yearly joint occurrence table of wave height and direction is given in Figure 3.19. The monthly joint occurrence tables and all other joint occurrence tables (like H_s versus

T_z and H_s versus T_p) are given in Appendix B.1. All joint occurrence tables are also available in the excel-file provided with this report.
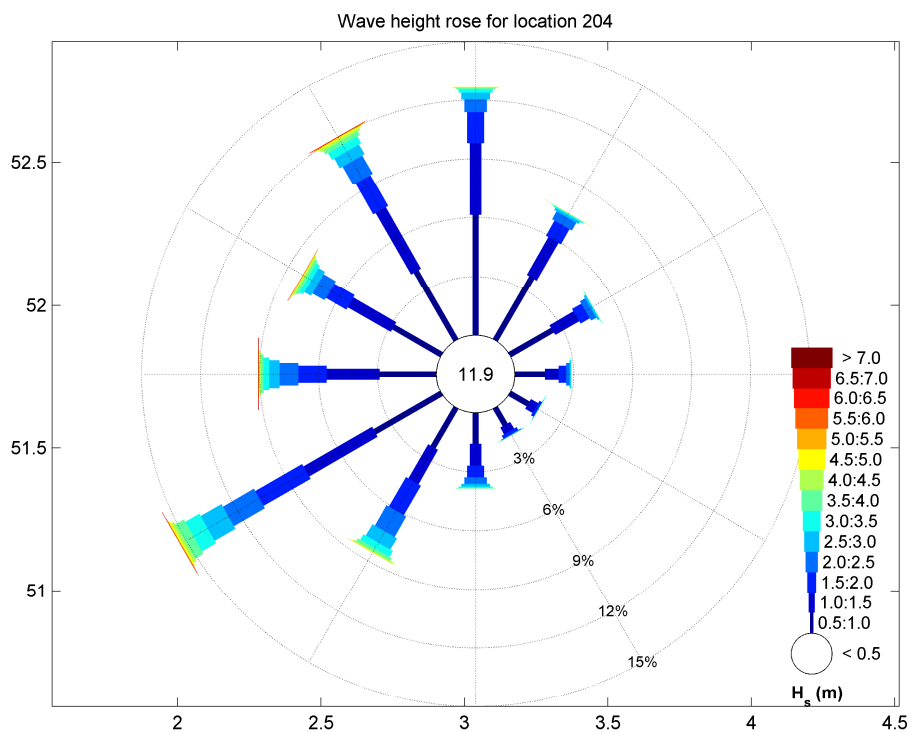
Figure 4.5   Annual wave rose at the selected location for Site I.

Deltares
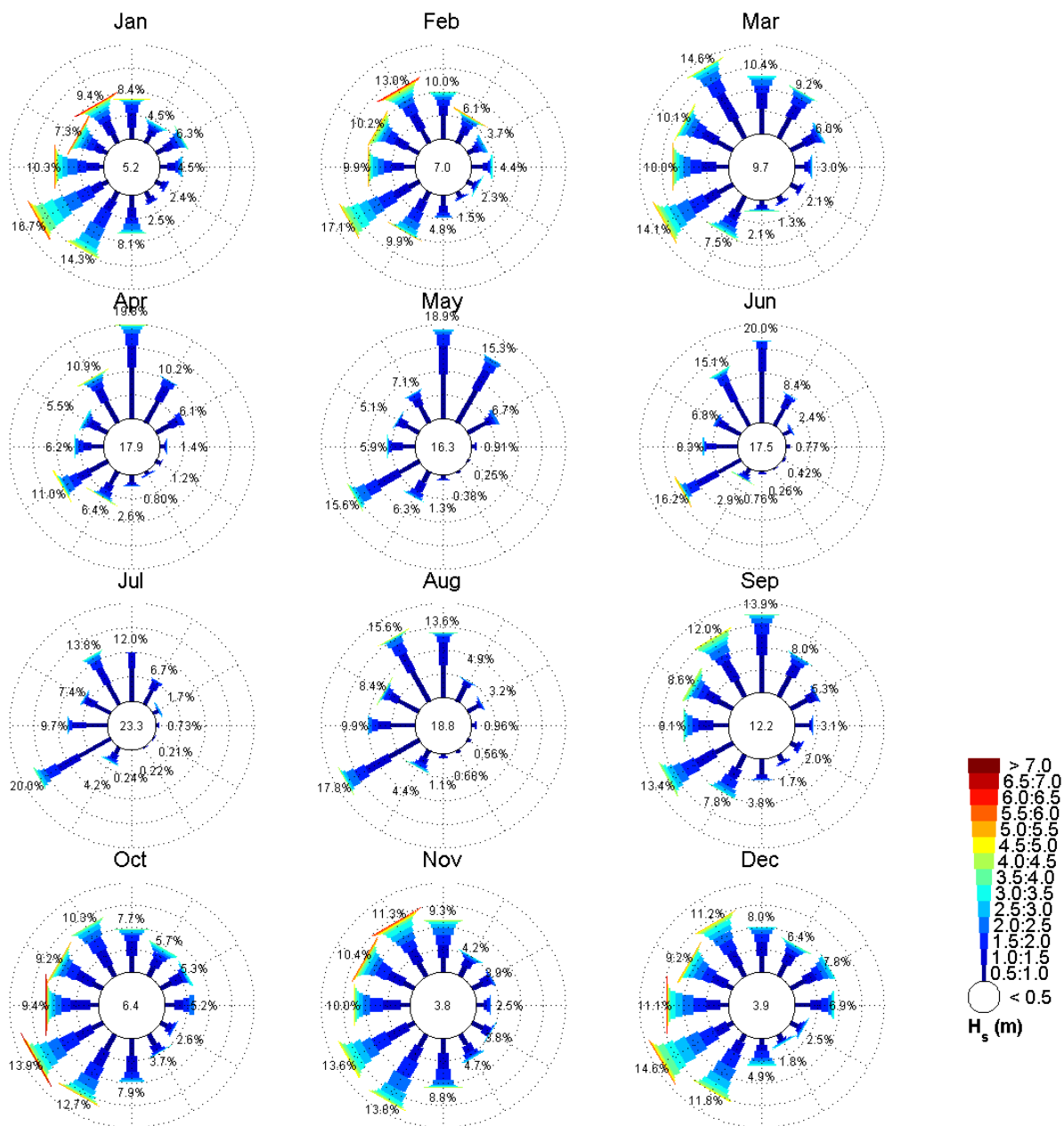
Data from 01-Jan-1992 until 31-Dec-2011 23:00:00 (mean=1.3m, max=6.8m)

Figure 4.6   Monthly wave roses at the selected location for Site I.

H_s (m)	345-15	15-45	45-75	75-105	105-135	135-165	165-195 (MWD °N)	195-225	225-255	255-285	285-315	315-345	Total
>7.0													
6.5-7.0									0.00	0.00			0.00
6.0-6.5									0.00	0.00		0.01	0.01
5.5-6.0	0.00								0.01	0.01	0.01	0.02	0.05
5.0-5.5	0.00	0.00						0.01	0.02	0.01	0.01	0.03	0.08
4.5-5.0	0.01	0.01						0.01	0.08	0.03	0.03	0.07	0.24
4.0-4.5	0.04	0.00					0.00	0.06	0.17	0.06	0.11	0.14	0.58
3.5-4.0	0.08	0.02	0.01				0.02	0.16	0.49	0.15	0.13	0.20	1.26
3.0-3.5	0.17	0.06	0.02	0.02	0.00	0.00	0.07	0.33	0.83	0.29	0.21	0.41	2.41
2.5-3.0	0.34	0.12	0.11	0.05	0.00	0.02	0.15	0.67	1.22	0.53	0.38	0.57	4.18
2.0-2.5	0.66	0.45	0.29	0.17	0.02	0.04	0.33	1.20	1.82	0.96	0.72	1.08	7.73
1.5-2.0	1.58	0.89	0.55	0.39	0.14	0.16	0.59	1.73	2.76	1.44	1.20	1.82	13.24
1.0-1.5	3.67	2.21	1.40	0.69	0.43	0.40	1.12	2.01	4.03	2.68	2.53	3.59	24.76
0.5-1.0	8.11	3.71	2.52	1.54	1.09	1.01	1.57	2.32	3.93	2.90	2.82	4.07	33.60
0.0-0.5	1.90	1.48	1.06	0.69	0.57	0.63	0.52	0.67	1.02	0.94	0.92	1.47	11.87
All year	14.56	8.95	5.95	3.55	2.25	2.26	4.38	9.17	16.37	10.00	9.07	13.48	100.00 (Total)

Table 4.4   Joint occurrence table of wave height versus wave direction at the selected location for Site I.

The wave roses, joint occurrences tables, Normal Sea States (NSS, cf. C402, DNV-OS-J101) and the wind-wave misalignment (the joint occurrence table of the wind direction and the mean wave direction) have been determined using the synchronous wave and wind data (hourly from 1992 until 2011, 20 years).

4.3.1   Wind-wave misalignment

Misalignment between wind and wave direction is an aspect to consider in the design of wind turbines. Figure 4.7 presents the annual joint occurrence table of the wind direction and the mean wave direction. The figure shows that the wind-wave misalignment can be high for waves coming from the North-Northwest, the main swell direction.

MWD (° N)

	345-15	15-45	45-75	75-105	105-135	135-165	165-195	195-225	225-255	255-285	285-315	315-345	Total
315-345	1.17	0.12	0.03	0.01	0.00	0.00	0.01	0.02	0.08	0.23	0.67	4.06	6.40
285-315	0.47	0.11	0.03	0.02	0.01	0.01	0.01	0.06	0.23	0.85	2.84	2.60	7.24
255-285	0.46	0.12	0.05	0.02	0.02	0.02	0.03	0.16	1.38	4.05	2.62	1.46	10.38
225-255	0.48	0.13	0.06	0.04	0.03	0.04	0.11	1.17	10.90	3.45	1.54	1.23	19.19
195-225	0.43	0.11	0.11	0.06	0.09	0.13	0.63	5.65	2.93	0.69	0.50	0.75	12.08
165-195	0.43	0.14	0.15	0.13	0.23	0.56	2.85	1.81	0.45	0.28	0.28	0.38	7.69
135-165	0.52	0.26	0.27	0.30	0.65	1.20	0.65	0.22	0.16	0.15	0.15	0.32	4.84
105-135	0.65	0.49	0.61	1.08	1.08	0.24	0.08	0.05	0.09	0.07	0.06	0.24	4.74
75-105	0.87	1.16	2.07	1.77	0.10	0.03	0.01	0.02	0.04	0.04	0.09	0.26	6.44
45-75	1.53	2.87	2.38	0.12	0.02	0.01	0.00	0.01	0.03	0.04	0.08	0.30	7.39
15-45	3.30	3.11	0.17	0.01	0.00	0.01	0.00	0.01	0.03	0.06	0.08	0.46	7.24
345-15	4.25	0.33	0.03	0.00	0.00	0.01	0.01	0.01	0.05	0.10	0.17	1.41	6.36
	14.56	8.95	5.95	3.55	2.25	2.26	4.38	9.17	16.37	10.00	9.07	13.48	100.00

Wind direction (° N)

All year

Figure 4.7   Joint occurrence table of the wind direction and the mean wave direction at the BWFZ (Site I).

The figures in Appendix B.1 show the misalignment between wind and wave direction for several wind speed classes. The tables show that the wind-wave misalignment significantly reduces with increasing wind speed.

The figures in Appendix B.2 show H_s distribution for wave height (0-7m H_s) – wind direction misalignment cases – wind speed (0-100m/s).

4.3.2   Individual wave height distribution
The individual wave height distribution for a 1-year period is presented in the accompanying excel file. The table presents per directional sector (12 in total) the joint occurrence of the individual wave height and wave period for several wave height and wave period classes.

4.3.3 Normal Sea States

A Normal Sea State (NSS) is characterised by a significant wave height and a peak period. Furthermore, it is associated with a concurrent mean wind speed or wind speed range. The significant wave height $H_{S,NSS}$ of the Normal Sea State is defined as the expected value of the significant wave height conditioned on the concurrent wind speed range. Thus the wind speeds are binned in specific classes, and the mean value of the concurrent (associated) wave height for each class is calculated. These values are presented in Table 4.5. The table also provides the associated peak wave period range, peak enhancement factor of the JONSWAP spectrum, maximum wave height and the percentage of the year characterized by such sea state. The peak enhancement factor is computed from the significant wave height and peak period using Torsethaugen et al. (1984). The associated range of wave periods is defined, as in the DNV standard (DNV-OS-J101, C402) as

$$11.1 \cdot \sqrt{H_s / 9.81} \le T \le 14.3 \sqrt{H_s / 9.81}. \tag{3.11}$$

Wind$_{10m}$ (m/s)	H_s (m)	T_p (s)	Spectrum (-)	Gamma γ (-)	duration (%)	T (s) min - max
< 4	0.6	6.0	JONSWAP	1.44	19.42	(2.8 - 3.6)
4 - 5	0.8	5.8	JONSWAP	1.44	10.99	(3.1 - 4.0)
5 - 6	0.9	5.7	JONSWAP	1.44	11.84	(3.3 - 4.3)
6 - 7	1.0	5.7	JONSWAP	1.44	11.15	(3.6 - 4.6)
7 - 8	1.2	5.8	JONSWAP	1.44	9.96	(3.9 - 5.0)
8 - 9	1.4	6.0	JONSWAP	1.44	8.58	(4.2 - 5.4)
9 - 10	1.6	6.2	JONSWAP	1.44	6.90	(4.5 - 5.8)
10 - 11	1.8	6.4	JONSWAP	1.44	5.59	(4.8 - 6.2)
11 - 12	2.1	6.6	JONSWAP	1.44	4.38	(5.1 - 6.6)
12 - 13	2.3	6.8	JONSWAP	1.44	3.33	(5.4 - 7.0)
13 - 14	2.6	7.1	JONSWAP	1.44	2.55	(5.8 - 7.4)
14 - 15	2.9	7.3	JONSWAP	1.44	1.78	(6.0 - 7.8)
15 - 16	3.2	7.5	JONSWAP	1.44	1.31	(6.3 - 8.2)
16 - 17	3.4	7.6	JONSWAP	1.44	0.89	(6.6 - 8.5)
17 - 18	3.7	7.8	JONSWAP	1.44	0.62	(6.8 - 8.8)
18 - 19	4.0	8.0	JONSWAP	1.44	0.31	(7.1 - 9.1)
19 - 20	4.3	8.2	JONSWAP	1.44	0.18	(7.3 - 9.5)
20 - 21	4.5	8.4	JONSWAP	1.44	0.10	(7.5 - 9.7)
21 - 22	4.7	8.4	JONSWAP	1.44	0.07	(7.7 - 9.9)
22 - 23	5.0	8.6	JONSWAP	1.44	0.02	(7.9 - 10.2)
23 - 24	5.3	8.9	JONSWAP	1.44	0.02	(8.1 - 10.5)
24 - 25	5.3	8.8	JONSWAP	1.44	0.01	(8.2 - 10.5)
25 - 27	5.9	9.3	JONSWAP	1.44	0.01	(8.6 - 11.1)
> 27	6.6	10.0	JONSWAP	1.44	0.00	(9.1 - 11.7)

Table 4.5 Normal Sea States at the BWFZ (Site I). Note that the given values are means and should not be used directly for turbine design without further considerations.

4.4 Extreme wave conditions

4.4.1 Introduction

The extreme conditions are described in terms of Severe Sea States (DNV-OS-J101, C404) and of Extreme Sea States (DNV-OS-J101, C406). For both sea states return values of significant wave height need to be estimated. These are estimated by means of the extreme value analysis method described in Section 1.3, the POT method. This method was used to determine the 50-yr return values of the significant wave height associated with certain classes of the wind speeds at hub height of the Severe Sea States and to determine significant wave height directional 1, 2, 5, 10, 50 and 100-yr return values of the Extreme Sea States.

The extreme wave climate at the BWFZ is described in terms of Severe Sea States, Section 4.4.2, and of Extreme Sea States, Section 4.4.3.

4.4.2 Severe Sea States

In the Severe Sea States analysis the synchronous SWAN wave hindcast and HARMONIE wind data (hourly from 1992 until 2011, 20 years) were used.

The Severe Sea States are defined for a number of hub height wind speed classes and consist of the 50-year return value of the H_s data falling in that class and the associated peak wave period, maximum wave height and wave period range. The associated parameters were determined as follows:

- The associated peak period is computed assuming a linear relationship of the form $T_p = aH_s + b$, with a and b being estimated using the whole 20 years dataset.
- The maximum wave height (H_{max}) is defined as the largest wave height in 1,000 waves ($H_{0.1\%}$) during a given sea state and was computed from the H_s estimates using the Rayleigh distribution[3], i.e.,

$$H_{0.1\%} = 1.86 H_s .$$ (3.12)

- The associated range of wave periods is computed using Eq. 4.2.

The Severe Sea State H_s and associated T_p, H_{max} and wave period range estimates are given in Table 4.6 for a number of classes of the hub height wind speed. Higher values of wind speed are associated with severer wave conditions, which indicate a high correlation between the wind speed and the wave conditions at the BWFZ.

---

[3] *We note that the Battjes and Groenendijk (2000) distribution is generally preferred to the Rayleigh distribution in regions where the highest waves in a sea state may be depth-limited, since it accounts for eventual depth-induced wave breaking. However, given that the area of interest is in an approximately constant depth region with a few depth/slope variations, the estimates of Battjes and Groenendijk (2000), which are based solely on data from foreshores with slopes ranging from 1:20 to 1:250, may be too low. In such situations, to avoid biased low estimates, the Battjes and Groenendijk (2000) distribution should be applied, as done here, using its deep water limit, the Rayleigh distribution, see Caires and van Gent (2012).*

Wind$_{100m}$ (m/s)	H$_s$ (m)	T$_p$ (s)	H$_{0.1\%}$ (m)	T (s) min - max
< 4	2.6	7.4	4.8	(5.7 - 7.3)
4 - 5	2.6	7.5	4.9	(5.8 - 7.4)
5 - 6	2.8	7.6	5.2	(5.9 - 7.6)
6 - 7	3.0	7.8	5.5	(6.1 - 7.9)
7 - 8	3.1	8.0	5.8	(6.3 - 8.1)
8 - 9	3.3	8.2	6.2	(6.5 - 8.3)
9 - 10	3.7	8.6	6.8	(6.8 - 8.7)
10 - 11	3.8	8.7	7.0	(6.9 - 8.9)
11 - 12	3.9	8.8	7.3	(7.0 - 9.1)
12 - 13	4.2	9.1	7.8	(7.2 - 9.3)
13 - 14	4.6	9.5	8.5	(7.6 - 9.8)
14 - 15	5.0	9.9	9.3	(7.9 - 10.2)
15 - 16	5.2	10.2	9.7	(8.1 - 10.4)
16 - 17	5.7	10.7	10.6	(8.5 - 10.9)
17 - 18	5.8	10.7	10.7	(8.5 - 11.0)
18 - 19	6.2	11.2	11.5	(8.8 - 11.4)
19 - 20	6.8	11.8	12.6	(9.2 - 11.9)
20 - 21	6.8	11.8	12.6	(9.2 - 11.9)
21 - 22	7.0	12.0	13.0	(9.4 - 12.1)
22 - 23	7.2	12.2	13.4	(9.5 - 12.3)
23 - 24	7.4	12.4	13.8	(9.6 - 12.4)
24 - 25	7.6	12.6	14.1	(9.8 - 12.6)

Table 4.6   Severe sea states at the BWFZ (Site I). Note that the given values are means and should not be used directly for turbine design without further considerations.

4.4.3 Extreme Sea States

The Extreme Sea States estimates are based on the full 35-year long ERA interim wave data (6-hourly from 1979 until 2013, 35 years) and the full 35-year long HARMONIE 10 m wind velocities. Return value estimates from these data are used to force the SWAN model. Different scenarios for each directional sector and each recurrence interval of 1, 2, 5, 10, 50 and 100 years were determined. The model was run in stationary mode, meaning that each computation calculates a single extreme condition. The resulting Extreme Sea States consist of directional 1-, 2-, 5-, 10-, 50- and 100-yr return values of the significant wave height and the associated peak wave period, MWD, maximum wave height and maximum wave crest. The significant wave height, associated peak wave period and MWD are the output of the SWAN computations. The maximum wave height is determined using Eq. 4.3. The extreme crest height (η_{max}) of the maximal wave height, is determined using the Rienecker-Fenton wave theory (Rienecker and Fenton, 1981). This maximum crest height is determined on the basis of the *total water depth* (accounting for the extreme wave levels in Chapter 5 and the local water depth), the maximum wave height ($H_{0.1\%}$) and the corresponding wave period which is taken equal to the peak wave period. In order to illustrate the variation of the extreme wave conditions over the BWFZ, Figure 4.8 presents an example output of significant wave height and peak wave period of 50-yr return value. The remaining figures for all other extreme wave conditions and 12 directional sectors are available in Appendix B.3 (maximum still water level) and B.4 (minimum still water level).
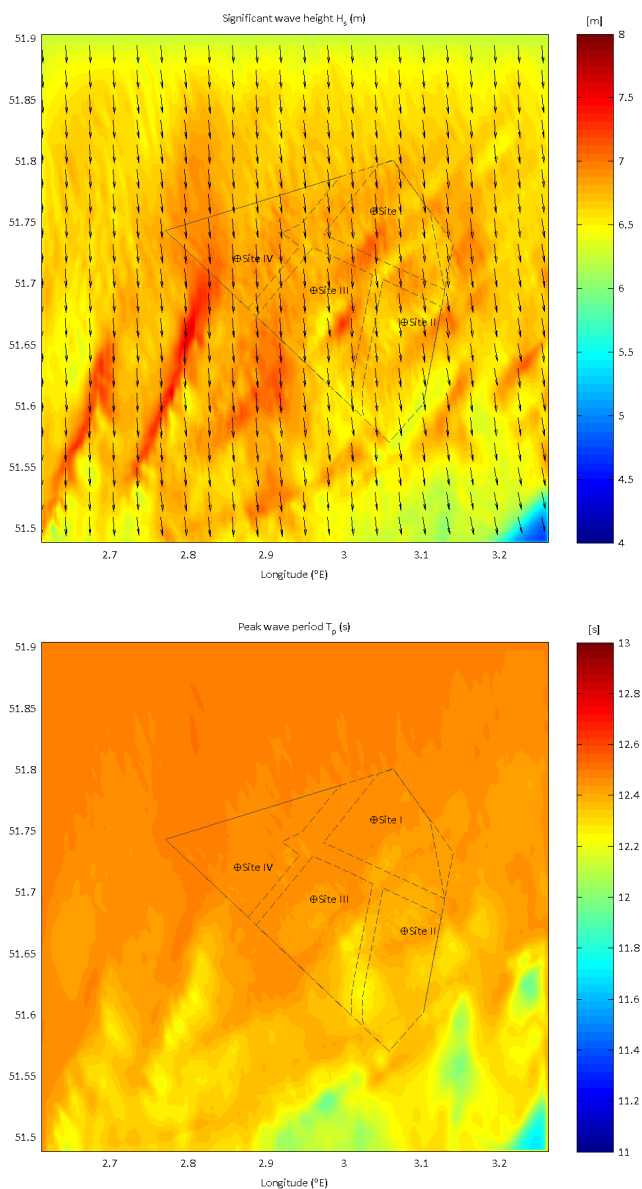
Figure 4.8   Extreme wave condition for 50yr return period and maximum still water level.

The ERA-interim significant wave height data were analysed using the POT method and 12 directional sectors (each 30° wide). These 12 sectors of mean wave direction are 345ºN-15ºN, 15ºN-45ºN, …, 285ºN-315ºN and 315ºN-345ºN. Only the data falling in the sector of interest are taken into account. As was the case in the EVA of the wind data, the data are stratified into sectors before the extreme value analysis is carried out, meaning that a given storm may be considered in more than one sector. The associated peak period is computed assuming a power relationship of the form $T_p = aH_s^b$, with a and b being estimated using the POT data used for the significant wave height GPD fit of the sector under consideration. The associated MWD is taken as the average MWD of the POT data used for the significant wave height GPD fit of the sector under consideration.

Deltares

The Extreme Sea State H_s and associated T_p, T_z, MWD, H_{max}, and η_{max} estimates can be found in the excel-file provided with this report. Also the wind speed return values are presented in the table there. As expected, return value estimates are higher for the Southwest-Northwest sectors and lower for the Northeast-Southeast sectors. For illustration, the return value plot of the ERA-interim data used to force the SWAN boundaries for the North-Northwest sector (NNW, 315°N: 345°N) sector is shown in Figure 4.9. As can be seen in the excel-file the omni-directional estimate of the 50-year return value of the significant wave height is of 8.7m with an associated U_{10} of 30 m/s.
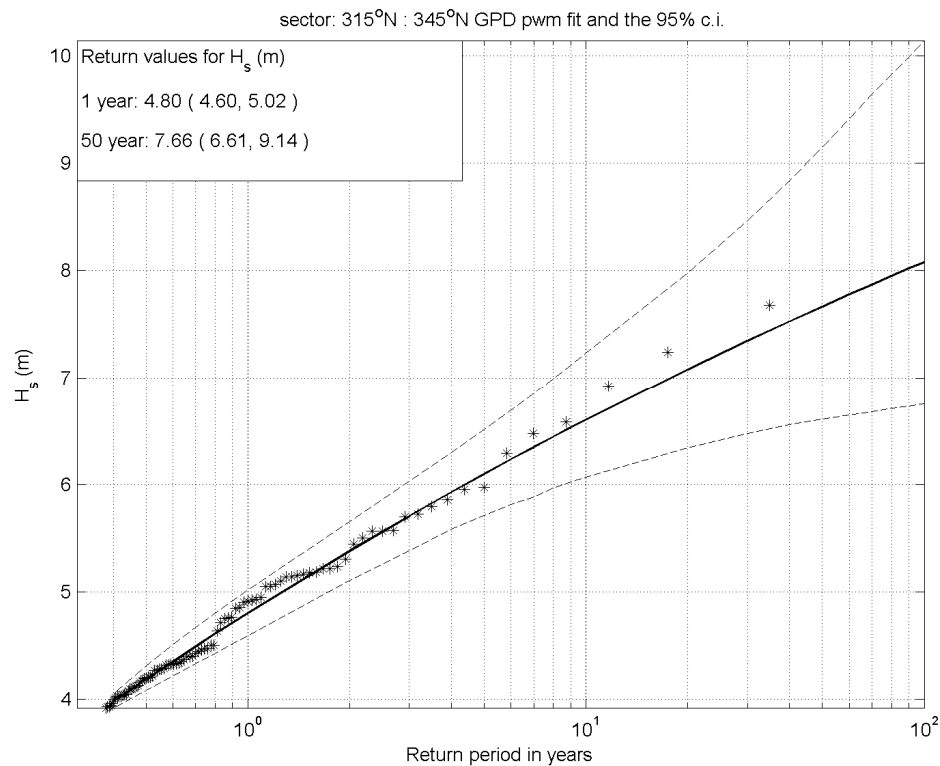

Figure 4.9 *Significant wave height return value plot for sector NNW (315°N: 345°N). The dashed lines are the associated 95% confidence intervals. The POT data are represented by the asterisks.*

In addition to the extreme parameters described above the wave parameters for the 10.000-yr sea state are determined and available the excel-file provided with this report.

4.4.4 Storm duration
Specifically, in the present application we have treated cluster maxima at a distance of less than 48 hours apart as belonging to the same cluster (storm).

In comparatively deep water, maximum wave height H_{max} is calculated from the wave parameters H_s and T_z according to the Rayleigh distribution assuming a sea state duration of 3 hours.

4.5   Shoaling and wave breaking

The considered wave data includes effects of shoaling and wave breaking. These effects lead to a spatial variation in the wave conditions in the BWFZ. Depth induced wave breaking may take place as a result of shoaling and limited water depth. Such breaking may take place either before the waves arrive at the site, or when they have arrived at the site. In both cases, the wave breaking implies that a depth-dependent limitation is imposed on the waves at the site. There are three types of wave breaking to be identified, which are based on the so-called surf similarity parameter, ξ:

- surging breaker ($\xi > 2$);
- plunging breaker ($0.4 < \xi < 2$) and
- spilling breaker ($\xi < 0.4$).

The surf similarity parameter can be determined by the following formula

$$\xi = \frac{\tan \beta}{\sqrt{H_s / L_0}} , \tag{3.13}$$

where β is the bottom slope angle and L_0 the deep water wave length. In order to determine the most severe type of wave breaking at the wind farm the surf similarity parameter was computed considering a wide range of bottom slopes and the upper limits of the 50 years return value estimates in the BWFZ (Figure 4.9) and in all cases the surf similarity parameter is lower than 0.4. Therefore, it is expected that only spilling breaker types are likely to occur in the BWFZ.

4.6   Wave spectra

Based on both measurements as model results the JONSWAP spectral form (Hasselmann et al., 1973, DNV-OS-J101, C300) is assumed to be valid for the waves in the BWFZ. Its form is

$$S(f) = \alpha g^2 \ (2\pi)^{-4} f^{-5} \ \exp\left(-\frac{5}{4}\left(\frac{f}{f_p}\right)^{-4}\right) \gamma^{\exp\left(-0.5\left(\frac{f-f_p}{\sigma f_p}\right)^2\right)}, \tag{3.14}$$

where
- f is the wave frequency,
- f_p is the peak frequency ($1/T_p$),
- σ is the spectral width parameter and takes a value of $\sigma=0.07$ for $f \leq f_p$ and $\sigma=0.09$ for $f > f_p$, and
- γ is the peak enhancement factor.

Furthermore, based on the relation found between the measurements of different wave period measures a JONSWAP spectrum with a peak enhancement factor (γ) of about 1.134 is expected to characterise the sea states in the BWFZ well.

4.7   Impact of currents and water level on waves

Currents may have an impact on the wave heights and to a lesser extent on the wave lengths. A significant impact of the currents on the waves is only expected for relatively strong

Deltares

currents (above 1 m/s, depth-averaged), and relatively low waves (in the order of a few meters). The expected effects would then be:

- reduced wave heights in cases of relatively strong following currents (currents with the same direction as the waves);
- increased wave heights in cases of relatively strong opposing currents (currents with opposite direction of the waves).

Given the expected magnitude and main directions of the currents at the BWFZ (see also chapter 6), the effect of currents on the waves are not considered to be significant at the BWFZ. This is explained by the fact that the waves are relatively high and that the currents are limited in speed and are directed parallel to the coast, not opposing the more extreme and common NW waves at the BWFZ.

Depth variations also may have an impact on the wave heights. The variations of the significant wave height within the BWFZ site are calculated by the SWAN computations and are therefore fully considered in this study. As explained in Section 4.5, the water depth is not taken into account in the computations of $H_{0.1\%}$, but it is taken into account in the computations of η_{max}. In shallower regions waves are more non-linear and therefore η_{max} can be higher. The η_{max} parameter mentioned in Section 4.4 and the values in the table representing the extreme sea state were computed considering a local depth and water level corresponding to the return period, following from the water level analysis (chapter 5).

5 Water levels

5.1 Methodology

The objective of this study task is to determine the operational and extreme water level conditions at the Borssele Wind Farm Zone. The operational and extreme conditions are based on the results of hydrodynamic modelling results for a period of 20 years (1992 - 2011) with Delft3D-FLOW. The model setup is briefly described in Section 5.2.

5.1.1 Determination of the normal conditions

The normal conditions consist of the average tidal levels at the BWFZ site (DNV-OS-J101, E101). The tide levels have been determined by harmonic analysis of the computed water levels (1992 – 2011) in the BWFZ. The resulting astronomical components were used to predict a 19 year period. The tidal levels were computed directly from the tidal time series based on the definitions given in the Admiralty Tide Tables (ATT, 2014).

5.1.2 Determination of the extreme conditions

Extreme high and low water levels were derived for five return periods (1-, 2-, 5-, 10-, 50-yr) by means of extreme value analysis of the BWFZ total (tide + surge) water level 20-year time series (1992 – 2011). The extreme value analysis approach used is based on the POT-GPD method.

5.2 Hydrodynamic modelling

5.2.1 Description of Delft3D-FLOW

The hindcast water level and current modelling was based on the Delft3D-FLOW modelling programme (Version 5.00.10.1983, Nov. 16, 2012). This program was developed by Deltares (formerly Delft Hydraulics) for the modelling of unsteady water flow and transport of dissolved matter. Delft3D-FLOW solves the three-dimensional shallow-water equations for given boundary conditions. The equations are solved by an implicit finite difference method (ADI) on a staggered (spherical or orthogonal curvilinear) grid. For the present application, Delft3D-FLOW was used in the one layer (depth-averaged) mode in spherical (geographical) space.

In the continuity equation, the mass balance for each grid cell is considered. In the momentum equations the following influences are included:
*   acceleration due to changes in the local velocity (convective accelerations);
*   earth rotation;
*   water level gradients;
*   bed friction;
*   horizontal momentum exchange due to eddy viscosity;
*   density differences (not in this study);
*   wind and air pressure variations.

The Delft3D-FLOW User Manual includes all technical background information and can be downloaded from: oss.deltares.nl/documents/21119/22242/Delft3D-FLOW_User_Manual.pdf.

5.2.2 Computational grids

In order to accurately simulate water level and current variations at the BWFZ, it is necessary to use both a large-scale model, which includes processes such as tidal propagation and storm surges, and a set of detailed models covering the area of interest which properly schematises the small-scale hydrodynamic processes. To this purpose, a combination of off-line nesting and *Domain Decomposition* (DD) was applied to dynamically link the large-scale Continental Shelf Model with the detailed models covering the BWFZ. Details of the various computational grids and method of nesting are given in Table 5.1. All computational grids used are shown in Figure 5.1. Figure 5.2 shows the two smaller domains in more detail.

Grid name	Max. extent [approx. km]	Nr. of active gridcells [-]	Resolution [m]	Colour in Figures	Nesting method
DCSM	1500 x 1500	18.931	9000	Blue	-
Regio	475 x 400	10.265	3000	Red	Offline in DCSM
DD600	114 x 85	17.687	600	Green	DD in Regio
DD200	45 x 45	52.650	200	Orange	DD in DD600

Table 5.1   Details of the various computational grids and method of nesting.
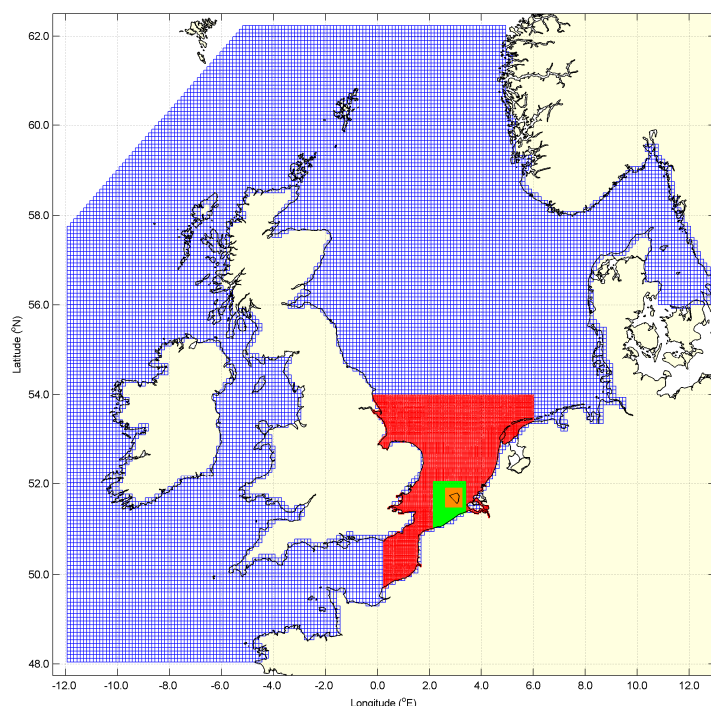

Figure 5.1   Computational grids of Continental Shelf Model (blue mesh) and detailed domains (respectively red, green, orange, black) covering the BWFZ.
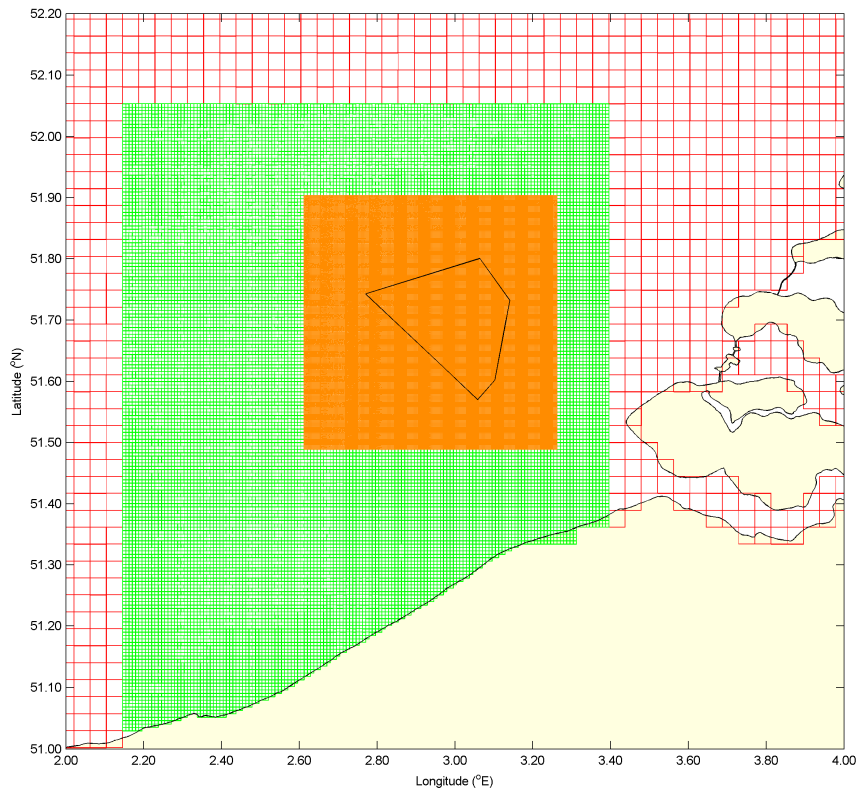
Figure 5.2   Computational grid of detailed domains (DD600 and DD200).

5.2.3   Depth schematisation

The depth schematisations of the detailed model domains were based on the bathymetry sources listed in Chapter 2. Depending on the density of the available depth samples in relation to the mesh size of the detailed model domain, the depth samples were interpolated onto the computational grid by means of gridcell-averaging or triangular interpolation.

The depth schematisations of all domains are presented in Figure 5.3. The depth schematisations of the detailed domains are presented in Figure 5.4. The sand waves are clearly visible on these figures.
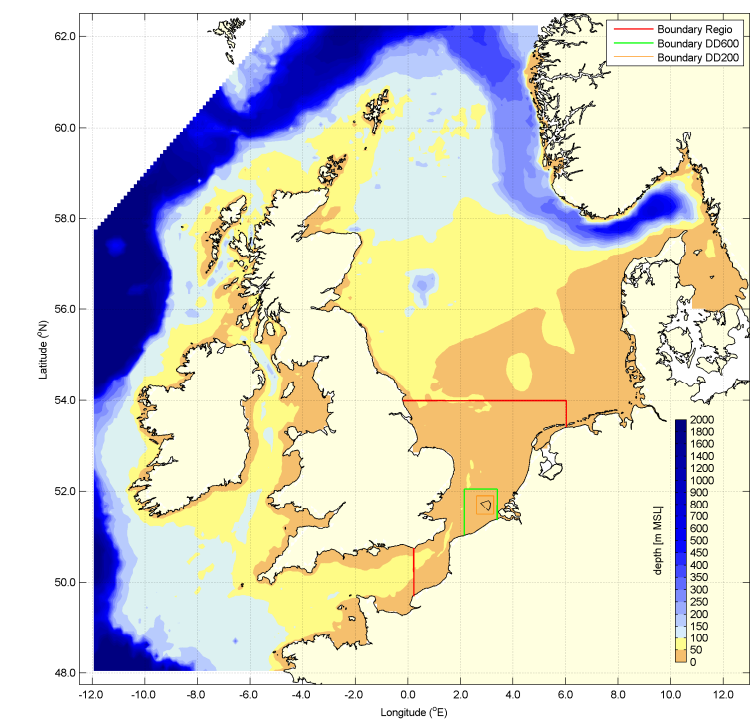
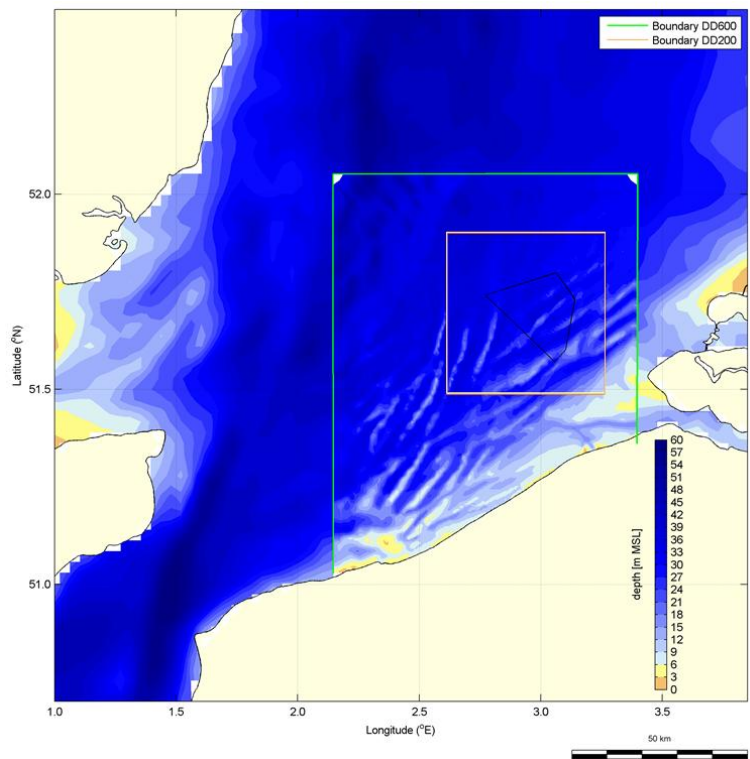*Figure 5.3   Depth schematisation of all model domains.*

Figure 5.4   Depth schematisation of the regio and detailed domains.

5.2.4 Boundary conditions

The tidal dynamics in the model are driven by tidal water level variations prescribed at the open boundaries of the Continental Shelf Model (DCSM) with astronomic constituents. A set of 11 main tidal constituents were applied, including M2, S2, N2, K2, O1 and K1. Note that the amplitudes and phases of the astronomic constituents have been thoroughly calibrated; see e.g. Gerritsen et al. (1995).

In addition to the tidal forcing, time- and spatial-varying wind and air pressure fields were forced to the model domains. These fields were based on the ERA-Interim global re-analysis database and include at 6-hour intervals hourly-mean wind and air pressure data on a 0.75° x 0.75° geographical mesh (see also Chapter 2).

5.2.5 Various model settings

Table 5.2 presents various model settings used in the regional and the detailed domains covering the BWFZ. The assessment of the model settings was based on sensitivity analyses and model calibration (e.g. Deltares, 2012). Note the decreasing values for the horizontal eddy viscosity and Manning bed roughness with the higher resolution domains. This is explained by the fact that higher resolution models are better able to solve relatively small-scale flow patterns as well as bed features, as compared to low resolution domains.

Model parameter	DCSM	Regio	DD600	DD200
Time integration step	10 min	7.5 s		
Horizontal eddy viscosity	10 m^2/s	10 m^2/s	2 m^2/s	2 m^2/s
Roughness (Manning)	spatially varying	0.03 $m^{1/3}$/s	0.03 $m^{1/3}$/s	0.026 $m^{1/3}$/s
Gravitational acceleration	9.81 m/s^2			
Wind drag coefficients	α_1 = 0.0015 (5 m/s) α_2 = 0.005 (40 m/s)			

Table 5.2   Various settings applied in the Delft3D-FLOW model domains.

5.2.6 Model validation

The hydrodynamic modelling for the BWFZ applies a similar model setup (overall grids and boundary conditions) as used for the an extensive modelling study for East Anglia Offshore Windfarm (Deltares, 2012). In the 2012 study the hydrodynamic models were calibrated, showing very good comparisons with a large set of water level and current measurements: root-mean-square errors of respectively about 0.1 m and 0.1 m/s, and correlation coefficients higher than 0.95 for both parameters.

In the present study, the modelling results (water levels and currents) were compared with similar results from the 2012 study for a location closest to BWFZ: ZW Ackaert. The time-series comparison between the two simulations is given in Figure 5.5. This figure shows that the results are very similar. Only incidentally the current magnitude shows a small bias (few cm/s), which is mainly explained by a different wind forcing (HARMONIE in the present study versus ERA-Interim in the 2012 study) and, to a lesser extent, by the different extents, dimensions and updated depths of the detailed domains (DD600 and DD200).
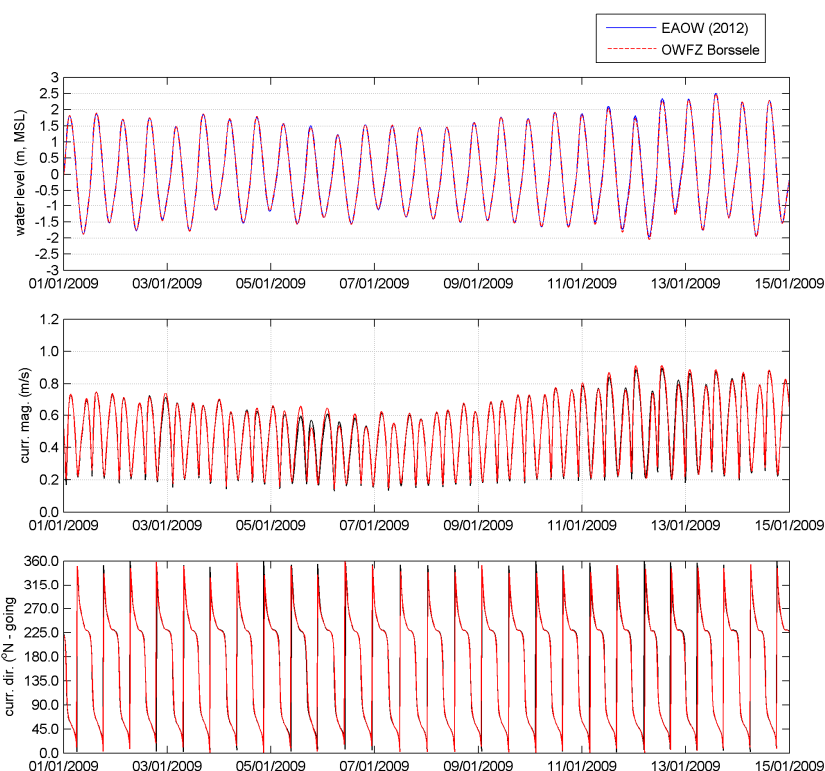
Figure 5.5   Comparisons between water level, current magnitude and direction at ZW Ackaert, as computed in the present study and the 2012 study for East Anglia Offshore Windfarm

5.2.7   Hindcast modelling

Hindcast modelling was carried out for a continuous period of 20 years: 1992 – 2011 under the forcing of tide, wind and air pressure gradients. Time-series of computed water levels and currents were stored for 239 locations in the BWFZ, given in Chapter 2. The stored time-series served as basis for the operational and extreme water level and current conditions as presented in the next sections.

5.2.8   Example time-series

Example time-series of wind speed, wind direction, water level, current magnitude and current direction are given in Figure 5.6 and Figure 5.7 for the period with respectively maximum positive and maximum negative surge in the hindcast period 1992 – 2011.

Figure 5.6   Time-series of wind speed, direction, water level, current magnitude and direction for a period of maximum positive surge in the hindcast period 1992 – 2011 at BWFZ (Site I).

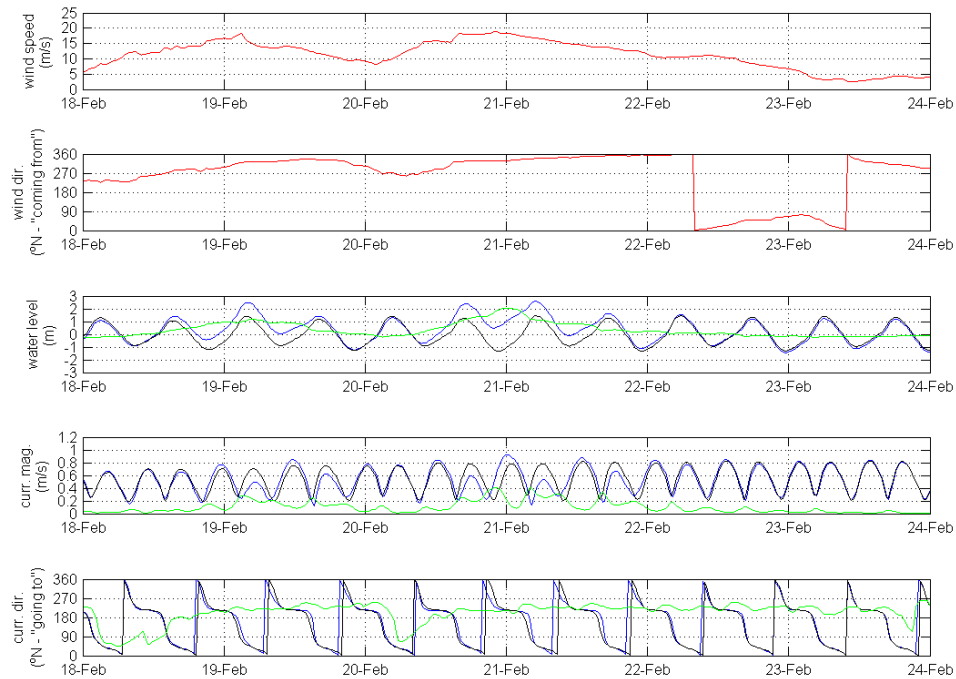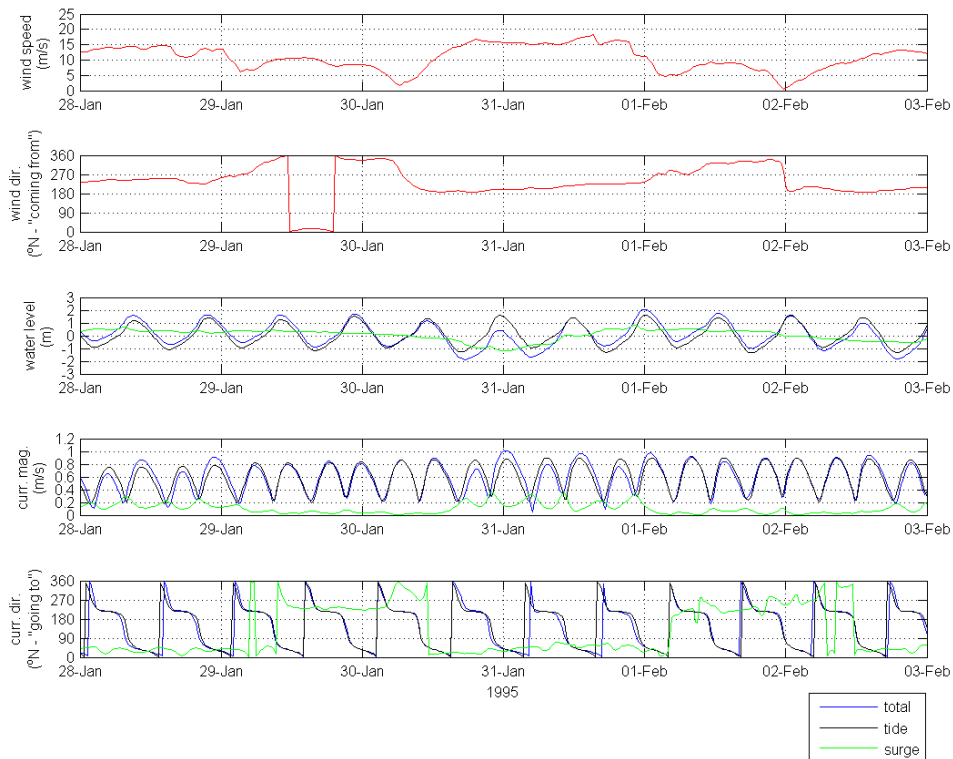*Figure 5.7   Time-series of wind speed, direction, water level, current magnitude and direction for a period of maximum negative surge in the hindcast period 1992 – 2011 at BWFZ (Site I).*

5.3 Reference water levels and tides

5.3.1 Average tide levels

The average tide levels derived from the BWFZ water levels for Site I are given in Table 5.3 relative to MSL and LAT. The levels are rounded to the nearest 0.05m.

Tide level	Relative to MSL (m)	Relative to LAT (m)
Highest Astronomical Tide (HAT)	1.90	3.40
Mean High Water Spring (MHWS)	1.45	2.90
Mean High Water Neap (MHWN)	0.85	2.30
Mean Water Level (MSL)	0.00	1.50
Mean Low Water Neap (MLWN)	-0.85	0.65
Mean Low Water Spring (MLWS)	-1.15	0.35
Lowest Astronomical Level (LAT)	-1.50	0.00

Table 5.3   Average tide levels at the BWFZ (Site I).

5.4 Extreme water levels

The results of the extreme value analysis for extreme high water levels (excluding sea level rise due to climate change) are given in Figure 5.8 and Table 5.4 and for extreme low water levels in Figure 5.9 and Table 5.5 (rounded to the nearest 0.05 m). The return value plots show the peak water levels (asterisks), the fit (straight line) as well as the 95%-confidence levels (dashed lines).

Return period (years)	relative to MSL (m)
1	2.30 (2.25 - 2.35)
2	2.40 (2.35 - 2.50)
5	2.60 (2.45 - 2.75)
10	2.70 (2.55 - 2.95)
50	3.00 (2.70 - 3.50)
100	3.15 (2.75 - 3.75)

Table 5.4   Extreme high water levels at the BWFZ (Site I).

Figure 5.8   High water levels return value plot for the BWFZ (Site I). The dashed lines are the associated 95% confidence intervals. The POT data are represented by the asterisks.

Return period (years)	relative to MSL (m)
1	-1.70 (-1.75 – -1.65)
2	-1.75 (-1.80 – -1.70)
5	-1.85 (-1.95 – -1.80)
10	-1.90 (-2.05 – -1.80)
50	-2.10 (-2.35 – -1.90)
100	-2.15 (-2.50 – -1.95)

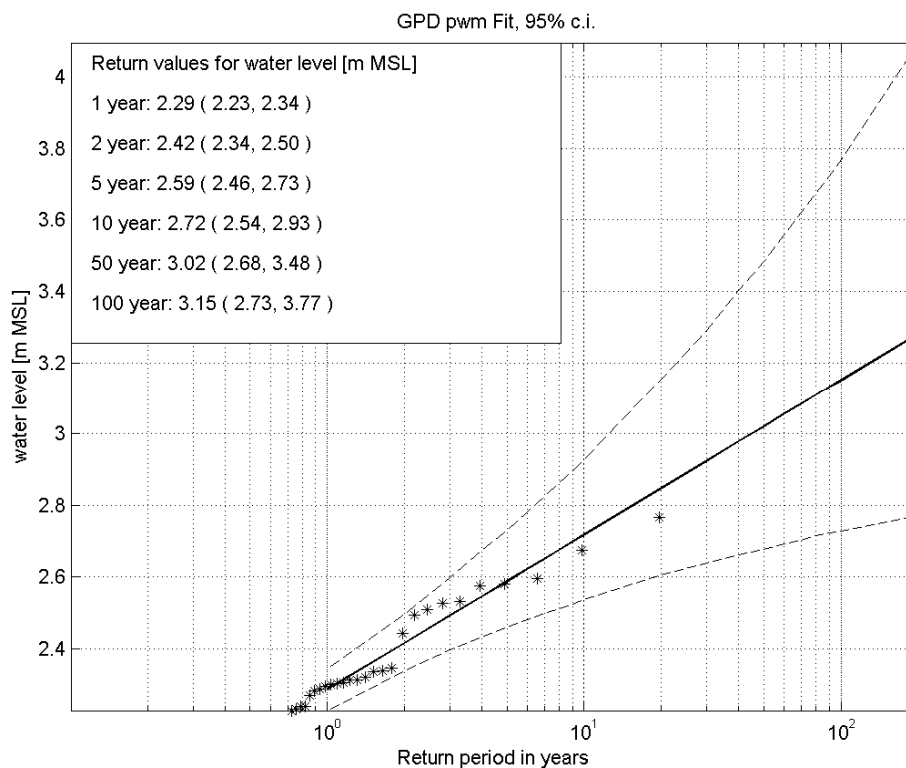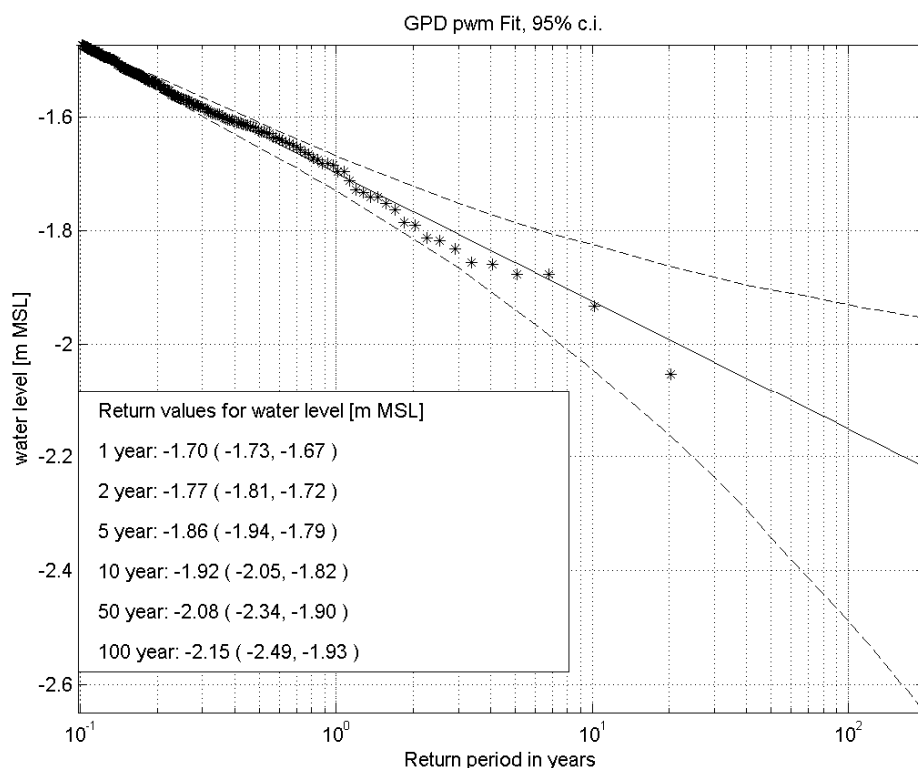*Table 5.5   Extreme low water levels at the BWFZ (Site I).*

Figure 5.9   Low water levels return value plot for the BWFZ (Site I). The dashed lines are the associated 95% confidence intervals. The POT data are represented by the asterisks.

5.5   Long term sea level change

The latest IPCC projections of global mean sea level rise until 2100 relative to 1986–2005 for four emission scenarios (RCP) are presented in Figure 5.10 (IPCC, 2013). The solid lines show the median projections, the dashed lines show the likely ranges for RCP4.5 and RCP6.0, and the shading the likely ranges for RCP2.6 and RCP8.5. This figure shows a projected global mean sea level rise of between 0.10 – 0.25 m in 2040, 0.20 - 0.5 m in 2065 and between 0.30 – 1.0 m in 2100.

Regionally the sea level changes may differ from the global mean sea level rise. Figure 5.11 shows that for the North Sea area the relative sea level changes varies between 0.3 – 0.7 m in the period 2081 – 2100 relative to 1986 – 2005 (IPCC, 2013) for the different emission scenarios. Note that this range is lower than the range of the global mean sea level rise.

Based on the available data on global and regional mean sea level rise, we recommend accounting for a sea level rise of 0.2 m in the coming 25 years and of 0.4 m in the coming 50 years.
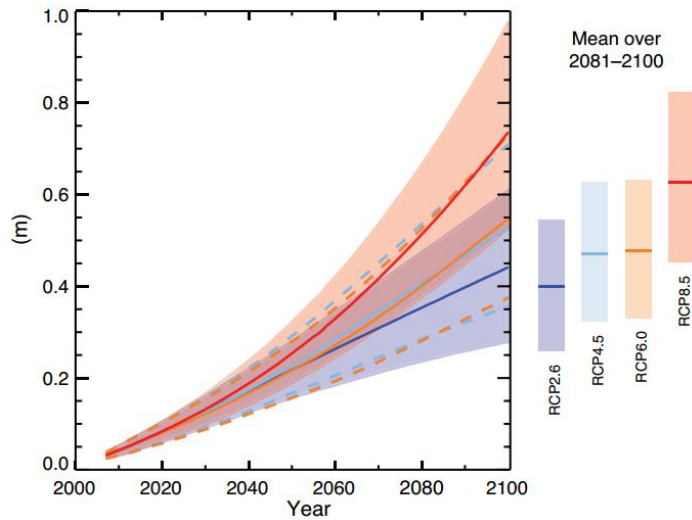
Deltares

Figure 5.10 IPCC projections of global mean sea level rise relative to 1986–2005 for four emission scenarios (IPCC, 2013, Fig. TS.22).
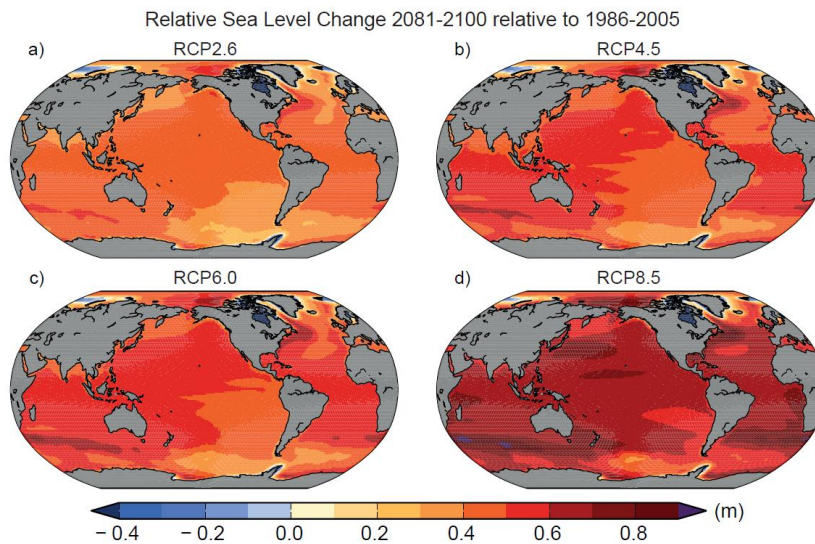

Figure 5.11 IPCC projections of regional relative sea level changes relative to 1986–2005 for four emission scenarios (IPCC, 2013, Fig. TS.23).

6 Currents

6.1 Methodology

The objective of this study task is to determine the operational and extreme current conditions at the BWFZ (Site I). These conditions were assessed by means of detailed analyses of the hindcast simulations with Delft3D-FLOW for the period 1992 – 2011 (Section 5.2). The oceanographic convention is used for the current directions, so all current directions are "going to" clockwise from North.

6.1.1 Determination of the normal conditions

Annual joint occurrence tables and roses of the total (tide + surge) currents were derived by analysing the 20-year current time-series. Currents at various depth layers were assessed by assuming a 7th-power profile in combination with 1.5% times the wind speed, following DNV (2010). The separation between total (tide + surge) and surge currents was based on subtraction of modelling results for 'tide + wind' and 'tide only'.

6.1.2 Determination of the extreme conditions

Extreme total current speeds were determined for 12 directional sectors (30° wide) for five return periods (1-, 2-, 5-, 10-, 50-yr) by means of extreme value analysis. The same POT-GPD approach was followed as for the extreme value analyses of the wind, waves and the water levels. Extreme current estimates at various depth layers were assessed by assuming a 7th-power profile in combination with 1.5% times the wind speed, following DNV (2010). This transformation assumed the associated extreme wind speed (in the direction of the current) and the associated extreme total water level.

6.2 Operational conditions

The joint occurrence table of the annual depth-averaged current speed (u_{mag}) and direction (u_{dir}) for the BWFZ (Site I) is given in Figure 6.1. The two dominant tide-related flow directions NNE and SSW can be clearly observed. Figure 6.2 shows the annual total current roses in and around the BWFZ for all four sites. Note that no large spatial variations are found.
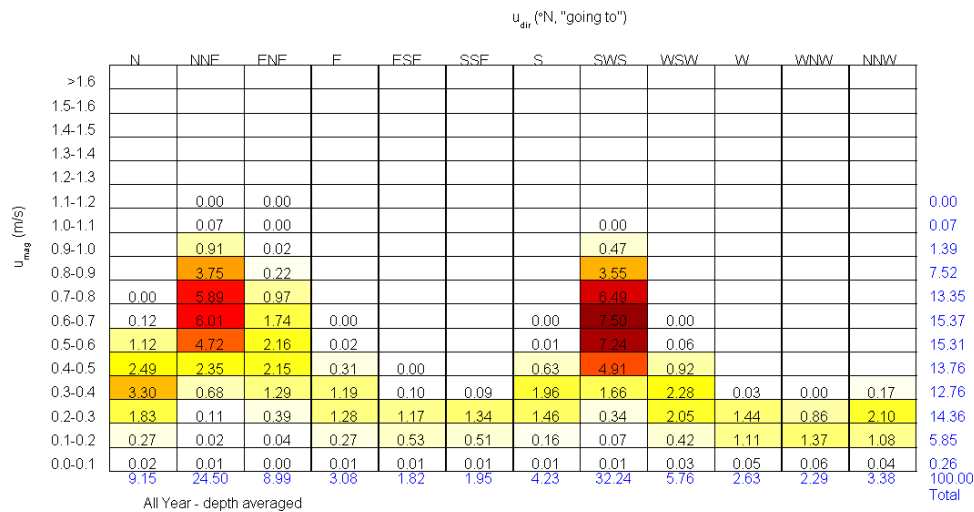
Figure 6.1   Joint occurrences of the depth-averaged current speed and direction at the BWFZ (Site I).
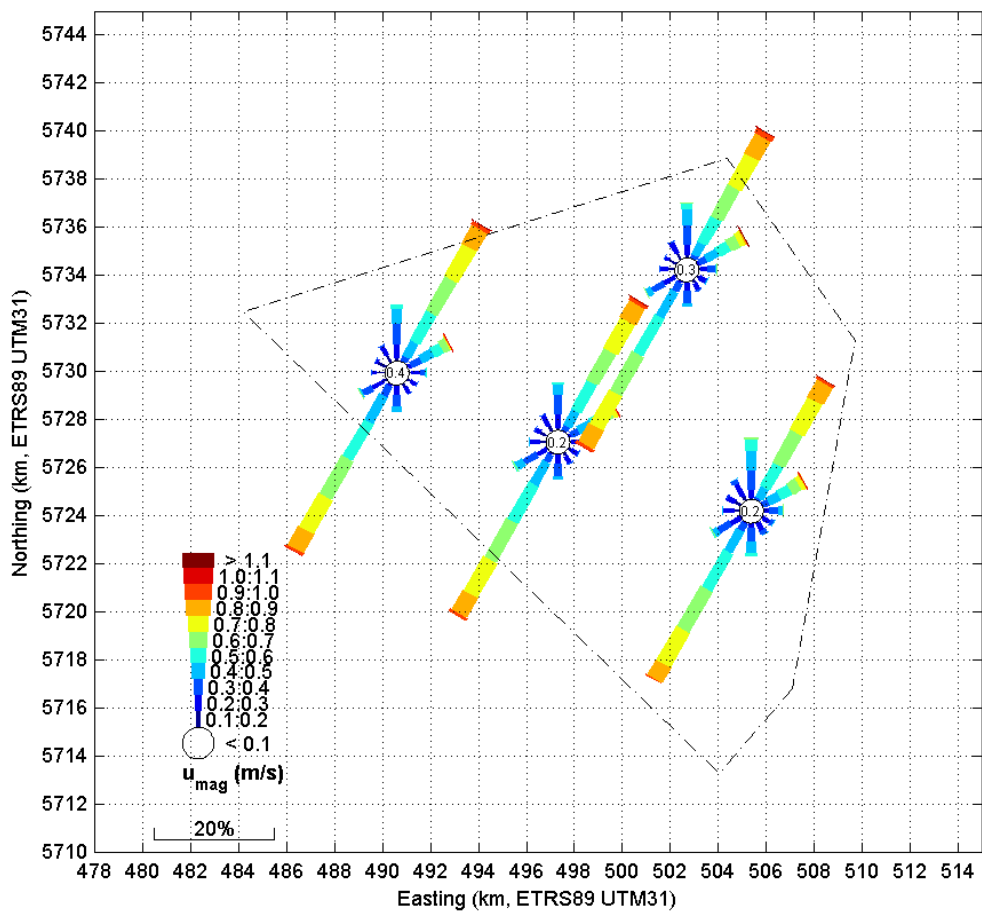
Figure 6.2   Annual current roses in the four wind farm sites of the BWFZ.

The depth-averaged currents were transformed to currents at various depth levels by assuming the DNV method (DNV, 2010). This method assumes the addition of:
3   1/7th-power current profile;
4   1.5% times the wind speed (U10), linearly decreasing to zero at the seabed.

Figure 6.3 presents two examples of a current profile with an opposing and following current with respect to the wind.
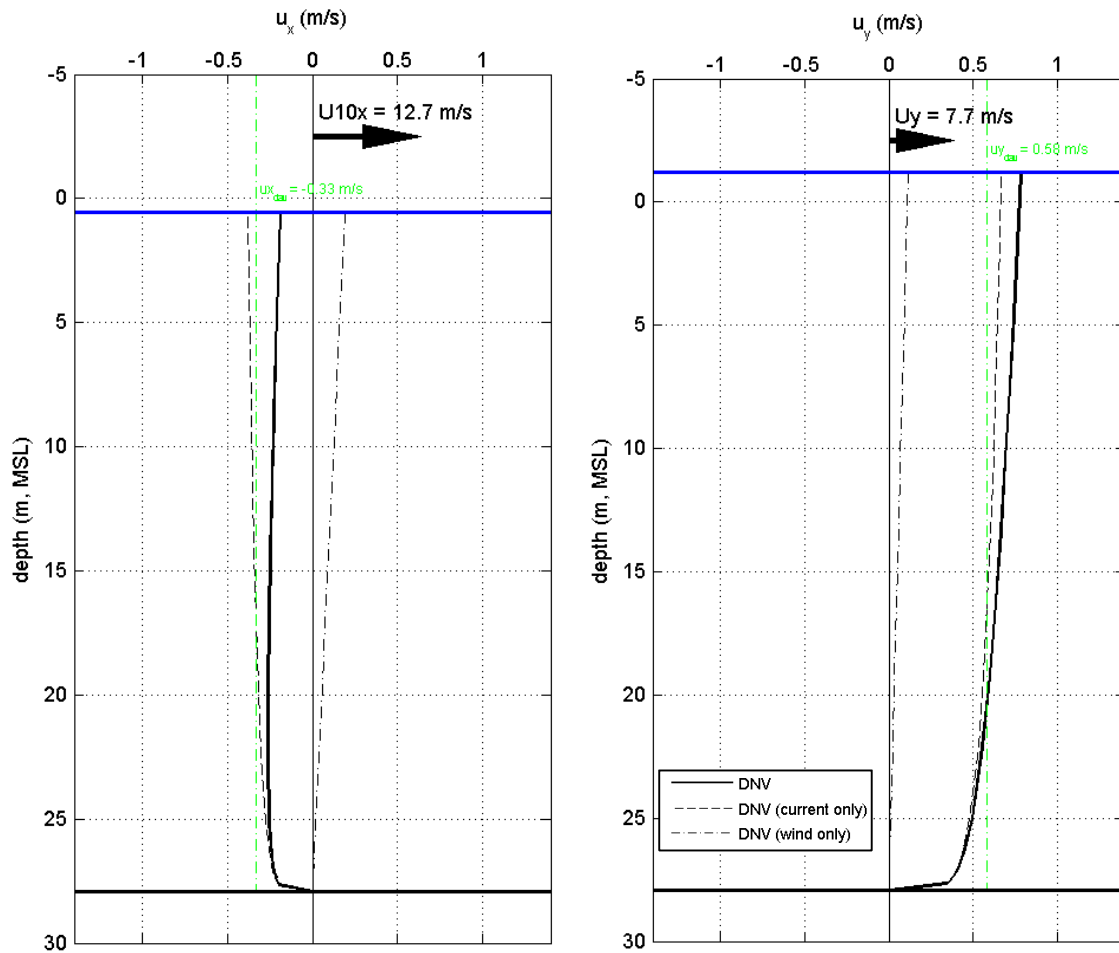
Figure 6.3   Illustration of DNV vertical current profiling method for opposing (left) and following (right) current with respect to the wind direction.

Joint-occurrence tables of current speed versus direction for respectively 100%, 75%, 50%, 25% and 5% of the total water depth are included in Appendix C.

6.3   Extreme conditions

The results of the POT-GPD fits resulting from the extreme value analysis for extreme current speeds for the two main current directions NNE and SSW are given respectively in Figure 6.4 and Figure 6.5. Polar plots of extreme current magnitudes are given in Figure 6.6.
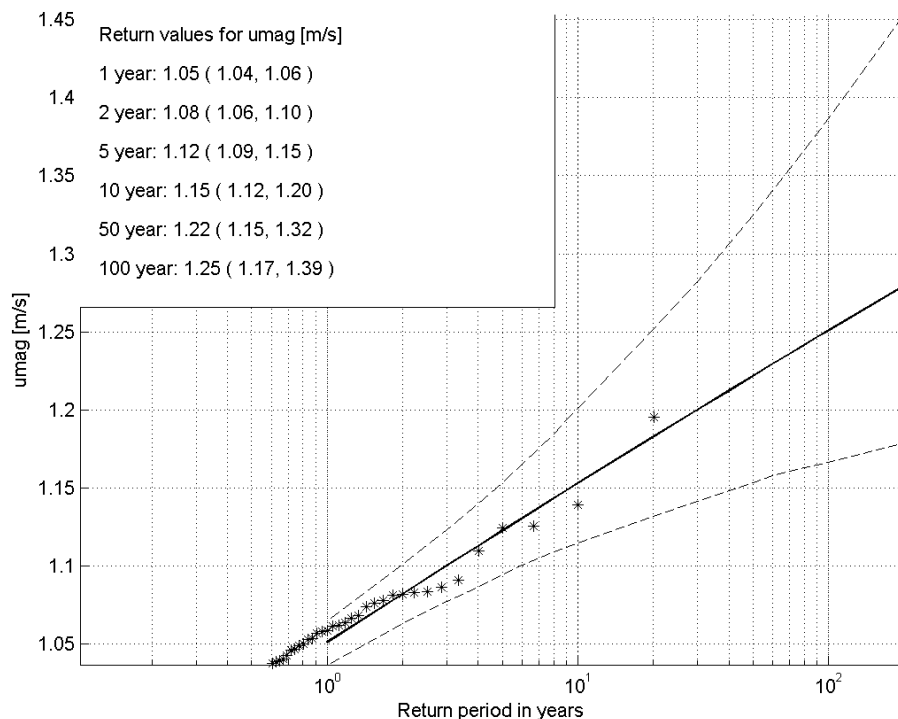
Figure 6.4   POT-GPD fit of extreme depth-averaged current magnitude for sector NNE at the BWFZ (Site I). The dashed lines are the associated 95% confidence intervals. The POT data are represented by the asterisks.
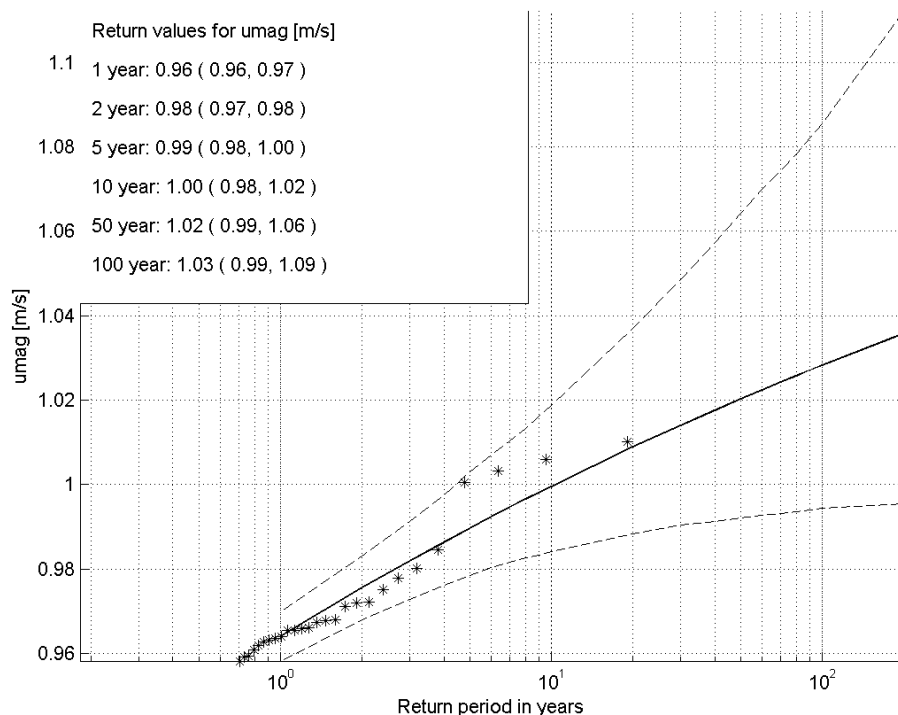
Figure 6.5   POT-GPD fit of extreme depth-averaged current magnitude for sector SSW at the BWFZ (Site I). The dashed lines are the associated 95% confidence intervals. The POT data are represented by the asterisks.
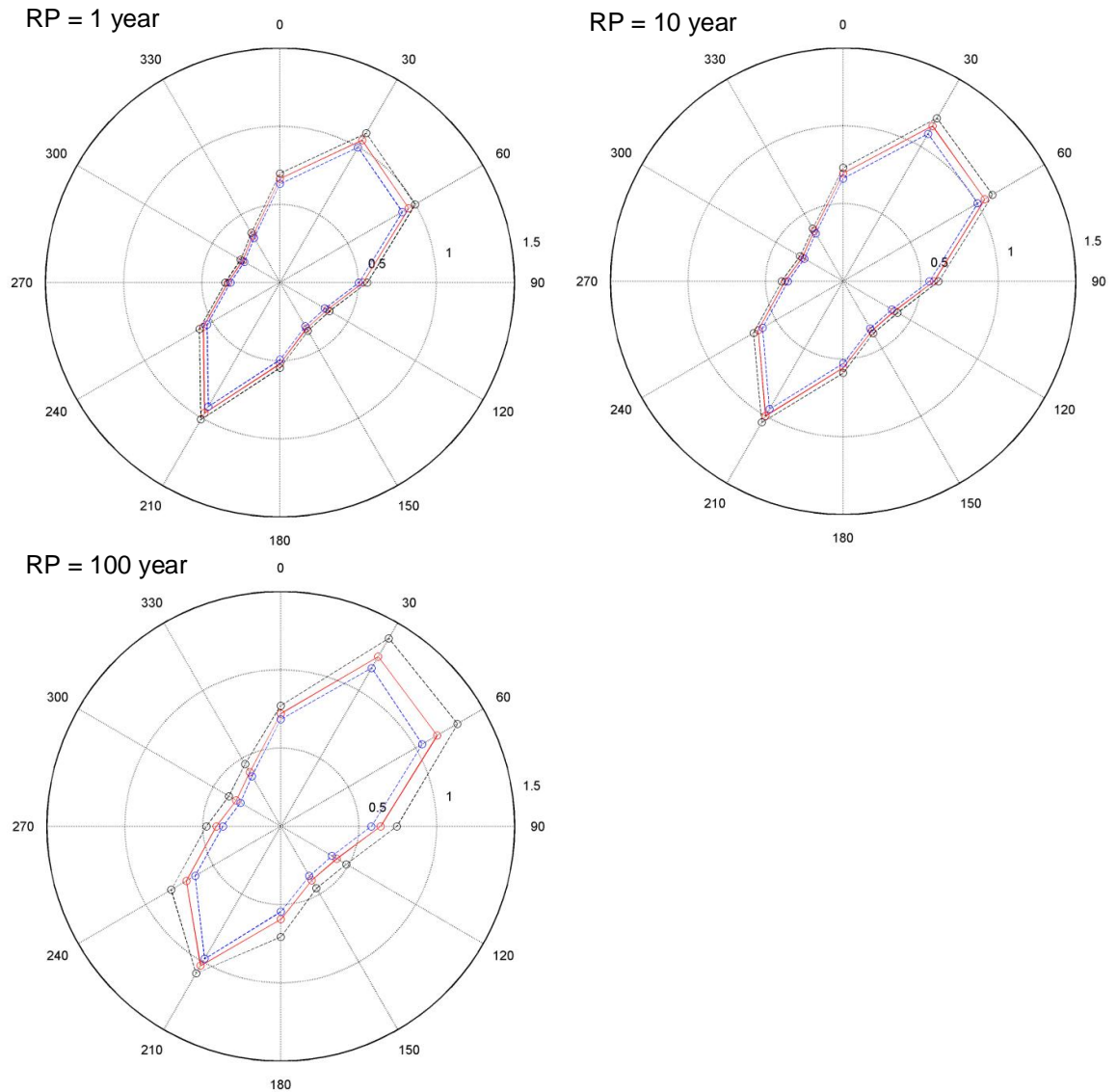
Figure 6.6 Polar plot of extreme depth-averaged current magnitudes at the BWFZ (Site I). The dashed blue and green lines are the associated 95% confidence intervals.

The depth-averaged extreme current magnitude estimates were transformed to currents at various depth levels by assuming the DNV method (DNV, 2010). The resulting extreme estimates for the main directional sectors NNE and SSW at the BWFZ are given in Table 6.1 and Table 6.2. The extreme current magnitude estimates at the various depth levels for all directional sectors are enclosed in Appendix C and are also given in the excel-table provided with this report.

Depth % total	RP = 1 year			RP = 2 years			RP = 5 year			RP = 10 year			RP = 50 year			RP = 100 year		
	low m/s	pnt m/s	up m/s	low m/s	pnt m/s	up m/s	low m/s	pnt m/s	up m/s	low m/s	pnt m/s	up m/s	low m/s	pnt m/s	up m/s	low m/s	pnt m/s	up m/s
100	1.36	1.43	1.49	1.41	1.48	1.55	1.47	1.55	1.62	1.51	1.60	1.68	1.60	1.71	1.87	1.62	1.75	1.97
90	1.32	1.39	1.45	1.37	1.44	1.50	1.43	1.50	1.57	1.47	1.55	1.63	1.55	1.65	1.81	1.57	1.70	1.91
80	1.28	1.34	1.41	1.32	1.39	1.46	1.38	1.45	1.52	1.42	1.50	1.57	1.50	1.60	1.75	1.52	1.64	1.84
70	1.24	1.30	1.36	1.28	1.34	1.41	1.33	1.40	1.47	1.37	1.44	1.52	1.44	1.54	1.68	1.46	1.58	1.77
60	1.19	1.25	1.31	1.23	1.29	1.35	1.28	1.35	1.41	1.32	1.39	1.46	1.39	1.48	1.61	1.40	1.52	1.70
50	1.14	1.20	1.25	1.18	1.24	1.30	1.22	1.29	1.35	1.26	1.33	1.39	1.33	1.41	1.54	1.34	1.45	1.62
40	1.08	1.14	1.19	1.12	1.17	1.23	1.16	1.22	1.28	1.19	1.26	1.32	1.26	1.34	1.46	1.27	1.37	1.53
30	1.02	1.07	1.12	1.05	1.11	1.16	1.09	1.15	1.21	1.12	1.18	1.24	1.18	1.26	1.37	1.20	1.29	1.44
20	0.94	0.99	1.04	0.97	1.02	1.07	1.01	1.06	1.11	1.04	1.09	1.15	1.09	1.16	1.26	1.10	1.19	1.32
10	0.83	0.88	0.92	0.86	0.90	0.95	0.89	0.94	0.98	0.91	0.96	1.01	0.96	1.02	1.11	0.97	1.05	1.16
5	0.74	0.78	0.82	0.77	0.81	0.85	0.79	0.84	0.88	0.82	0.86	0.90	0.86	0.91	0.99	0.87	0.93	1.03

Table 6.1   Extreme current magnitude estimates at the various depth levels for sector NNE at BWFZ (Site I). Note that no more than 1 digit after the comma must be considered when using these estimates further. If possible all point estimates should be rounded up to dm/s.

Depth % total	RP = 1 year			RP = 2 years			RP = 5 year			RP = 10 year			RP = 50 year			RP = 100 year		
	low m/s	pnt m/s	up m/s	low m/s	pnt m/s	up m/s	low m/s	pnt m/s	up m/s	low m/s	pnt m/s	up m/s	low m/s	pnt m/s	up m/s	low m/s	pnt m/s	up m/s
100	1.36	1.43	1.49	1.39	1.46	1.52	1.43	1.50	1.57	1.45	1.53	1.61	1.50	1.60	1.72	1.51	1.63	1.77
90	1.31	1.38	1.44	1.34	1.41	1.47	1.38	1.45	1.51	1.40	1.47	1.55	1.44	1.54	1.65	1.45	1.56	1.70
80	1.26	1.32	1.38	1.29	1.35	1.41	1.32	1.39	1.45	1.34	1.41	1.49	1.38	1.47	1.57	1.39	1.49	1.62
70	1.21	1.27	1.33	1.24	1.29	1.35	1.26	1.33	1.39	1.28	1.35	1.42	1.32	1.40	1.50	1.33	1.42	1.54
60	1.16	1.21	1.27	1.18	1.24	1.29	1.20	1.27	1.33	1.22	1.29	1.35	1.25	1.33	1.42	1.27	1.35	1.46
50	1.10	1.15	1.20	1.12	1.17	1.23	1.14	1.20	1.26	1.16	1.22	1.28	1.19	1.26	1.34	1.20	1.28	1.38
40	1.04	1.09	1.14	1.05	1.10	1.16	1.07	1.13	1.18	1.09	1.15	1.20	1.11	1.18	1.26	1.13	1.20	1.28
30	0.96	1.01	1.06	0.98	1.03	1.08	1.00	1.05	1.10	1.01	1.06	1.12	1.03	1.10	1.16	1.04	1.11	1.18
20	0.88	0.93	0.97	0.89	0.94	0.99	0.91	0.96	1.00	0.92	0.97	1.02	0.94	0.99	1.05	0.95	1.00	1.07
10	0.77	0.81	0.85	0.78	0.82	0.86	0.79	0.83	0.88	0.80	0.84	0.89	0.82	0.86	0.91	0.82	0.87	0.92
5	0.68	0.72	0.75	0.69	0.73	0.76	0.70	0.74	0.77	0.71	0.74	0.78	0.72	0.76	0.80	0.73	0.77	0.81

Table 6.2   Extreme current magnitude estimates at the various depth levels for sector SSW at BWFZ (Site I). Note that no more than 1 digit after the comma must be considered when using these estimates further. If possible all point estimates should be rounded up to dm/s.

7 Joint probability conditions

7.1 Introduction
This chapter describes the joint probability conditions. All persistence tables are presented in a separate excel table on persistence. The joint probability concerns the following combination of parameters:
- Wind and waves
- Current & waves
- Water levels & waves
- Water levels & current directions

7.2 Extreme
The extreme joint probability of waves and wind is presented in Section 4.4.

7.3 Operational
These tables are presented in the excel table and/or Appendices both accompanied with this report. Below it is described which combinations are determined.

7.3.1 wind and waves
- Joint occurrence of wind direction at hub height versus wave height (for wind speed from 0m/s to 100 m/s) Appendix B.2
- H_s distribution of wave-wind misalignment cases (for wind speed from 0m/s to 100 m/s) (excel table)
- H_s distribution for wave height (0-7m H_s) – wind direction misalignment cases – wind speed (0-100m/s) (excel table)
- Directional wind speed versus wave height for 10m height and hub height (excel table)

7.3.2 current and waves
- H_s versus still water level – total of tide and surge (excel table)
- H_s versus residual water level (surge height) Appendix D.1
- H_s versus depth averaged current speed – total of tide and surge (excel table)
- H_s versus depth averaged residual (surge) current speed (excel table)
- H_s distribution for misalignment cases (excel table)

7.3.3 water level and waves
- Water level versus significant wave height: (excel table)
- Residual water level versus significant wave height by direction (excel table)

7.3.4 water level and current directions
- Joint occurrence of water level and current (residual) direction (excel table)
- Joint occurrence of water level and current (total of tide and surge) direction (excel table)

8 Other metocean data

8.1 Snow and ice accretion criteria

According to ISO19906 (2010), ice accumulation, or icing of structures or structural members can result from fog, freezing rain, green water trapped on decks, wind- and wave-driven seawater spray, or tidal variation. Icing modifies the aerodynamic and hydrodynamic properties, static stability and dynamic responses of the structure and as a consequence significantly raise the levels of wind, wave and current actions on a structure due to changes in projected area, volume and surface roughness. Besides, the aerodynamic characteristics of the turbine blades may be affected by ice accumulation (Figure 8.1).

Figure 8.1   Ice accumulation on a wind turbine blade (Source: http://www.windpowerengineering.com).

Two types of icing exist: atmospheric icing due to precipitation and marine icing due to sea spray by breaking waves in combination with a strong wind. Atmospheric icing will be more relevant for the turbines, whereas marine icing for the lower part of the turbine, the platform and vessels.

Atmospheric icing can produce a uniform layer of ice on all surfaces over the height of the structure starting from a few metres above the waterline. Atmospheric icing normally occurs when the air temperature is between 0°C and -20°C and wind speed is less than 10m/s. As a result of atmospheric icing, the higher elevations of a structure can be covered with 1 to 2 cm of ice (ISO19906, 2010).

Marine icing caused by sea spray is the most frequent form of icing at sea. Sea spray will be formed when the wind blows droplets of water off wave crests, depending on the form and steepness of the waves and wind speed. The stronger the wind and waves, the higher the

spray is lifted. Typically icing due to waves reaches heights of up to 15 to 20 m above the sea surface. Conditions under which marine icing will occur according to ISO19906 (2010) are:

- Air temperature below the freezing point of sea water (approx. -2°C);
- Wind speed of 10 m/s or more;
- Seawater temperature less than 8°C.

The joint occurrence of the above conditions were assessed by making a joint-occurrence table for air temperature versus surface water temperature, but only at times when the wind speed is higher than 8 m/s. The simultaneous datasets were based on hindcast time-series from the National Center for Environmental Prediction – Climate Forecast System Reanalysis (NCEP-CFSR) at the BWFZ. The NCEP-CFSR data are based on a combination of a global, high resolution, coupled atmosphere-ocean-land surface-sea ice modelling system and numerous conventional and satellite observations. NCEP-CFSR atmospheric, oceanic and land surface output products are available at an hourly time resolution and 0.5° horizontal resolution around the globe (Saha et al., 2010).

The conditional joint-occurrence table is presented in Figure 8.2. This figure shows that:

- Marine ice accretion can be expected to occur on average during occur for 0.27 % of time (the sum of the occurrences with air temperature below -2°C and seawater temperature below 8°C), which is almost one day per year on average.
- Atmospheric icing can be expected to occur on average during occur for 0.64% of time (the sum of the occurrences with air temperature below 0°C), which is almost two and a half days per year on average.

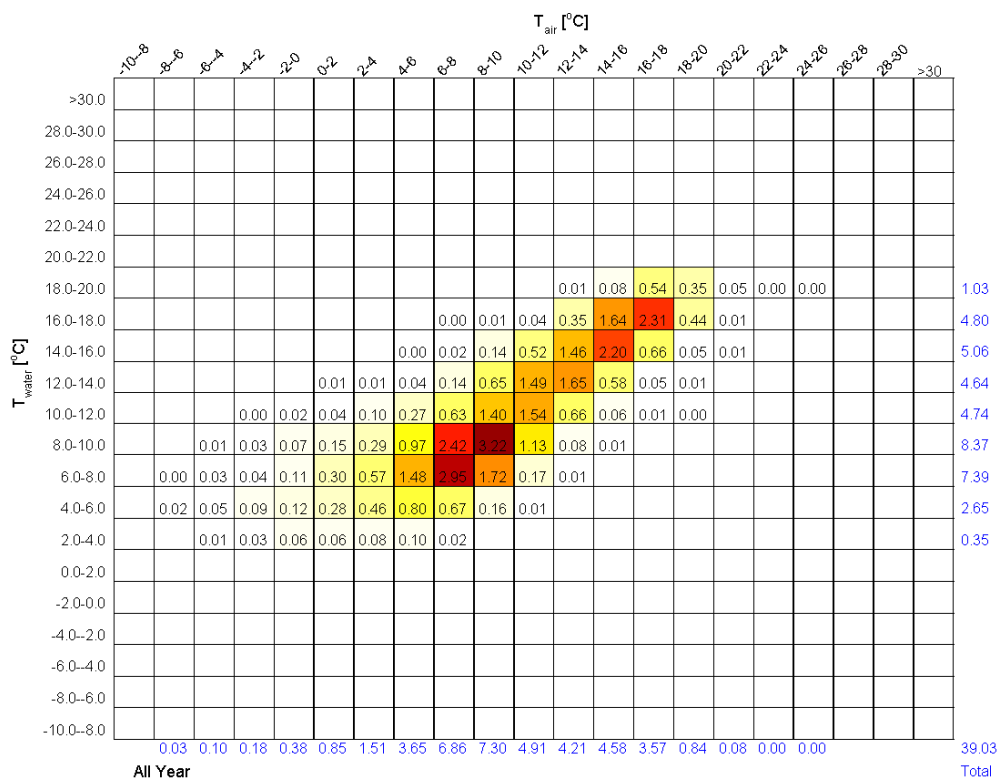

T_{water} [°C] \ T_{air} [°C]	-10--8	-8--6	-6--4	-4--2	-2-0	0-2	2-4	4-6	6-8	8-10	10-12	12-14	14-16	16-18	18-20	20-22	22-24	24-26	26-28	28-30	>30	
>30.0																						
28.0-30.0																						
26.0-28.0																						
24.0-26.0																						
22.0-24.0																						
20.0-22.0																						
18.0-20.0												0.01	0.08	0.54	0.35	0.05	0.00	0.00				1.03
16.0-18.0									0.00	0.01	0.04	0.35	1.64	2.31	0.44	0.01						4.80
14.0-16.0								0.00	0.02	0.14	0.52	1.46	2.20	0.66	0.05	0.01						5.06
12.0-14.0						0.01	0.01	0.04	0.14	0.65	1.49	1.65	0.58	0.05	0.01							4.64
10.0-12.0				0.00	0.02	0.04	0.10	0.27	0.63	1.40	1.54	0.66	0.06	0.01	0.00							4.74
8.0-10.0			0.01	0.03	0.07	0.15	0.29	0.97	2.42	3.22	1.13	0.08	0.01									8.37
6.0-8.0		0.00	0.03	0.04	0.11	0.30	0.57	1.48	2.95	1.72	0.17	0.01										7.39
4.0-6.0		0.02	0.05	0.09	0.12	0.28	0.46	0.80	0.67	0.16	0.01											2.65
2.0-4.0			0.01	0.03	0.06	0.06	0.08	0.10	0.02													0.35
0.0-2.0																						
-2.0-0.0																						
-4.0--2.0																						
-6.0--4.0																						
-8.0--6.0																						
-10.0--8.0																						
All Year		0.03	0.10	0.18	0.38	0.85	1.51	3.65	6.86	7.30	4.91	4.21	4.58	3.57	0.84	0.08	0.00	0.00				39.03 Total

Figure 8.2 *Joint-occurrence of air temperature versus surface water temperature for wind speeds of more than 8 m/s, based on CFSR hindcast data (1979-2010) for a location near the BWFZ.*

8.2 Sea ice conditions

Sea ice will not occur at BWFZ during normal winters since the temperature of the seawater will generally be higher than -2°C (Figure 8.2), which is the freezing temperature of salt water. Only during very extreme winters, sea ice occurs in the North Sea. According to anecdotal information published on internet, it was possible to walk into the sea (over the ice) for kilometres during the winter of 1963, which is the most extreme winter in more than 100 years. Figure 8.3 shows a photo taken on the top of a dune at an unknown location along the Dutch coast. The photo shows that the sea ice extends until just before the horizon (cf. the dark blue seawater line just in front of the horizon). Assuming that the photo was taken at a height of 10 to 15m above the level of the sea, the horizon, and thus the upper bound of the ice extent, will be about 10 to 15 km from the coastline. For BWFZ this would mean that it is outside this shore-fast ice zone during extreme winters.

Figure 8.3   Sea view at an unknown location along the North Sea coast during the winter of 1963 (Source: http://fieggentrio.blogspot.nl/2012/02/de-barre-winter-van-1963.html).

In KNMI (1964) observations of sea ice are reported at (amongst other locations) "Lightvessel Goeree". This manned (until 1971) vessel acted as a lighthouse and marine observation station, and was located about 30 km to the west of Hoek van Holland, which is about 50 km north-northeast of BWFZ. The following observations at Lightvessel Goeree are made in KNMI (1964):
- on two days during the 1963 winter there was heavy ice cover (70% coverage);
- on 3 days an ice coverage of between 10 – 70 % was observed;
- the size of the largest floating ice sheets was estimated to be only a few metres;
- the speed of the floating ice was estimated at about 5% of the wind speed;
- the origin of the floating ice was expected from the land-fast ice along the South-Holland coast and Southwest Delta estuary (note that the Haringvliet and Grevelingen barriers were under construction in 1963);
- ice was observed during periods with ENE to SSE winds;
- it was estimated that ice occurred four times in the period 1880 – 1964.

Based on the above observations, it must be concluded that there is a chance that sea ice will occur at the BWFZ during extreme long and cold winters with ENE to SSE wind conditions. Given, however, that (1) the Grevelingen and Haringvliet are presently not directly connected to the sea and (2) higher water and air temperatures as a result of climate change, the probability of sea ice at the BWFZ is less than in 1963.

8.3 Seismicity

The last hazard analysis for the southern part of the Netherlands was carried out in 1996. Currently KNMI is performing an update of that hazard analysis, where 260 Events in the Netherlands, Belgium and Germany from 1750 - 2007 are used. The magnitude of the events ranges from 2.5 to 6.0, the depth from 5 - 20 kilometres.

Following the analyses carried out in 1996, the seismicity in the Netherlands and Belgium and Germany is presented in the figure below.
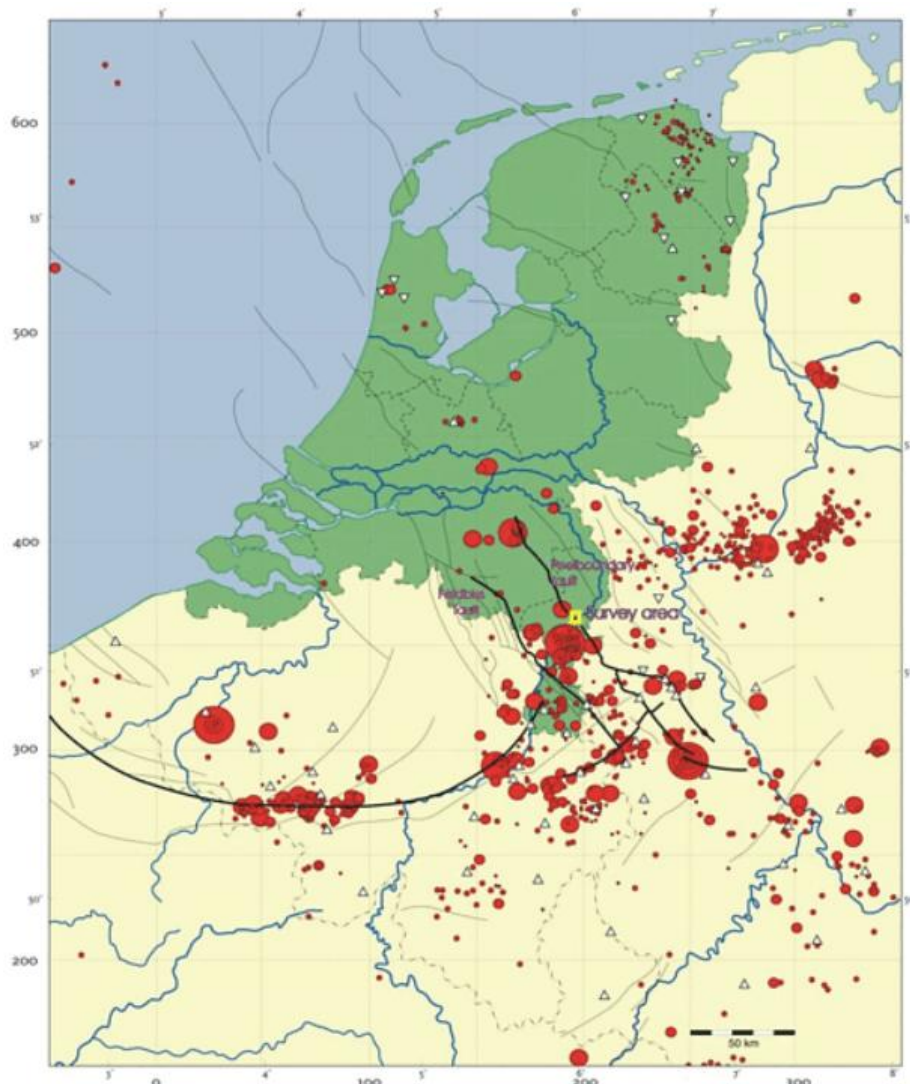
Figure 8.4 Seismicity in The Netherlands between 1900 and 1996 (red circles). (source: www.KNMI.nl)

This figure indicates that natural seismicity is mainly restricted to the Southern part of the Netherlands. The BWFZ being only ~100km away shows that the area could be subject to tectonic activity.

Figure 8.5 shows the seismic hazard in the Netherlands by tectonic earthquakes with a return period of 475 years. This implies that in the red areas intensity VII can be reached ones every 475 years, or with a probability of 10% in 50 years. For the areas with intensity lower than V, there are not enough data to specify in more detail. The hazard due to induced earthquakes in the northern part of the Netherlands is not included in this map. The intensities are according to the European Macroseismic Scale (EMS).
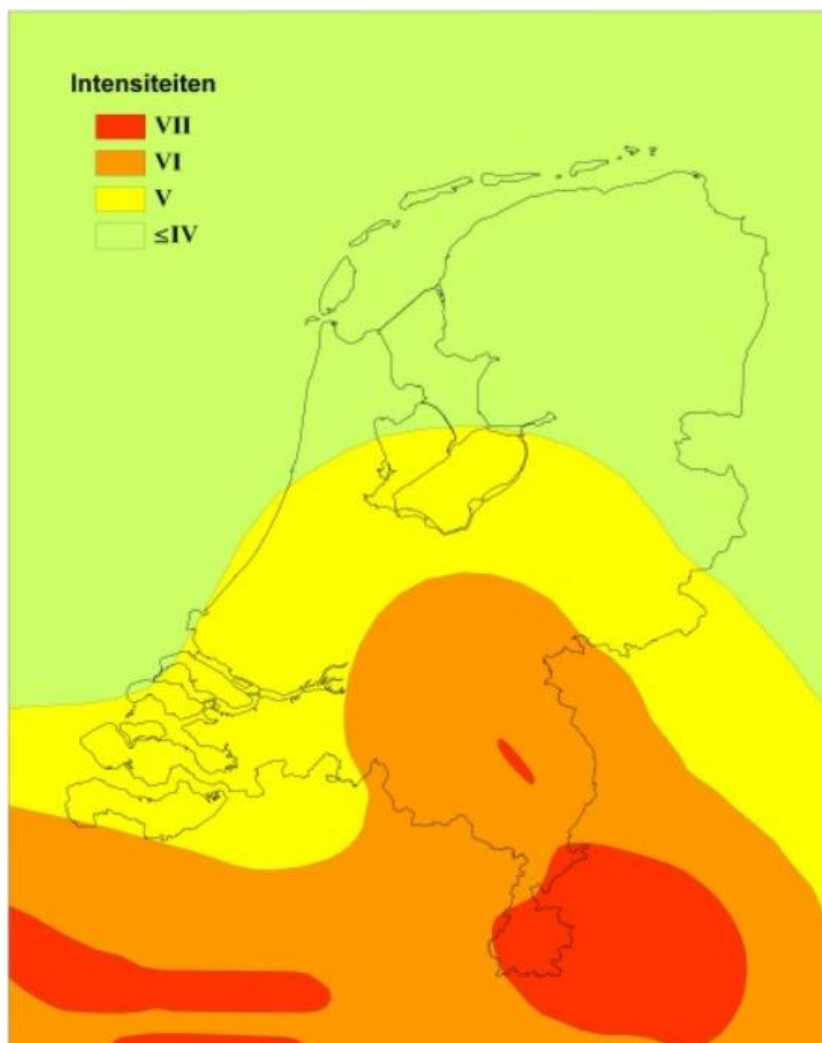
Figure 8.5   Results from Crook, 1996. The study is performed using intensities to determine the seismic hazard, and afterwards the intensities are translated to peak ground accelerations.
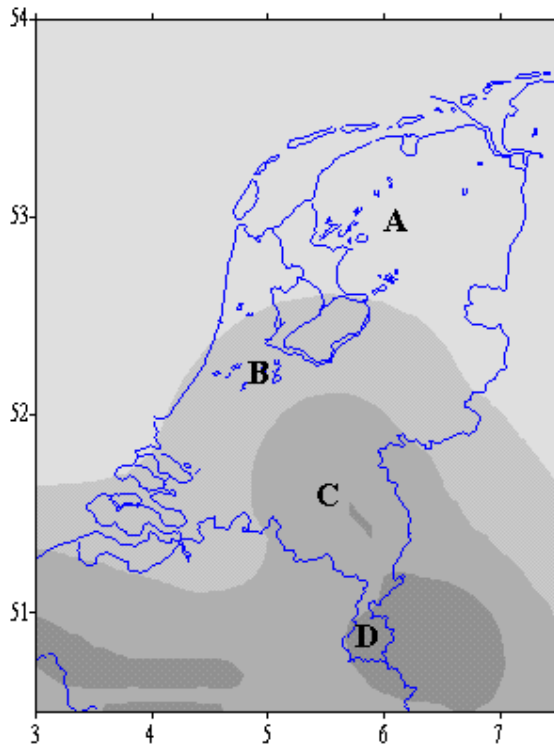
Figure 8.6   Seismic zones in the Netherlands and adjacent North Sea. In this map a zonation is applied based on the expected horizontal Peak Ground Acceleration (PGA). PGA for zones A, B, C and D are 0.1, 0.22, 0.5 and 1 m/s^2 respectively. It is assumed that at the ground surface/sea bottom the horizontal component of the movement is the greatest. (Bron: de Crook, 1996).

In recent years similar maps have been made for the British and Belgian sectors of the North Sea. Based on archive research it was concluded that historical earthquakes of magnitudes up to M=6 in the adjacent area of the English Channel could be deduced from the historical documents. Incorporation of these earthquakes in the calculation of the seismic hazard map contours of North Western Europe has produced a higher value of Peak Ground Acceleration (PGA), when extrapolated onto the offshore area (Grünthal et al. 1999). The map shows that in the BWFZ a PGA with a probability of 10% in 50 years may be expected in the order of at least 0.3-0.4 m/s^2. Although it is not entirely clear from the map, even a PGA of between 0.4 and 0.5 may be expected. The PGA contours were adjusted in 2003 (Jiménez et al, 2003) using up-to-date ground motion prediction equations. This resulted in generally lower PGA values. From the latter study a design PGA value of 0.3 m/s^2 for stiff subsoil is advised. This is also in line with the UK seismic hazard map (Musson and Sargeant, 2007).

It should be noted that these values apply to stiff upper ground conditions. When soft layers, like Holocene clays or peats are encountered at foundation locations the amplitudes may be amplified. In that case adjusted PGA values should be derived using Eurocode 8.
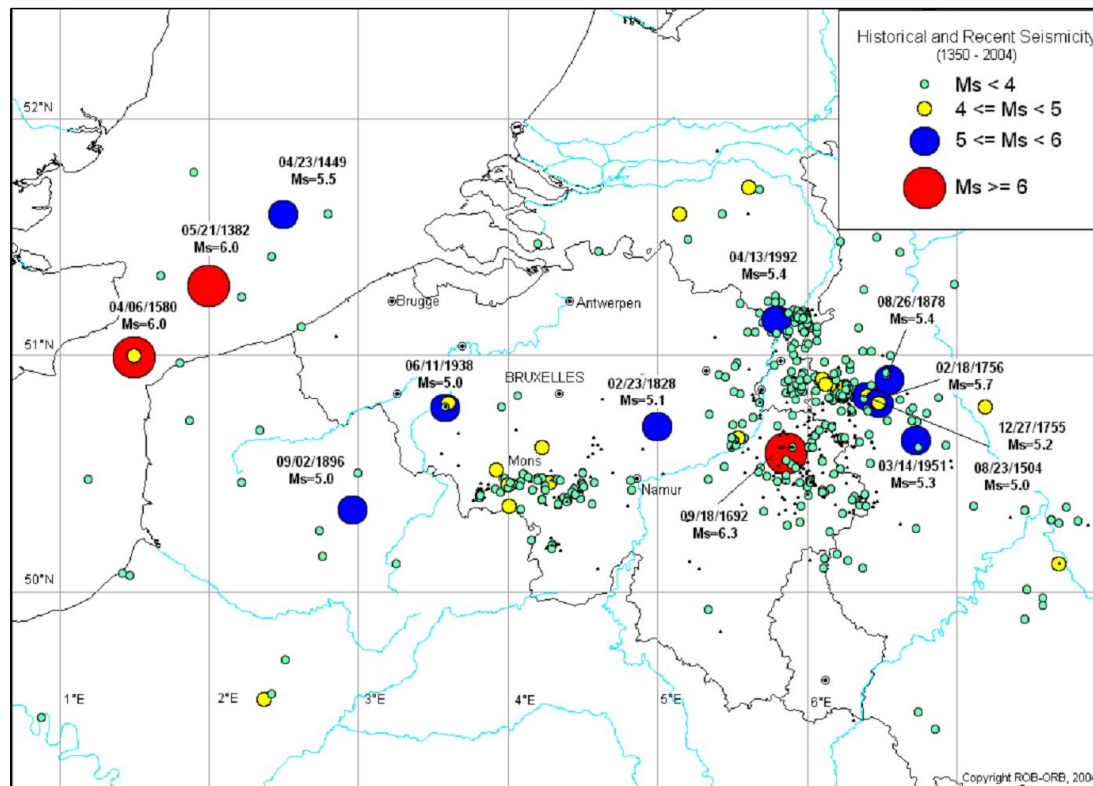
Figure 8.7   Catalog of historical and recent earthquake. Epicenter and Magnitude of the earthquakes are indicated [Philippe Rosset, ORB 2004].
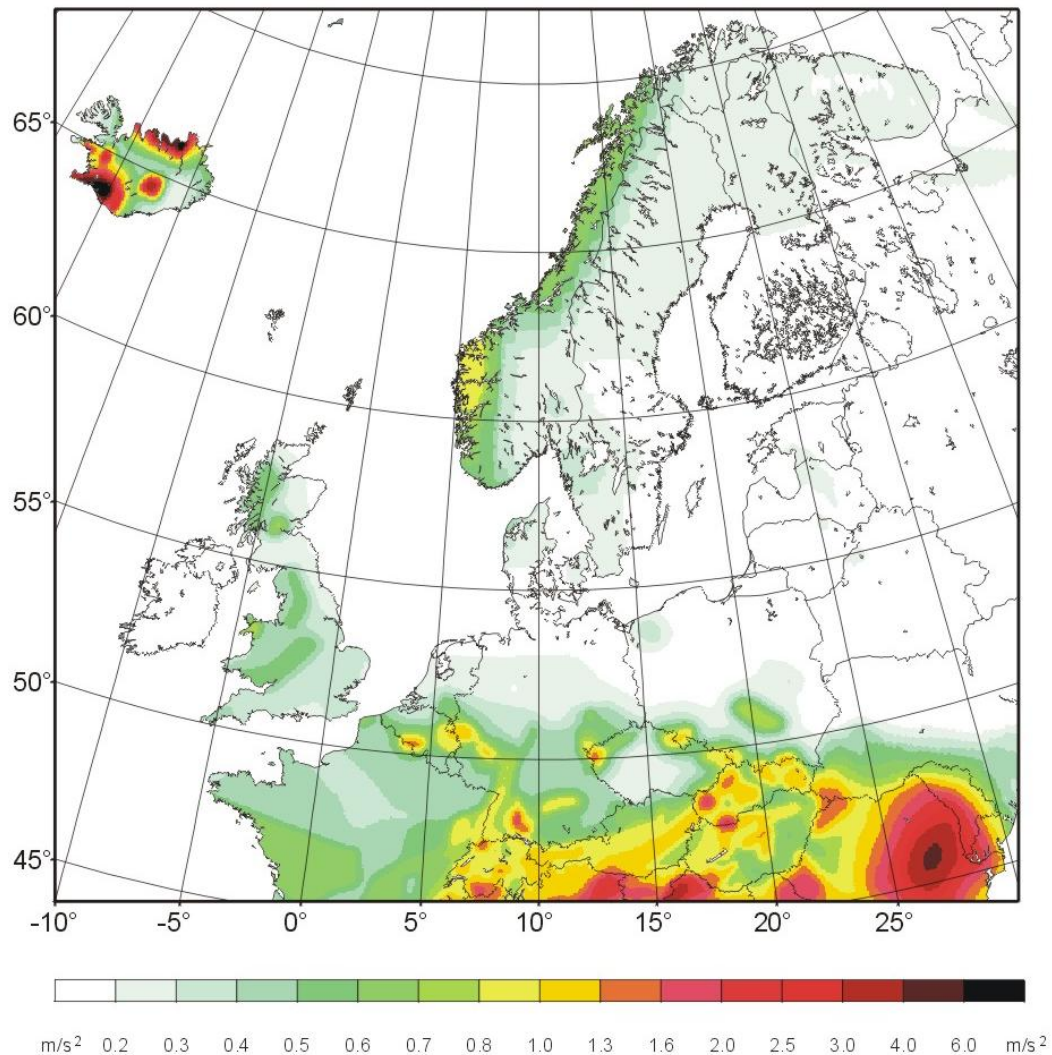
Deltares

Figure 8.8   Horizontal peak ground acceleration seismic hazard map representing stiff site conditions for an exceedance or occurrence rate of 10% within 50 years for the GSHAP Region 3 (Grünthal et al, 1999).

The extraction of natural gas is known to produce induced earthquakes. The BWFZ does not lie in an area of existing gas exploration. The nearest zone of natural gas extraction is located at a distance of 80 km to the North-East. The seismic hazard of these gas fields is assumed to be comparable to the hazard determined for the gas fields in the Rotterdam near- and onshore area. This hazard is considered to be very low to negligible (TNO report TNO-rapport 2012 R10198) and will not add to the predicted PGA.

8.4   Air temperature and air density

The table below presents the monthly distribution of mean, min and max daily averaged air temperature at 10m above sea level including standard deviation, based on HARMONIE database.

	mean (°C)	min (°C)	max (°C)	st. deviation (°C)
January	5.9	-8.2	13.1	3.2
February	5.6	-7.6	12.4	2.8
March	6.7	-3.6	14.5	2.3
April	8.5	1.2	17.1	2.0
May	11.3	4.8	19.5	2.0
June	14.0	7.5	24.7	1.9
July	16.5	11.7	23.7	1.6
August	17.6	12.9	25.2	1.5
September	16.2	10.4	23.4	1.7
October	13.4	4.8	19.9	2.3
November	9.9	-1.8	17.1	2.6
December	7.1	-4.8	14.2	2.9

Table 8.1 Monthly distribution of mean, min and max daily averaged air temperature including standard deviation, based on HARMONIE database.

The table below presents the monthly distribution of mean, min and max daily averaged air density at 10m above sea level including standard deviation, based on HARMONIE database.

	mean (kg/m^3)	min (kg/m^3)	max (kg/m^3)	st. deviation (kg/m^3)
January	1.265	1.191	1.348	0.025
February	1.266	1.182	1.348	0.023
March	1.261	1.195	1.327	0.019
April	1.249	1.197	1.299	0.016
May	1.239	1.188	1.284	0.014
June	1.226	1.177	1.273	0.013
July	1.214	1.170	1.251	0.011
August	1.209	1.171	1.240	0.011
September	1.216	1.169	1.258	0.013
October	1.226	1.164	1.295	0.018
November	1.243	1.178	1.315	0.020
December	1.258	1.186	1.330	0.024

Table 8.2 Monthly distribution of mean, min and max daily averaged density including standard deviation, based on HARMONIE database.

8.5 Seawater

This section describes the parameters salinity, seawater temperature and seawater density. The analyses are based on the hindcast time-series from the National Center for Environmental Prediction – Climate Forecast System Reanalysis (NCEP-CFSR) at the BWFZ. The NCEP-CFSR data are based on a combination of a global, high resolution, coupled atmosphere-ocean-land surface-sea ice modelling system and numerous conventional and satellite observations. NCEP-CFSR atmospheric, oceanic and land surface output products are available at an hourly time resolution and 0.5° horizontal resolution around the globe (Saha et al., 2010).

Where available the hindcast database is validated with data from measurement stations located in the vicinity of the BWFZ.

8.5.1 Salinity

The table below presents the monthly distribution of mean, min and max air daily averaged temperature including standard deviation, based on CFSR database.

	Mean(PPT)	min (PPT)	max (PPT)	st. deviation (PPT)
January	33.1	32.8	34.9	0.5
February	33.0	32.9	33.3	0.5
March	33.0	32.9	33.2	0.5
April	33.0	32.9	33.1	0.5
May	33.0	32.9	33.2	0.5
June	33.0	32.9	33.1	0.5
July	33.0	32.8	33.1	0.5
August	33.0	32.9	33.1	0.5
September	33.0	32.9	33.2	0.5
October	33.0	32.9	33.3	0.5
November	33.0	32.9	33.2	0.5
December	33.1	32.8	34.2	0.5

Table 8.3 Monthly distribution of mean, min and max air daily averaged temperature including standard deviation, based on all available years 1906 – 2012.

Information about salinity was obtained from the DONAR-database of the Dutch government. From 1975 till 1983 the seawater salinity was measured on a monthly base 30 km out of the coast at Schouwen (51.8°N 3.27°E), which is nearby the BWFZ. This is also measured at other transects along the Dutch coastline, at Hook of Holland, Egmond aan Zee, etc. These stations do not show significant variation.

Since these are the most recent publicly available measurements, these data are used for characterizing the seawater salinity and the calculation of the seawater density. The average salinity (1975-1983) at the BWFZ is between 33 and 34 PSU (Figure 8.9).
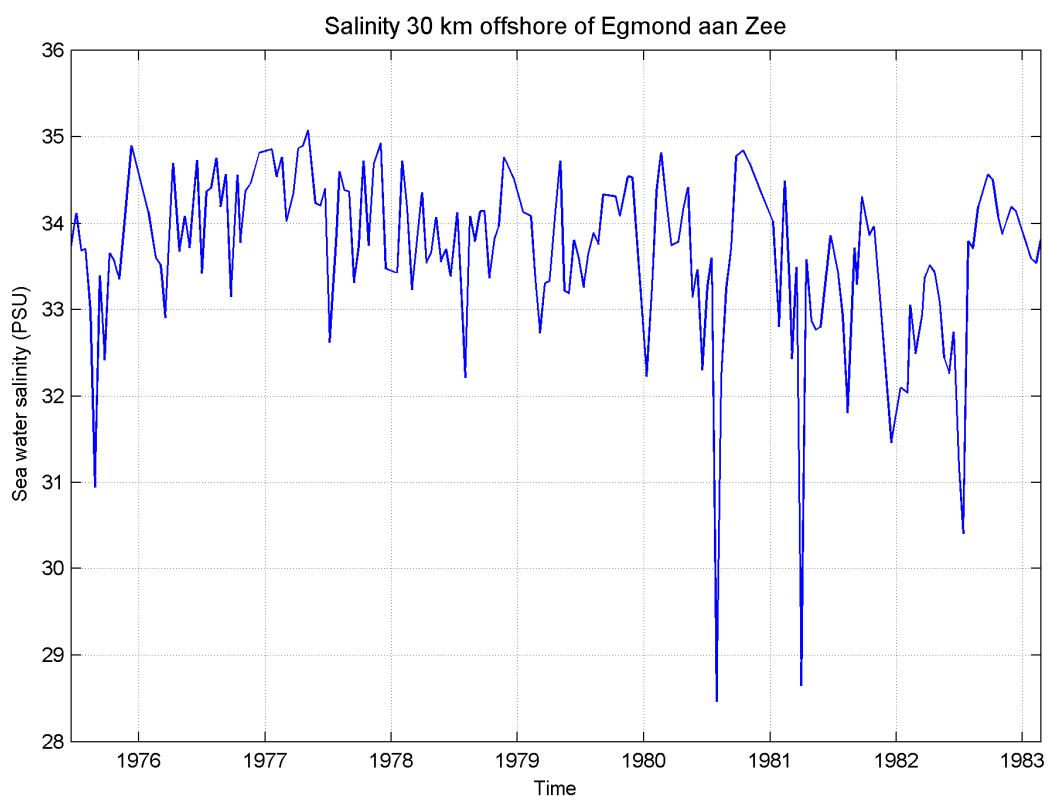
Figure 8.9   Salinity measurements 30km offshore of Egmond aan Zee.

8.5.2   Seawater temperature

The table below presents the monthly distribution of mean, min and max air daily averaged temperature including standard deviation, based on CFSR database.

	mean (°C)	min (°C)	max (°C)	st. deviation (°C)
January	7.0	2.7	10.3	1.3
February	5.9	1.8	8.7	1.4
March	6.1	1.4	9.1	1.4
April	7.8	3.9	12.1	1.2
May	10.4	6.1	13.9	1.4
June	13.4	9.6	16.4	1.2
July	15.9	12.8	19.5	1.1
August	17.4	15.0	20.0	1.0
September	16.7	14.2	19.1	1.0
October	14.6	11.6	17.8	1.1
November	11.7	7.6	15.3	1.3
December	9.0	5.8	12.1	1.1

Table 8.4 Monthly distribution of mean, min and max air daily averaged temperature including standard deviation, based on CFSR database.

Recent temperature measurements at the IJmuiden Munititiestortplaats (YM6) have also been obtained from the DONAR-database for the period 1989-2013. The temperature over this period varied roughly between 7°C during winter periods and 19°C during summer periods.

8.5.3 Seawater density

Using the UNESCO equation of State of Seawater 1980 (UNESCO, 1981), this leads to a water density range of 1023-1026 kg/m^3 for the BWFZ.

8.6 Extreme temperatures

The extreme value analysis is carried out for the water and air temperature. The hindcast database used for the water temperature is explained above, in Section 8.5. The high and low extreme water temperature is illustrated in the two figures below.
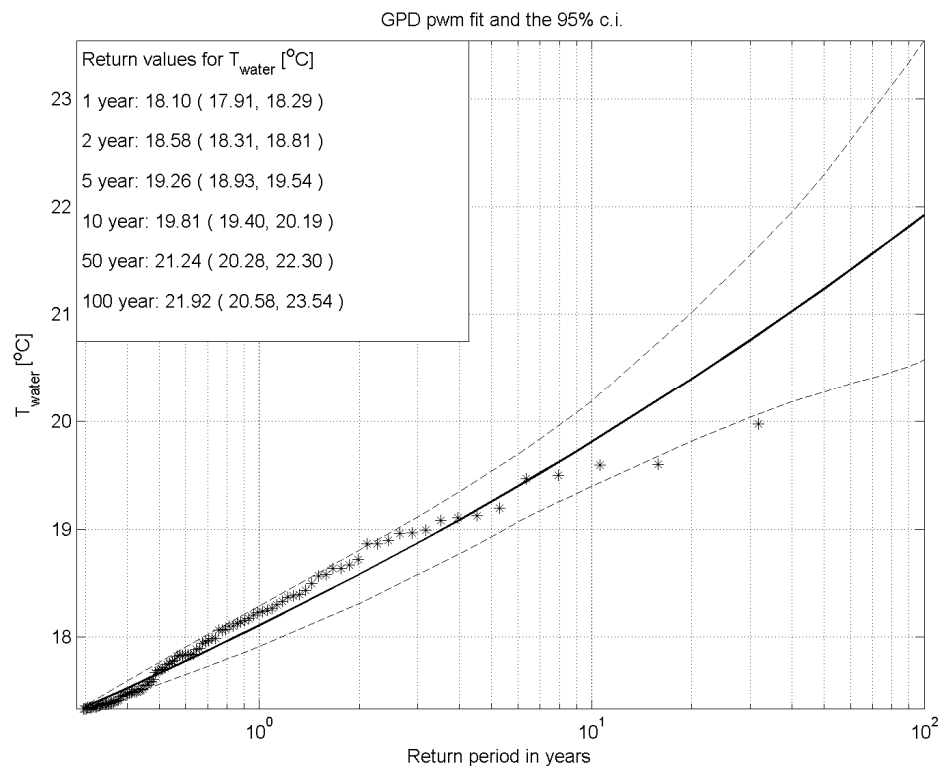
Figure 8.10 Return value plot of the water temperature.

The hindcast database used for the air temperature is HARMONIE and is explained in Section 2.3. The high and low extreme air temperature is illustrated in the two figures below.
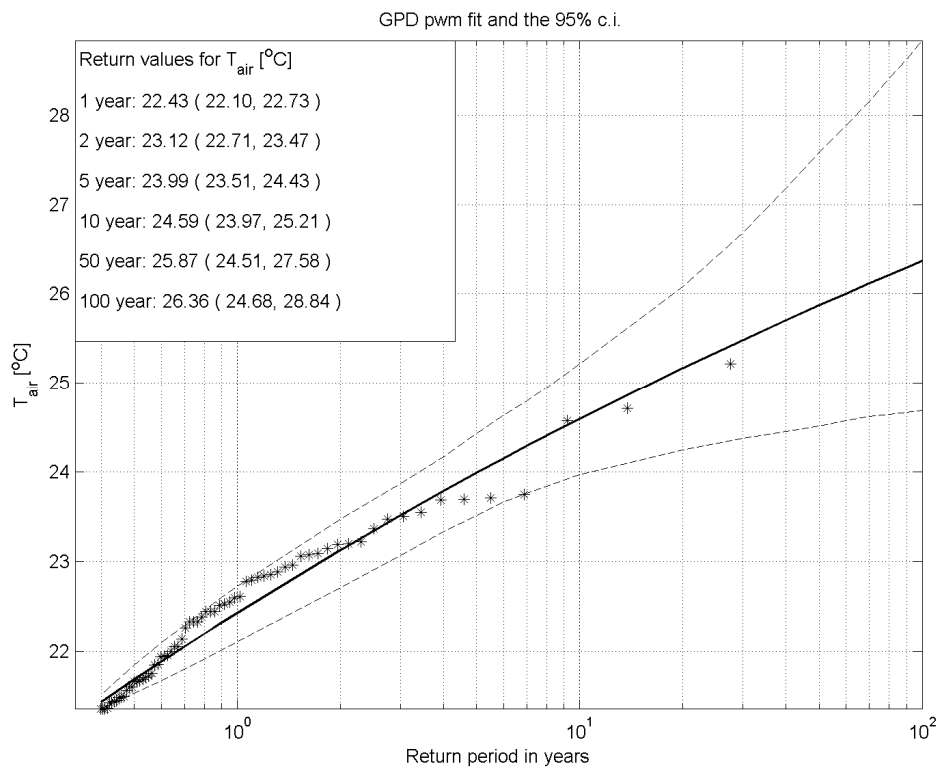
Deltares

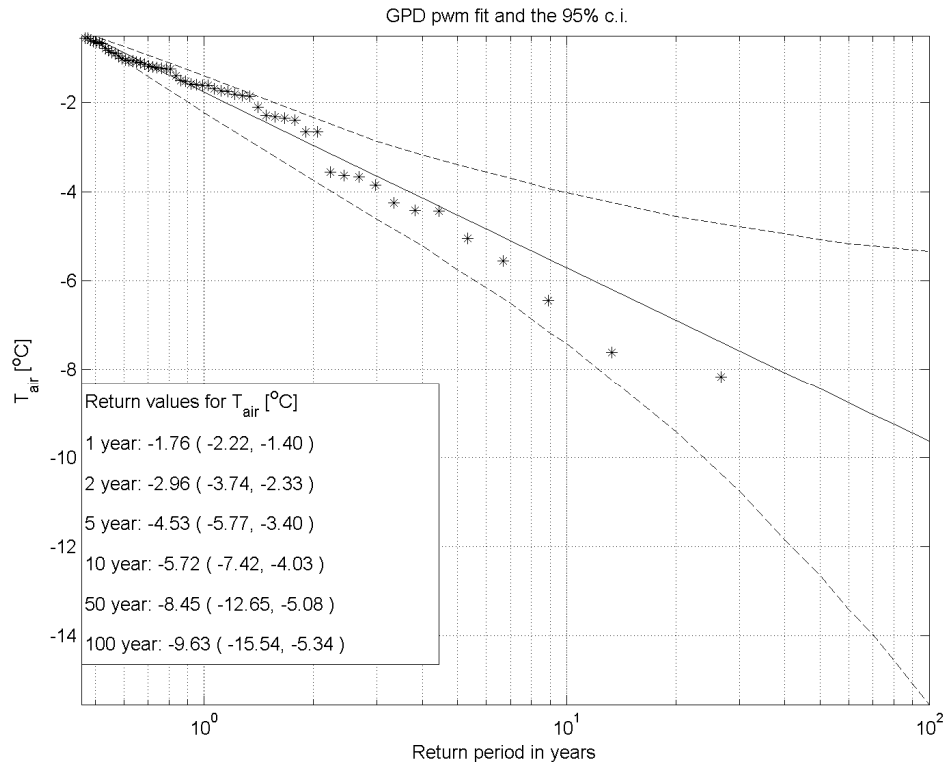*Figure 8.11 Return value plot of the high air temperature.*

Figure 8.12 Return value plot of the low air temperature.

8.7 Marine growth

8.7.1 Marine growth on wind turbines

Marine growth, or biofouling, is the attachment of organisms to a man-made surface within an aquatic environment (Cooksey and Wigglesworth-Cooksey, 1995). On any structure installed in an aquatic environment, numerous types of fouling organisms may be found on its submerged surfaces after a certain time.

Marine growth is broadly divided into "hard" (generally animals such as mussels and barnacles) and "soft" (algae, sponges), where hard growth is generally thinner but rougher than soft growth. Fouling organisms generally colonize a structure soon after installation but the growth tapers off after a few years (Jusoh and Wolfram, 1996).

Marine growth influences the mass, the geometry, and the surface texture of the support structure of an offshore wind turbine. Consequently, marine growth may influence hydrodynamic loads, dynamic response, accessibility and corrosion rate of the structure and must therefore be taken in to account during design (DNV, 2014; Quarton, 2005).

Firstly, if marine growth forms a consistent layer around a pile, increasing its thickness; the pile will incur more drag. Secondly, irrespective of the total thickness of the pile, hard organism assemblages (such as mussels and oysters) can strongly increase the surface drag in comparison to a smooth hard surface (Green et al. 1998, Järvelä 2002, Crimaldi et al.

2007). The drag on the structure is partly caused by friction drag (determined by the total amount of wetted surface area) and in case of larger structures and higher flow velocities also by form drag. The net effect of flexible organisms is more difficult to predict. Very flexible biota, such as seagrass can actually reduce the drag on the overlying boundary layer (Bouma et al. 2005, Dijkstra and Uittenbogaard 2010). Although the increased total width of the pillar will incur more form drag. The total effect of biota on drag is therefore determined by 1) properties (size, shape) of the organisms and 2) the ambient hydrodynamics. (Järvelä 2002).

Marine growth has not only negative effects. The North Sea has very little natural hard substrate. Hard substrate tends to be richer (in terms of biomass and biodiversity) than soft (sandy) sediments. Artificial hard substrates (such as wrecks, oil and gas infrastructure, wind farms etc.) are often rich oases (Krone et al. 2013). This also attracts other biota that live off the attached marine growth such as cod (Lindeboom et al. 2011) and marine mammals (Lindeboom et al. 2011, Scheidat et al. 2011). Whether this higher occurrence of these animals is a consequence of marine growth, or if it is a consequence of the fact that within wind farms (and certainly close to the turbines) no fishing is allowed, remains to be established.

The extra hard substrate provided by wind farms and other structures also has possible negative consequences for the North Sea: the higher density of hard substrate makes dispersal for hard substrate species easier. The probability to encounter suitable substrate within a certain time window is larger (Adams et al. 2014). This means that natural barriers for invasive species decrease. Particularly on hard substrate we find a lot of marine invasive species. The net effect of the positive and the negative effects of hard substrate on the North Sea ecosystem are currently not well documented (Thorpe 2012).

The weight of marine growth may add significant extra load on pillars and other structures. There will be differences between hard and soft organisms. The density of soft growth is close to that of the surrounding seawater and does not add much in terms of loading, but hard growth, especially oyster shells can add significantly. For marine structures the density of marine growth is generally assumed to be 1325 kg /m^3 (DNV 2010).

8.7.2   On marine growth

From the initial adsorption of macromolecules to the development of complex and diverse plant and animal communities, marine growth affects most solid surfaces permanently or temporarily immersed in saline, brackish and freshwater environments (Richmond and Seed, 1991). The development of marine growth in aquatic environments typically follows a regular sequence of events: 1) development of a conditioning film (within seconds), 2) microfouling (within a week), and then 3) macrofouling (within two to three weeks) (Wells and Sytsma, 2009).

Macrofouling organisms tend to have rapid metamorphosis and growth rates and are highly adaptable to water temperature, flow patterns, salinity, and substrate type (Yebra et al., 2004). Macrofouling species tend to be filter feeders that form dense colonies.

8.7.3   Thickness and profile of marine growth

The level of marine growth (most commonly expressed in thickness in mm) depends strongly on a number of factors: the biodiversity at the location, temperature, season, salinity, flow, substrate type.

Guerin (2009) studied marine growth communities of North Sea offshore platforms and found typical shallow fouling assemblages at the shallowest parts of a platform, corresponding to the intertidal and shallow sublittoral zones of a typical rocky shore (algae, barnacles, mussels). Below this depth, platforms are colonized with a mix of hard and soft fouling species. By the time a structure has been in place for 20 years, hard fouling species are dominant over much of the platform, although coverage remains thinnest near the base of the platform.

Most recent studies that address zonation on artificial structures, address biodiversity and abundance in relation to depth (Kerckhof et al. 2010; Vanagt & Faasse, 2014). Although these studies show a clear decrease of species abundance with increasing depth, these studies do not provide any relationships between thickness of marine growth and depth. In the study by Vanagt & Faasse (2014), the deeper strata showed actually a higher biomass. An old study by Jusoh and Wolfram (1996) looked into average thickness of marine growth on all kinds of offshore structures including monopoles (ranging from 10 to 40mm) and found that the thickness of marine growth decreases with increasing depth (see Figure 8.13).
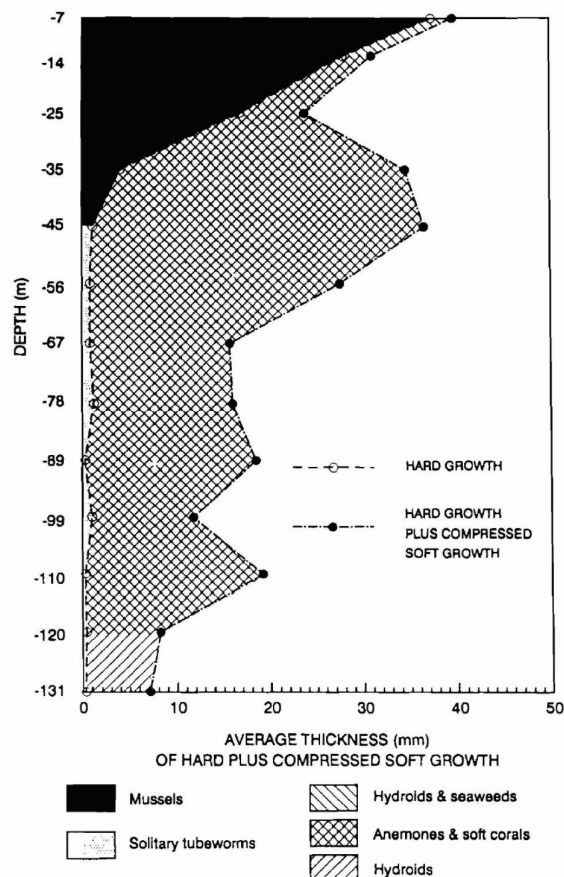

Figure 8.13 Depth/Thickness Profile for a Typical Jacket in the North Sea (from Jusoh and Wolfram, 1996).

DNV standard (DNV-OSJ-101, DNV, 2014, E800) use higher marine growth values for their standard and indicate that the following marine growth profile may be used for design in

Norwegian and UK waters: Central and Northern North Sea: -2 to -40: 100mm, >40: 50mm; and somewhat higher values (up to 150 mm between sea level and LAT –10 m) in the Southern North Sea. This is supported by Larsen et al. (2004), who present similar values of the expected marine growth for the OWP Borkum Riffgrund in the North Sea; although they found on certain piles a relatively thinner fouling layer in the upper 20 m (see Table 8.5, note that this table only shows the zonation in the upper 32 m). The differences between the general findings of Jusoh and Wolfram (1996), and Larsen et al. (2004) and DNV (2014) indicate local variation in marine growth thickness and zonation, which makes it necessary to investigate local data on marine growth (where available).

Water depth (m)	Marine growth thickness (mm)
0-10	50
10-20	45
20-25	65
25-32	90

Table 8.5   Thickness of marine growth of OWP Borkum Riffgrund according to Larsen et al. 2004.

8.7.4   Marine growth surveys in the North Sea

From 2008 to 2010, KEMA performed surveys of marine growth on turbine support structures of the Offshore Windfarm Egmond aan Zee (OWEZ), constructed in 2006 at 6-14m depth (KEMA, 2010). It was predicted (KEMA, 2006) and observed (Bouma and Lengkeek 2009; KEMA 2010) that a clear vertical zonation in marine growth communities would develop on the three monitored OWEZ structures in two to four years after construction. The upper zone was dominated by a relative thick layer of mussel fouling communities (50-150 mm*: M. edulis* and starfish) down to a depth of ~7 m . Below 7 m to the bottom, the marine growth community mainly consisted of soft fouling species, forming a relatively thin layer (10-50mm: anemones, bryozoan, barnacles, Japanese oysters) (KEMA 2010).

The Princess Amalia Wind Farm (constructed in 2007, at 19-24m depth) was sampled for marine growth communities in 2011 by eCOAST Marine Research, 3.5 years after construction (eCOAST, 2013). They compared the results of the Princess Amalia Wind Farm to survey results by Bouma and Lengkeek (2009) on OWEZ and reported a similar depth zonation, but a significantly higher species diversity at PAWF. Also, OWEZ densities of mussel *M. edulis* were slightly lower than at PAWF. This could be explained by that Bouma and Lengkeek (2009) surveyed OWEZ two years after construction whereas eCOAST (2011) surveyed PAWF after 3.5 years.

An elaborate monitoring scheme on biofouling has been executed on the C-Power wind park on the Thornton Bank in the Belgian part of the North Sea, constructed at around 30m depth (Degraer & Brabant (2009). The monitoring, however, did not address the thickness of marine growth layer. Fast and intense colonization of the concrete foundations was observed (Degraer & Brabant 2009, Kerckhof et al. 2009); after 3.5 months, a surprisingly high species richness (49 spp.) was found, including crustaceans, mussels, scallops and oysters. Mussels and oysters were expected to eventually dominate the marine growth communities. While the number of species found was high compared to species richness on hard substrata in the Southern North Sea, it is not expected that this results in a higher thickness of marine growth.

KEMA (2010) indicated that when clusters of mussels are >150 mm thick, due to currents during the tides (up to 3 m/s) and mortality of the specimens attached to the surface (underneath), patches and clusters of mussels are expected to come loose from the surface,

leaving open spaces where new marine growth can develop. This was indeed observed on the OWEZ structures. It is therefore expected that marine growth thickness will mostly remain <150 mm.

8.7.5   Borssele Wind Farm Zone

The Borssele Wind Farm Zone is located more than 22 km west of the coast of Zeeland, the Netherlands, at a similar water depth as Princess Amalia (18-38m). It is to be expected that the biofouling communities at the BWFZ will develop in similar ways to the observed communities at the C-Power and Princess Amalia wind farms. As the Princess Amalia wind farm showed a higher biodiversity and higher densities of mussel *M. edulis* after a longer period (3.5 years) of operation, it is advised to take into account a marine growth thickness of 150 mm for the top 7 m below water level of the BWFZ monopoles and 50 mm for the lower zone.

References

Adams, T. P., R. G. Miller, D. Aleynik, and M. T. Burrows. 2014. Offshore marine renewable energy devices as stepping stones across biogeographical boundaries. Journal of Applied Ecology 51:330-338.

ATT, 2014. Admiralty Tide Tables. United Kingdom Hydrographic Office NP-201. Volume 1.

Dee, D. P. and co-authors, 2011: The ERA-Interim reanalysis: configuration and performance of the data assimilation system, Q. J. R. Meteorol. Soc., 137 (656), 553-597, doi:10.1002/gj.828.

Baas, P., 2014: *Final report of WP1 of the WTI2017-HB Wind Modelling Project*. KNMI Scientific Report; WR 2014-02 (http://www.knmi.nl/bibliotheek/knmipubWR/WR2014-02.pdf), August 2014.

Baas P., Bosveld F. C., and Burgers G., 2015: The impact of atmospheric stability on the near-surface wind over sea in storm conditions, *Wind Energ*., doi: 10.1002/we.1825.

Bouma B. and W. Lengkeek, 2009: Development of underwater flora- and fauna communities on hard substrates of the offshore wind farm Egmond aan Zee (OWEZ). Report Bureau Waardenburg nr 08-220.

Bouma, T. J., M. B. De Vries, E. Low, G. Peralta, I. C. Tánczos, J. Van De Koppel, and P. M. J. Herman. 2005. Trade-offs related to ecosystem engineering: A case study on stiffness of emerging macrophytes. Ecology 86:2187-2199.

Crimaldi, J. P., J. R. Koseff, and S. G. Monismith. 2007. Structure of mass and momentum fields over a model aggregation of benthic filter feeders. Biogeosciences 4:269-282.Cooksey, K. E., and B. Wigglesworth-Cooksey, 1995: Adhesion of bacteria and diatoms to surfaces in the sea: a review. Aquat. Microb. Ecol. 9:87–96.

Crook, Th. de, [1996], A seismic zoning map conforming to Eurocode 8, and practical earthquake parameter relations for the Netherlands, Geologie en Mijnbouw, 75, pp 11-18.

Degraer S, Brabant R (Eds.) 2009. Offshore wind farms in the Belgian part of the North Sea: State of the art after two years of environmental monitoring. Royal Belgian Institute for Natural Sciences, Management Unit of the North Sea Mathematical Models. Marine ecosystem management unit. 287 pp. + annexes.

Dijkstra, J. T. and R. E. Uittenbogaard. 2010. Modeling the interaction between flow and highly flexible aquatic vegetation. Water Resources Research 46.

DNV, 2010: recommended practice Det Norske Veritas DNV-RP-C205, environmental conditions and environmental loads, October 2010

DNV, 2014:. Offshore Standard DNV-OS-J101. Design of Offshore Wind Turbine Structures. May 2014.

eCOAST, 2013: Development of hard substrate fauna in the Princess Amalia Wind Farm, Monitoring 3.5 years after construction. (Vanagt T, Van de Moortel L, Faasse M.) Report eCOAST Marine Research report 2011036.

Graaff, R.F. de, S. Caires, A.C.S. Mol, J.J. Schouten, P.R. Wellens. 2011: West of Duddon Sands Offshore wind farm, task 1 : metocean conditions. *Deltares report 1202877-000 HYE* (for Dong Energy West of Duddon Sands (UK) Ltd.), 578 p., Feb. 2011.

Green, M. O., J. E. Hewitt, and S. F. Thrush. 1998. Seabed drag coefficient over natural beds of horse mussels (*Atrina zelandica*). Journal of Marine Research 56:613-637.

Grünthal, G., GSHAP Region 3 Working Group (1999): Seismic Hazard Assessment for Central, North and Northwest Europe: GSHAP Region 3. - *Annali di Geofisica*, *42*, 6, p. 999-1011.

Guerin, A. J.. 2009: Marine Communities of North Sea Offshore Platforms, and the Use of table Isotopes to Explore Artificial Reef Food Webs. University of Southampton, School of Ocean and Earth Science, Doctoral Thesis , 244pp.

ISO19906, 2010. Petroleum and natural gas industries – Arctic offshore structures. NEN-EN-ISO 19906:2010. Section 8.3.1.2.

Järvelä, J. 2002. Flow resistance of flexible and stiff vegetation: A flume study with natural plants. Journal of Hydrology 269:44-54.

Jiménez, M.-J., Giardini, D., Grünthal, G. (2003) The ESC-SESAME unified hazard model for the European-Mediterranean region. EMSC/CSEM Newsletter 19, 2-4.

Jusoh I. and J. Wolfram, 1996: Effects of marine growth and hydrodynamic loading on offshore structures. Jurnal Mekanikal, Jilid 1, 1996.

KEMA, 2006: Biological Fouling. Pre-survey of marine fouling on turbine support structures of the Offshore Windfarm Egmond aan Zee. OWEZ_R_112_July 19 2006. 50562062-TOS/MEC 06-9409.

KEMA, 2010: Biological Fouling. Survey of marine fouling on turbine sypport structures of the Offshore Windfarm Egmond aan Zee. OWEZ_r_112_T1_20100114_biofouling. 50863231-TOS/MEC 08-9096.

Kerckhof F, Norro A, Jacques TG, Degraer S. 2009. Early colonisation of a concrete offshore windmill foundation by marine biofouling on the Thornton Bank (southern North Sea). In: Offshore wind farms in the Belgian part of the North Sea: State of the art after two years of environmental monitoring. Degraer & Brabant (Eds). MUMM.

Kerckhof, F., B. Rumes, A. Norro, T. G. Jacques & S. Degraer, 2010b. Seasonal variation and vertical zonation of the marine biofouling on a concrete offshore windmill foundation on the Thornton Bank (southern North Sea). In Degraer, S., R. Brabant & B. Rumes (eds), Offshore wind farms in the Belgian Part of the North Sea: Early environmental impact assessment and spatio-temporal variability. Royal Belgian Institute of Natural Sciences. Management Unit of the North Sea Mathematical Models, Marine ecosystem management unit, Brussels: 53–68

KNMI, 1964. Drijfijswaarnemingen van Nederlandse lichtschepen in Januari - Maart 1963. (in Dutch) Dr. R. Dorrestein. Overdruk uit De Zee, nr. 3, jaargang 1964. www.knmi.nl/~koek/NTT%20De%20Zee/DeZee-083.pdf

Krone, R., L. Gutow, T. J. Joschko, and A. Schröder. 2013. Epifauna dynamics at an offshore foundation - Implications of future wind power farming in the North Sea. Marine Environmental Research 85:1-12.

Larsen S.T. and coauthors, 2004: Wind and Wave Loads to Borkum Riffgrund Offshore Wind Farm, European Wind Energy Conference, 22-25 November 2004, London, UK.

Lindeboom, H. J., H. J. Kouwenhoven, M. J. N. Bergman, S. Bouma, S. Brasseur, R. Daan, R. C. Fijn, D. De Haan, S. Dirksen, R. Van Hal, R. Hille Ris Lambers, R. Ter Hofstede, K. L. Krijgsveld, M. Leopold, and M. Scheidat. 2011. Short-term ecological effects of an offshore wind farm in the Dutch coastal zone; Acompilation. Environmental Research Letters 6.

Mol, A.C.S., 2009: Metocean conditions at OWP Godewind. *WL | Delft Hydraulics report H5277*, Jan. 2009.

Musson, R.M.W. and Sargeant, S.L., 2007. Eurocode 8 seismic hazard zoning maps for the UK. CR/07/125, British Geological Survey Technical Report, Edinburgh.

Quarton, D.C., 2005: An International Design Standards for Offshore Wind Turbines: IEC 61400-3

Richmond MD, Seed R. 1991. A review of marine macrofouling communities with special reference to animal fouling. Biofouling: The Journal of Bioadhesion and Biofilm Research Volume 3, Issue 2, 1991, pp 151-168.

Rosset P. Et Barszez A-M., 2005: Mapping The Local Seismic Hazard And Its Influence On Built Environnement : Case Study In The Mons Basin (Hainaut - Belgium). Actes du symposium : Deuxième journée des géographes belges. 2005.

Scheidat, M., J. Tougaard, S. Brasseur, J. Carstensen, T. Van Polanen Petel, J. Teilmann, and P. Reijnders. 2011. Harbour porpoises (*Phocoena phocoena*) and wind farms: a case study in the Dutch North Sea. Environ. Res. Lett. 6:10.

Standards Norway, 2007: Norsok Standard N-003, Edition 2, September 2007, Actions and action effects.

Thorpe, S. A. 2012. On the biological connectivity of oil and gas platforms in the North Sea. Marine Pollution Bulletin 64:2770-2781.

TNO-rapport 2012 R10198 Deterministische hazard analyse voor geïnduceerde seismiciteit in Nederland , Karin van Thienen-Visser, Manuel Nepveu, Jenny Hettelaar

Unesco, 1981. Background papers and supporting data on the International Equation of State of Seawater 1980. Unesco Technical Papers in Marine Science, No. 38, 192 pp

Unesco, 1981. Background papers and supporting data on the International Equation of State of Seawater 1980. Unesco Technical Papers in Marine Science, No. 38, 192 pp

Vanagt T. and Faasse M. (2014). Development of hard substratum fauna in the Princess Amalia Wind Farm. Monitoring six years after construction. eCOAST report 2013009

Wells, S. and M. Sytsma, 2009: A Review of the Use of Coatings to Mitigate Biofouling in Freshwater - prepared for the Bonneville Power Administration and the Pacific Marine Fisheries Commission. Center for Lakes and Reservoirs Portland State University.

Yebra, D.M., Kiil S. and K. Dam-Johansen, 2004: Antifouling technology-past, present and future steps towards efficient and environmentally friendly antifouling coatings. Progress in Organic Coatings. 50:75-104.